UNIVERSITY OF OKLAHOMA

GRADUATE COLLEGE

FROM NITRITE REDUCTASE TO ALZHEIMER'S DISEASE:
DESIGN, SYNTHESIS, AND REACTIVITY OF NEW NITROGEN-, OXYGEN-, AND
SULFUR-CONTAINING LIGANDS AND THEIR COPPER COMPLEXES.

A Dissertation

SUBMITTED TO THE GRADUATE FACULTY

in partial fulfillment of the requirements for the

degree of

Doctor of Philosophy

By

ERIC L. KLEIN
Norman, Oklahoma
2006

UMI Number: 3203325

UMI®

FROM NITRITE REDUCTASE TO ALZHEIMER'S DISEASE:
DESIGN, SYNTHESIS, AND REACTIVITY OF NEW NITROGEN-, OXYGEN-, AND
SULFUR-CONTAINING LIGANDS AND THEIR COPPER COMPLEXES.

A Dissertation APPROVED FOR THE
DEPARTMENT OF CHEMISTRY AND BIOCHEMISTRY

BY

_____
Robert P. Houser

_____
George B. Richter-Addo

_____
Paul F. Cook

_____
Kenneth M. Nicholas

_____
David P. Nagle

ACKNOWLEDGEMENTS

As I complete with this dissertation the great challenge of earning my doctoral degree and now reflect on the past five years of my life that I have largely spent in its pursuit, I find myself faced with the truly daunting task of adequately expressing my gratitude to the many people who have helped make this experience possible, worthwhile, and its successful conclusion a reality. These are the people who have offered friendship, words of encouragement or a smile at just the right moment, motivation when I was ready to give up, selflessly their time, expertise, and resources whenever and wherever I needed them, and who have simply shared with me, in great and small ways, the highs and lows of my life as a graduate student. I am, and will always be, grateful to everyone who has graced this time of my life with their presence and will always remember what they have done for me.

Jenny, my best friend and wife of six years, has absolutely convinced me that I am married to the most fantastic woman any man could ever wish for himself. She has been my crown and joy; a terrific and necessary partner, without whom I would never have found within myself the strength or courage to begin, much less continue and complete, this work. I look forward to our years ahead and to better showing her, as she has done so well for me, just how much I love and cherish her.

I owe my mentor and advisor, Prof. Robert P. Houser, my sincere appreciation for allowing and encouraging me to be a member of his group, even before his group existed. As an undergraduate under his direction, he gave me the valuable experience of learning to set up and run a research lab almost from day one. His tremendous patience, trust, and excellent skill as a teacher during that process persuaded me to continue working under

his direction and to become his first graduate student. I appreciate very much his direction, outstanding character, and kind financial support over the years I have known him.

I am thankful for my past and present colleagues in the Houser Research Group, particularly for Deping Cheng, Arunendu Mondal, Urmila Pal Chauhuri, and Lei Yang, for their collaboration and friendship. It has been a genuine pleasure to work with each of them.

To my graduate advisory committee members, Professors Houser, Richter-Addo, Cook, Nicholas, Nagle, and formerly Wehmschulte, I am appreciative of their constructive criticism, continual encouragement, and sound advice over the years. I have enjoyed and anticipated our meetings together and getting to know each of them.

I am indebted to Prof. Dr. Andreas Grohmann and his group at the Technische Universität Berlin for allowing me to work in Berlin during the summer of 2004. I consider Prof. Grohmann and each member of his group to be great friends and am thankful for all of the time we were able to enjoy together in Berlin and for the unique experience they made possible for me in Germany.

I appreciate all of the current and past students and faculty of the Inorganic Division who have freely shared their knowledge, correction, and friendship with me, especially during Inorganic Seminar. I have learned a great deal from our conversations and friendly debates, and have enjoyed knowing and interacting with each of them over the years.

Finally, I would like to thank the support staff in the Department who worked behind the scenes to make my job here possible. Thanks to Arlene Crawford, Sandra

CONTENTS

LIST OF TABLES

ABBREVIATIONS

AA	Amino acid
AcOH	Acetic acid
AD	Alzheimer's Disease
Ala	Alanine
Asp	Aspartic acid
bipy	Bipyridine
Boc	*tert*-Butyloxycarbonyl
(Boc)₂TACN	1,4-Di(*t*-butyloxycarbonyl)-1,4,7-triazacyclononane
BOC-ON	2-(*t*-Butoxycarbonyloxyimino)-2-phenylacetonitrile
Br	Broad
Bz	Benzyl
COSY	Correlation spectroscopy
CT	Charge transfer
CuNiR	Copper-containing nitrite reductase
CV	Cyclic volammetry
Cys	Cysteine
DCC	Dicyclohexylcarbodiimide
DCU	Dicyclohexylurea
deg	Degrees
DMF	Dimethylformamide
DMSO	Dimethylsulfoxide
EI-MS	Electron impact ionization mass spectrometry

EPR	Electron paramagnetic resonance
ESI-MS	Electrospray ionization mass spectrometry
Et_3N	Triethylamine
Et_2O	Diethyl ether
EtOAc	Ethyl acetate
FeNiR	Iron-containing nitrite reductase
Fmoc	Fluorenylmethyloxycarbonyl
FTIR	Fourier transform infrared spectroscopy
GC-MS	Gas chromatography mass spectrometry
Gly	Glycine
HOBt	Hydroxybenzotriazole
His	Histidine
HOMO	Highest occupied molecular orbital
Ile	Isoleucine
iPr_2TACN	1,4-Diisopropyl-1,4,7-triazacyclononane
IR	Infrared
LMCT	Ligand-to-metal charge transfer
LUMO	Lowest occupied molecular orbital
m	Medium
Me	Methyl
MeCN	Acetonitrile
MeOH	Methanol
Met	Methionine

MLCT	Metal-to-ligand charge transfer
MW	Microwave
MS	Mass spectrometry
NiR	Nitrite reductase
NMR	Nuclear magnetic resonance spectroscopy
OTf	Trifluoromethanesulfonate
OTs	*p*-toluenesulfonate
Phe	Phenylalanine
Py	Pyridine
rbf	Round bottom flask
ROS	Reactive oxygen species
r.t.	Room temperature
s	Strong
sh	Sharp
TACN	1,4,7-Triazacyclononane
TBA	Tetrabutylammonium
TBAH	Tetrabutylammonium hexafluorophosphate
TBAB	Tetrabutylammonium Bromide
TFA	Trifluoroacetic acid
THF	Tetrahydrofuran
TIS	Triisopropylsilane
TLC	Thin layer chromatography
TOF	Time of flight

Tosyl	*p*-Toluenesulfonyl
Trityl	Triphenylmethyl
Trt	Triphenylmethyl
Ts	*p*-Toluenesulfonyl
UV	Ultraviolet
UV-vis	Ultraviolet visible spectroscopy
w	Weak

ABSTRACT

Transition metal ions are essential for a wide range of biochemical transformations and are found in more than one half of all known enzymes. Our interest in the bioinorganic chemistry of copper prompted us to develop new model complexes that more accurately mimic structural aspects of the copper-containing nitrite reductase (CuNiR) active site, which contains a type 1 ("blue") electron transfer center that is coupled via a His-Cys bridge to a type 2 ("normal") catalytic center. Preliminary attempts to achieve this goal by covalently linking 1,4,7-triazacyclononane (TACN) and His were thwarted by synthetic challenges. Using less reactive amino acids, however, the first structurally characterized copper(II) complexes of TACN-Ala, -Gly, and -Phe were obtained and studied. These new complexes provide insight into the copper coordination chemistry of TACN, where one of its secondary amines has been converted to a tertiary amide. As an offshoot of this project, mononuclear copper(II) complexes of a new N_2S(thioether) ligand were also obtained and fully characterized. The reactivity of these complexes with thiolates was investigated in an effort to produce new N_2S(thioether)S(thiolate) type 1 copper center models. Although stable copper(II)-thiolate complexes could not be obtained, the redox decomposition of one of these proceeds by way of an unprecedented pathway that requires two equivalents of thiolate to fully reduce copper(II) to copper(I). Finally, a related ligand that contains two thioethers was also prepared. Attempts to produce copper(II) complexes of this ligand result in unanticipated redox decomposition that is dependent on the presence of both thioether sulfurs. This work has direct relevance to a recent proposal implicating Met sulfur in Alzheimer's Disease amyloid-β neurotoxicity.

By taking a long and thoughtful look at what God has created, people have always been able to see what their eyes, as such, cannot see; eternal power, for instance, and the mystery of his divine being…

Romans 1:20

CHAPTER 1.

INTRODUCTION AND BACKGROUND: COPPER-CONTAINING NITRITE REDUCTASE AND COPPER-MEDIATED NEUROTOXICITY IN ALZHEIMER'S DISEASE

1.1 Introduction

Redox-active transition metals are found in more than one half of all known enzymes and are essential for a wide range of biochemical transformations and processes.[1,2] Of these metals, copper plays a particularly interesting and diverse role in metalloenzyme electron transfer,[2,3] oxygen transport,[4] and catalytic sites.[5,6] Regrettably, copper has also been directly implicated in a number of deleterious processes and is known to be central to several human disorders,[7] including Alzheimer's Disease (AD).[8] The diverse biological reactivity of copper can be directly attributed to two principal factors; (1) its inherent electronic structure and (2) its coordination environment.

Although copper can form stable complexes in the 1+, 2+, or 3+ oxidation states, it is known to definitively exist only in the 1+ or 2+ oxidation states in biological systems. The electronic structure and preferred coordination environment of the metal in these two oxidation states differ considerably from each other.[9] Copper(I) has completely occupied d-orbitals ($3d^{10}$), tends to adopt a flexible, but often tetrahedral, coordination geometry and is stabilized by relatively soft ligands. Conversely, copper(II) has incompletely filled *d*-orbitals ($3d^9$), prefers tetragonal or trigonal coordination geometries, and is stabilized by comparatively hard ligands. Furthermore, as a consequence of unequal electron occupation of their degenerate *d*-orbitals, copper(II) complexes typically exhibit significant Jahn-Teller distortions,[10] where the orbital degeneracy is broken and the complex is stabilized by axial metal-ligand bond elongation or compression. While the coordination geometry of copper in small molecule complexes is principally dictated by the electronic structure of the metal and ligand constraints, the rigid protein structure of a metalloenzyme has the ability to effectively

impose a fixed geometry on its coordinated metal ion. The ability of the protein to control both the coordination geometry of the metal ion and the identity of its coordinating ligands (amino acids) allows it to elegantly modulate the electronic properties and reactivity of copper.

One method that is employed by chemists to gain a better understanding of the structure-function relationship occurring at the active site of metalloenzymes is the synthesis and characterization of small-molecule model complexes. Such model complexes are usually designed to mimic specific aspects of the metal coordination site as it exists in the protein, including the structures and properties of proposed substrate-bound reactive intermediates that are difficult to characterize in the actual enzyme. By comparing the reactivity and/or spectroscopic features of the model complexes to that of the metalloenzyme, analogies can be drawn that provide insight into its structure and mechanism. Furthermore, factors that promote substrate activation can often be probed in model complexes in ways that are not always possible or practical in the enzyme. Thus, the continual development of new and improved model systems is important to the pursuit of a deeper understanding of specific metalloenzyme function.

Our efforts toward the synthesis and characterization of next-generation model complexes that more accurately mimic structural aspects of the dinuclear copper-containing nitrite reductase (CuNiR) active site, which contains a copper electron transfer site and a copper catalytic site, are presented in chapters 2 and 3. An extension of this project is presented in chapter 4 and deals with the debated mode of copper reduction and subsequent reactive oxygen species (ROS) generation in AD. As a general background for each of these projects, the environmental role and structure of CuNiR are described in

section 1.2 of this chapter along with studies of several important CuNiR-related model

complexes that have been reported to date. Finally, section 1.3 of this chapter presents a

brief background of some of the current AD research with respect to the role of copper.

1.2 **Copper-Containing Nitrite Reductase**

1.2.1. The Terrestrial Nitrogen Cycle

Nitrogen exists in a large number of stable oxidation states, ranging from 3- to

5+.[11] The enzymatic interconversion of nitrogen between its many oxidation states is a

vital part of the bioenergetic processes of many bacteria and fungi.[12] As a consequence,

these organisms collectively have direct control over the natural balance of nitrogen in

the environment and, as such, a far-reaching influence over all life on earth. Figure 1-1

shows a schematic representation of the terrestrial nitrogen cycle.[5] The cycle is presented
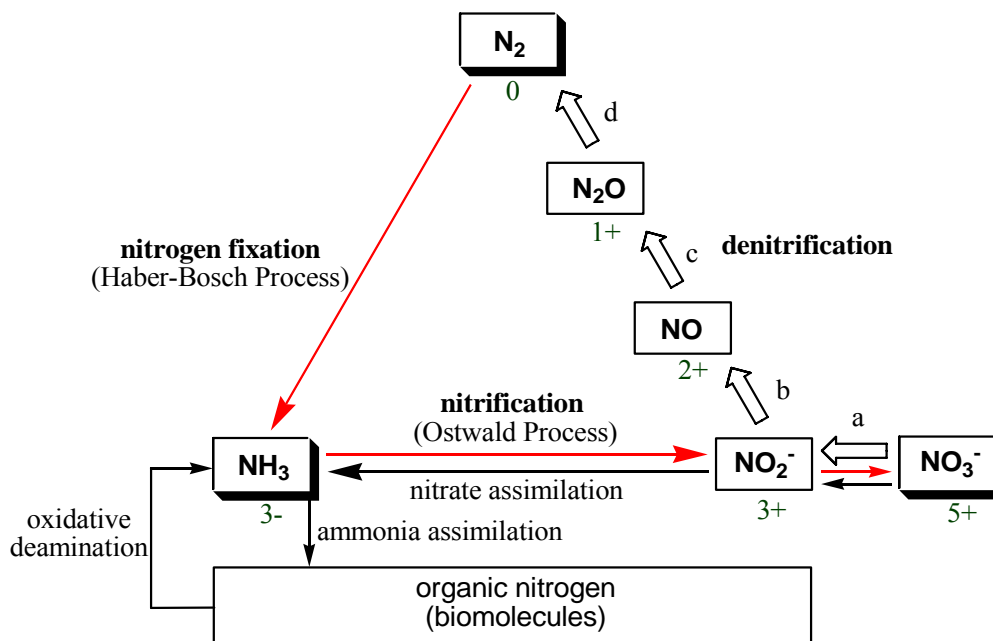
Figure 1-1. Schematic representation of the terrestrial nitrogen cycle adapted from reference 5. The red arrows indicate areas of significant anthropogenic influence on the nitrogen cycle through the Haber-Bosch and Ostwald processes.

in terms of the principal environmental nitrogen species, nitrate (N^{5+}), dinitrogen (N^0), and ammonia (N^{3-}), and is divided into three central processes; nitrogen fixation, nitrification, and denitrification.

Because nitrogen is required for assimilation into the cells of all organisms, its availability in a biologically useful form generally limits organism growth. This is particularly important in agriculture, where useful nitrogen is often depleted from the soil and must be artificially replenished with nitrogen-based fertilizers in order to achieve adequate crop yields. The vast supply of dinitrogen (N_2) in the atmosphere is of no use to most organisms because of the very high stability of the N_2 triple bond. While a few, namely nitrogen fixing bacteria and archaea, have the ability overcome this high energetic barrier and convert N_2 directly to NH_3,[13] all others must obtain their cellular nitrogen requirements by converting nitrate and nitrite to ammonia through the process of nitrate assimilation or, alternatively, through the liberation of ammonia from the decomposition of organic material by oxidative deamination.[14] Nitrification is the complimentary process to nitrate assimilation, where nitrifying bacteria use ammonia directly as an energy source under aerobic conditions and produce nitrate.[15]

As a means of meeting the ever-increasing human demand for agricultural fertilizer (ammonium nitrate) the Haber-Bosch (fixation) and Ostwald (nitrification) processes, both developed in the early twentieth century, have also enabled the industrial-scale production of large quantities of ammonium nitrate from atmospheric N_2.[16] The impact of the artificial introduction of huge quantities of nitrate, released into almost every ecosystem through agricultural runoff, is enormous and accounts for many emerging ecological problems including river, pond, and lake eutrofication.[17] Thus, the

human-instigated imbalance of the nitrogen cycle, as indicated by the red arrows in Figure 1-1, is a growing concern.

Completing the nitrogen cycle, denitrification is the dissimilatory process by which nitrate and nitrite are reduced to gaseous nitric oxide (NO), nitrous oxide (N_2O), and ultimately N_2.[18] Denitrification is carried out in several steps (Figure 1-1, steps a-d) by denitrifying bacteria, which use reducible nitrogen species as terminal electron acceptors in their metabolic processes.[19] In the first step (step a), nitrate reductase, an enzyme that contains Mo(VI)O, heme iron, and non-heme iron sites, mediates the two-electron reversible reduction of nitrate to nitrite.[20] In the second step, nitrite is then irreversibly reduced to nitric oxide by either heme iron (FeNiR)[21] or copper-containing (CuNiR)[5, 22] nitrite reductase (step b). Nitric oxide reductase,[23] also a heme iron enzyme, further reduces nitric oxide to nitrous oxide (step c).[19, 24] In the final step of the denitrification pathway (step d), nitrous oxide reductase, which contains Cu_A and Cu_Z sites, catalyzes the reduction of nitrous oxide to dinitrogen.[25]

Because they efficiently mediate the natural pathway by which nitrogen oxides can be converted into gaseous products, the enzymes and organisms that are involved in denitrification have received much attention. It is hoped that a better understanding of the relationship between the structures of these enzymes and the details of their catalytic mechanisms will ultimately lead to the design of new synthetic catalysts that can be specifically implemented on a global scale to reverse increasing nitrate pollution. Of these enzymes, the copper and iron nitrate reductases have received particular attention since they catalyze the first irreversible step in denitrification.

Our interest in the biological chemistry of copper, particularly with respect to denitrification, has prompted us to undertake the development of next-generation model complexes of the dinuclear CuNiR active site. While the currently reported CuNiR-related model complexes have provided much structural information about mononuclear copper-bound reactive intermediates (see section 1.2.2), at the inception of this work, no efforts to synthesize more complete models that could accurately mimic the dinuclear structure or reactivity of the CuNiR active site had been reported.

1.2.2   CuNiR Structure and Proposed Mechanisms

CuNiR has been isolated from several different bacteria and fungi. The first reported crystal structure of the enzyme was obtained from *Achrobacter cycloclastes* in 1991.[26-28] Since then, the structures from *Alcaligenes faecalis*[29, 30] and *Alcaligenes xylosoxidans*,[31] as well as a number of related mutants, have also been reported. In each case, the wild-type CuNiR protein and copper binding site structures are nearly identical to each other, differing only slightly in their spectroscopic features as a result of subtle variations in the copper ion coordination geometries.

The 1.8 Å resolution crystal structure of NO_2^--bound CuNiR from *A. faecalis* is shown in Figure 1-2.[30] This 37 kDa enzyme is composed of three identical subunits, each containing two copper ions, and is representative of the known CuNiR enzyms. Each of the subunits consists of two domains, I and II, that are joined to each other by a 12 amino acid loop. Domain I is located toward the interior of the enzyme, forming a $4-6$ Å channel around a 3-fold central axis, and interacts with domain II of its adjacent subunit. While the exterior surface of the protein is hydrophilic, the interior and subunit interface regions are largely hydrophobic.
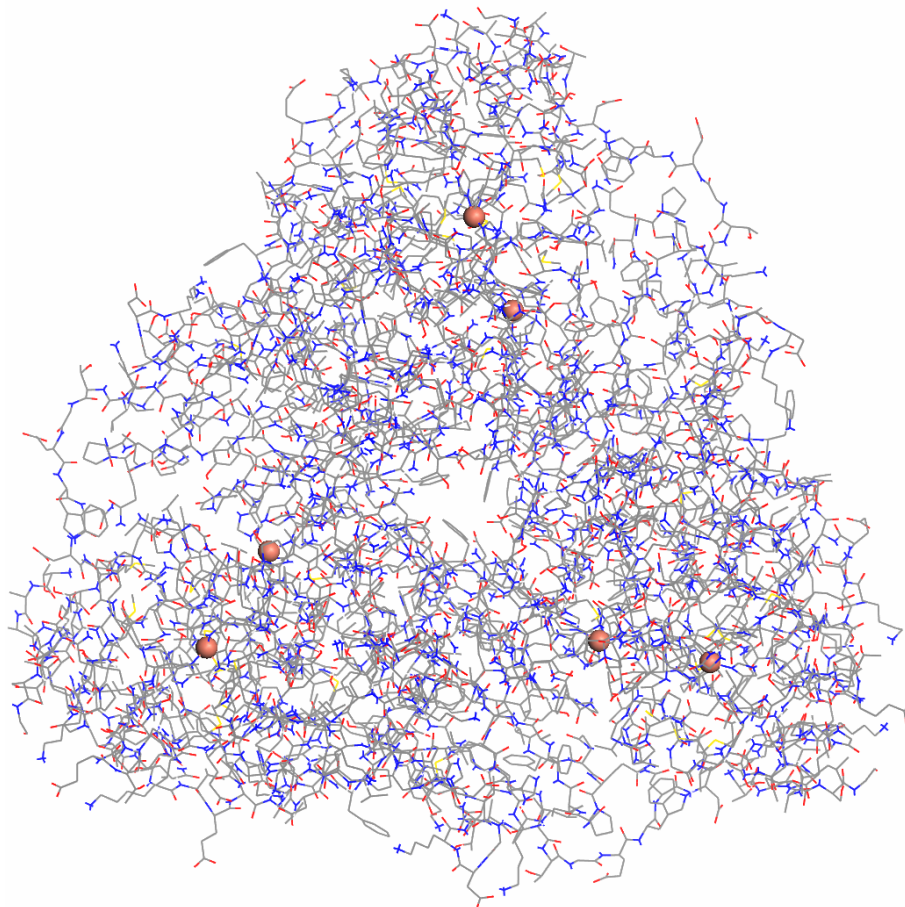
Figure 1-2. Representation of the 37 kDa homotrimeric CuNiR protein structure from *A. faecalis*. The copper ions are displayed as CPK spheres. Water molecules and hydrogen atoms have been omitted for clarity.

A close-up of one of the binuclear copper sites is shown in Figure 1-3. Buried within domain I is a single type 1 copper (Cu-I) electron transfer site, where the copper ion is bound by one cysteine (Cys), one methionine (Met), and two histidine (His) residues in a distorted trigonal planar geometry. The second copper ion, separated by ~12.5 Å from the Cu-I site via a His-Cys bridge and located at the subunit interface, forms a type 2 copper (Cu-II) site and is bound in a tetrahedral geometry by two His residues from domain I of one subunit, one His from domain II of its neighboring

subunit, and one exogenous ligand. Prior to catalysis, the exogenous ligand, water or chloride depending on the source, is displaced by substrate, which diffuses into the active site between the subunits. Accordingly, the accessible Cu-II site serves as the location of substrate binding and catalysis, while the His-Cys bridge connecting it to the Cu-I electron transfer site within the same subunit is believed to serve as the route of electron transfer to the catalytic site and ultimately to bound NO_2^-, yielding NO.[32]
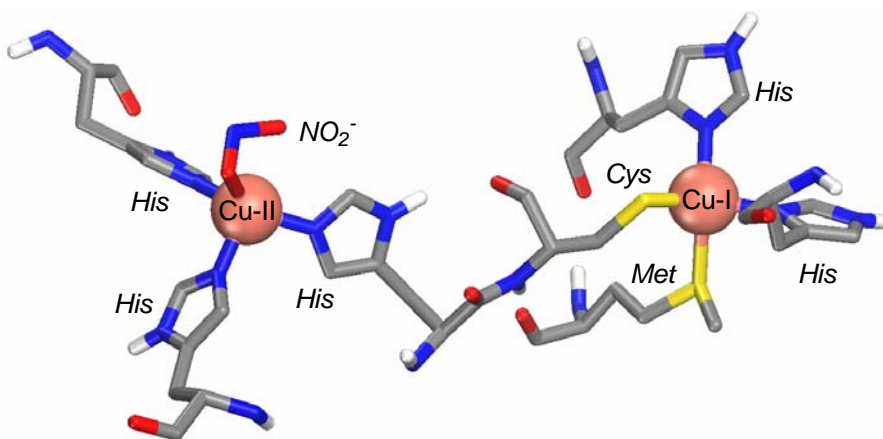
Figure 1-3. Representation of the X-ray crystal structure of the NO_2^--bound CuNiR active site from *A. faecalis*.

Despite the fact that the function and structural aspects of CuNiR are now well understood, the details of its catalytic mechanism are still unfolding. At the inception of this work, two very different mechanisms for NO_2^- reduction by CuNiR had been proposed in the literature. The first, and more simplistic of the two, was reported by Hulse and Averill (Figure 1-4).[24, 33] This mechanism is centered on the η^1-N coordination of NO_2^- to the reduced catalytic site and does not specifically address potential interactions of the bound substrate with amino acid residues in the active site vicinity. In
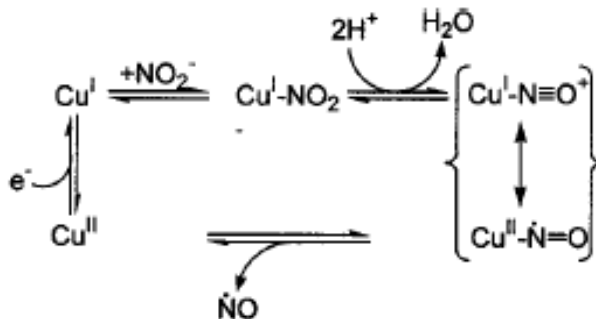
Figure 1-4. CuNiR catalytic mechanism proposed by Hulse and Averill.

the presence of protons, the *N*-bound copper(I)-NO_2 adduct eliminates water, forming a copper nitrosyl intermediate that subsequently evolves NO. The copper ion is then reduced by an electron transfer event from the Cu-I site prior to the next cycle.

The second mechanism, initially reported by Adman, *et al.*, draws upon the involvement of His and aspartic acid (Asp) residues in the vicinity of the catalytic site, as suggested by X-ray crystallography (Figure 1-5).[26, 30] In this mechanism, NO_2^- binds to the oxidized copper ion at the catalytic site, thereby forcing the release of OH^- in the first step. Instead of an η^1-*N* coordination mode as described in the previous mechanism, NO_2^- is proposed to bind in an η^2-*O,O'* fashion via its oxygen atoms to the oxidized copper ion. The binding of NO_2^- has also been suggested to increase the redox potential of the copper ion and, as a result, to possibly facilitate electron transfer from the reduced Cu-I site.[34] The copper(I)-NO_2^- intermediate that is then generated at the catalytic site quickly reduces its bound NO_2^- following electron transfer, releasing NO and dehydrating in a concerted step. In the final step of the mechanism, the enzyme is reset by protonation of His and reduction of the Cu-I site. Throughout the mechanism, the His and Asp residues serve as general acid-base catalysts and provide, or shuttle, the required

10

protons. Based on a very recent report of the first structurally characterized side-on copper nitrosyl coordination in CuNiR, a revision to this mechanism has also been proposed by Murphy, *et al.*,[35] where the electron transfer step from the Cu-I site reduces the copper at the catalytic site and results in a coordination rearrangement of NO_2^- from η^2-O,O' to η^1-N prior to NO release, thus unifying aspects of both proposed mechanisms.[35]
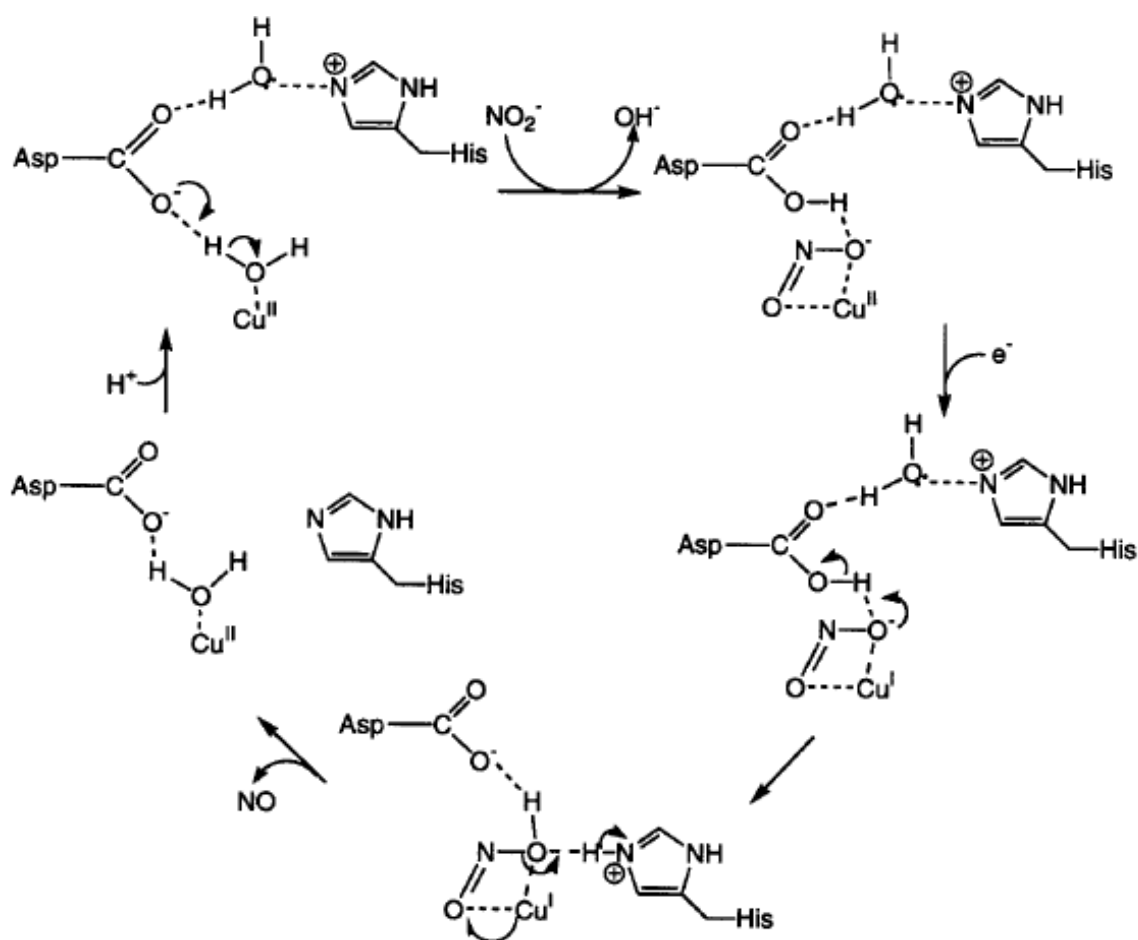
Figure 1-5. Proposed CuNiR catalytic mechanism by Adman, *et al.*

Each of the mechanisms described above involve the initial binding of NO_2^- at the catalytic site, followed by dehydration and NO elimination. In the first mechanism, an η^1-N-bound NO_2^- adduct is proposed, where the copper ion is suggested to, but not necessarily, be reduced prior to substrate coordination. In the second mechanism, an asymmetric η^2-O,O'-bound NO_2^- adduct is proposed, where NO_2^- coordination to copper(II) may also facilitate electron transfer from the Cu-I site. Moreover, the second mechanism implies the formation of an O-bound copper-nitrosyl intermediate, which is unprecedented in the copper literature. At the time these proposals were published, particularly that of Hulse and Averill, very little was known about the coordination chemistry of NO_2^- or NO to mononuclear copper in either of its oxidation states. The chemical feasibility of the different proposed reactive intermediates was, consequently, difficult to assess using precedent from synthetic chemistry. This fact led to a considerable effort early on to synthesize and structurally characterize model complexes specifically designed to provide information about the coordination chemistry of copper-NO_2^- and copper-NO adducts.

1.2.3. CuNiR Model Complexes

The CuNiR-related model complexes that have been reported to date can be divided into three general categories. First, there are those designed to model the structure and/or spectroscopic features of the Cu-I electron transfer site.[36] Next, there are those that model the structure and/or properties of the Cu-II catalytic site, including proposed catalytic intermediates.[37-41] Finally, there are functional models that mimic the reactivity of CuNiR.[39, 42] A recent example of a binuclear copper complex that mimics structural aspects of the His-Cys bridge has also been reported.[43] Since the Cu-I site is

not unique to CuNiR and is present in many other biological copper electron transfer systems, the focus of this section will be on the important mononuclear structural models of the Cu-II site that feature bound NO_2^- or NO.

Several examples of structurally characterized NO_2^- and NO adducts for a number of metals had been reported prior to the time of the proposed CuNiR mechanism by Hulse and Averill.[44]   However, the coordination chemistry of NO_2^- and NO in mononuclear copper(I) or copper(II) complexes reminiscent of the Cu-II site remained unknown. To provide structural information for these and, in so doing, to investigate the viability of the proposed intermediates in the mechanism, model complexes of the Cu-II site with bound NO_2^- and NO began to appear in the literature shortly after the first report of the CuNiR structure from *A. cycloclastes*.[27]   Since the Cu-II site, where substrate binding and catalysis occur, was known to contain a copper ion ligated by three His residues in an unusual tetrahedral motif, appropriate supporting ligands that could closely mimic the Cu-II site coordination environment were required.

Using a pyrazole ligand, based on designs developed primarily by Kitajima,[45] Tolman reported the first structural characterization of a mononuclear copper-NO_2^- complex with a His_3-like ligand set.[38] The anionic supporting ligand in the complex, $[HB(t\text{-}Bupz)_3]^-$, is composed of three *tert*-butyl substituted pyrazole groups around a central boron. This arrangement creates a facially coordinating ligand, where a sterically protected pocket is formed by the *tert*-butyl groups after metal coordination.   The addition of $K[HB(t\text{-}Bupz)_3]$ to equimolar amounts of aqueous $CuCl_2$ and $NaNO_2$ in methanol results in the instantaneous formation of $[HB(t\text{-}Bupz)_3]Cu(NO_2)$ (**1**). The X-ray crystal structure of **1** shows the 5-coordinate copper(II) ion, around which the three
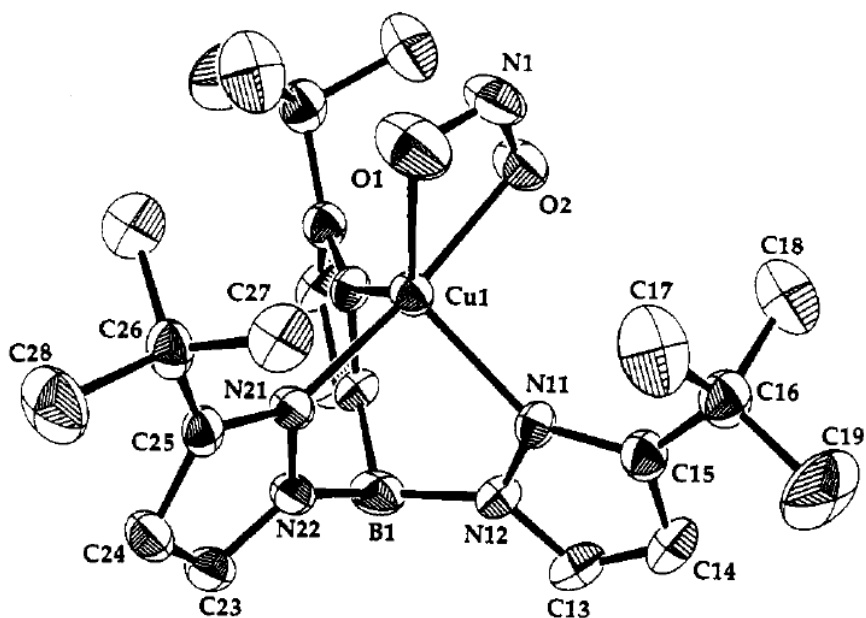
Figure 1-6. Representation of the X-ray crystal structure of [HB(t-Bupz)$_3$]Cu(NO$_2$) (**1**), adapted from reference 37, showing 40% thermal ellipsoids. All hydrogen atoms have been omitted for clarity.

pyrazole nitrogens and the η^2-*O,O'*-bound NO$_2^-$ form a distorted trigonal bipyramidal geometry (Figure 1-6). Presuming the requirement for an η^1-*N* bound copper-nitrosyl for NO elimination to occur (see Figure 1-4), it is speculated that substantial molecular rearrangements would be required to convert η^2-*O,O'*-bound NO$_2^-$, as in **1**, to η^1-*N*-bound NO. The coordination mode of NO$_2^-$ in this copper(II) complex, thus, lends support to the notion that the copper is likely reduced prior to NO$_2^-$ coordination, where an *N*-bound arrangement should be preferred and the need for a rearrangement step would be circumvented altogether.

The same pyrazole ligand system was later used by Tolman to produce the first structurally characterized mononuclear copper complex having a terminal nitrosyl

ligand.[40]   In this case, Tl[HB(*t*-Bupz)₃][46] is reacted with CuCl in THF, affording a colorless dimeric complex, {[HB(*t*-Bupz)₃]Cu}₂, that is composed of linear 2-coordinate copper(I) ions linked by η^2-[HB(*t*-Bupz)₃]⁻ ligands. Subsequent reaction of this dimeric species with NO at 1 atm in an aromatic solvent yields a deep red product, [HB(*t*-Bupz)₃]Cu(NO) (**2**), that forms X-ray quality crystals upon cooling of the reaction mixture to -20 °C. The X-ray crystal structure of **2** is very similar to **1** with respect to the supporting ligand coordination and copper ion, but possesses η^1-*N*-bound NO instead of η^2-*O,O'*-bound NO₂⁻ (Figure 1-7).
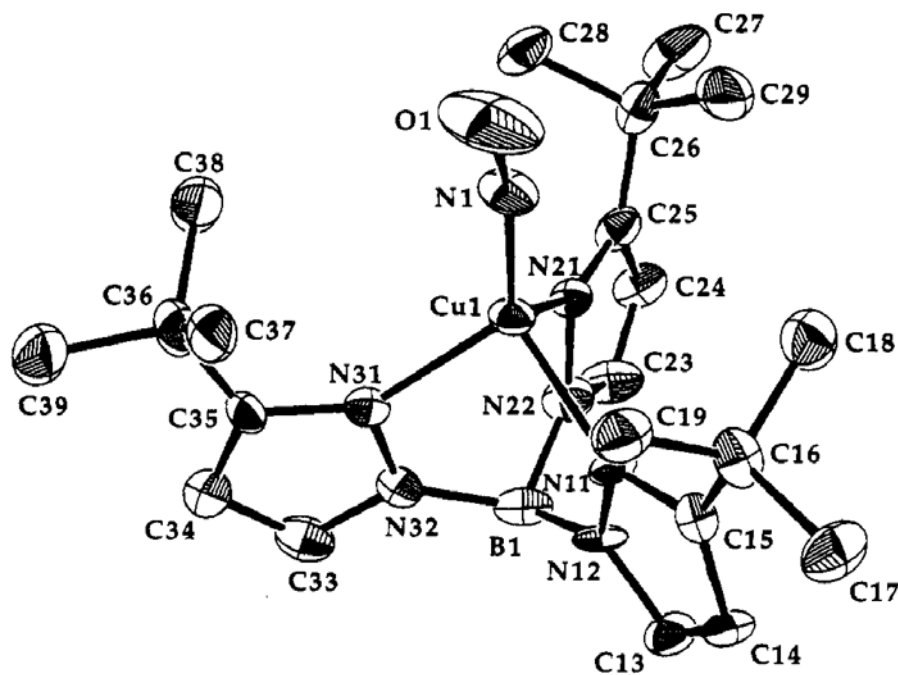
Figure 1-7. Representation of the X-ray crystal structure of [HB(t-Bupz)₃]Cu(NO) (**2**), adapted from reference 39, showing 40% thermal ellipsoids. All hydrogen atoms have been omitted for clarity.

In addition to the X-ray crystal structure, the assignment of the copper-NO coordination mode of **2** was further supported by FTIR and low temperature EPR experiments using ^{14}NO and ^{15}NO. The FTIR spectra exhibit strong absorptions at 1712 cm^{-1} and 1679 cm^{-1} assigned to $v(^{14}$NO$)$ and $v(^{15}$NO$)$, respectively. The X- and S-band EPR spectra of these complexes clearly reveal the hyperfine coupling of the unpaired electron to copper and NO, providing conclusive evidence for the copper-NO interaction. While the similarity of **2** to the copper(I)-NO intermediate(s) of the proposed mechanism is obvious, evidence for the evolution of gaseous NO from the model complex has not been reported.

Having successfully synthesized and structurally characterized the copper(II)-NO$_2^-$ and copper(I)-NO model complexes, efforts ensued to prepare mononuclear copper(I)-NO$_2^-$ complexes that would be more representative of the proposed Cu-II catalytic site immediately after substrate coordination. The first reported structurally characterized example was prepared by reaction of a copper(I) complex of the tridentate capping ligand 1,4,7-triisopropyl-1,4,7-triazacyclononane (iPr$_3$TACN)[47] with excess NaNO$_2$ in methanol, affording the binuclear copper(I) complex [(iPr$_3$TACN)$_2$Cu$_2$(μ^2-(η^1-N:η^1-O)-NO$_2$)]PF$_6$ (**3**).[41] X-ray quality crystals of **3** were obtained by slow evaporation of the solvent from the reaction mixture. The structure of **3** consists of two copper(I)-iPr$_3$TACN units, located at either end of the complex, with a single NO$_2^-$ ligand bridging between the copper(I) ions (Figure 1-8). The NO$_2^-$ coordinates one copper(I) ion in an η^1-N fashion and the other copper(I) ion weakly by the *syn* lone pair of one of its oxygen atoms (O2) in an η^1-O mode. This type of bridging arrangement had also been previously
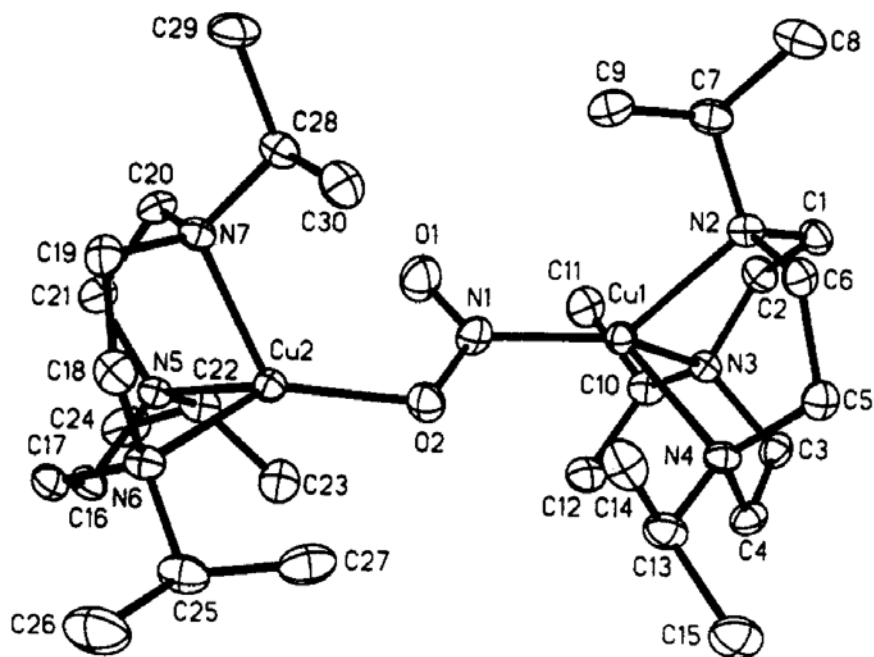
Figure 1-8. Representation of the X-ray crystal structure of $[(iPr_3TACN)_2Cu_2(\mu^2-(\eta^1-N:\eta^1-O)-NO_2)]PF_6$ (**3**), adapted from reference 40, showing 50% thermal ellipsoids. All hydrogen atoms have been omitted for clarity.

reported for several polynuclear transition metal NO_2^- species, but always through the *anti* oxygen lone pair.[48]

In addition to the obvious precedent that **3** provides for copper(I)-NO_2^- coordination, albeit in a binuclear complex, chemical oxidation of **3** with ferrocenium hexafluorophosphate also afforded the unprecedented mixed-valence complex, $[(iPr_3TACN)_2Cu_2(\mu^2-(\eta^1-N:\eta^2-O)-NO_2)](PF_6)_2$ (**4**), where the remaining copper(I) is η^1-N-bound and the copper(II) is η^2-O,O'-bound. The characterization of **4** was achieved by analytical, spectroscopic, and preliminary X-ray crystallographic experiments. Most notably, the integration of the axial X-band EPR signal accounts for about 46% of the total copper in the system. Furthermore, an intense ($\varepsilon = 2500$ M^{-1}cm^{-1}) visible transition

17

at λ_{max} = 444 nm is observed, believed to arise from a CT transition involving the NO_2^-

bridge. Thus, the preferred coordination mode of NO_2^- to both copper(I) and copper(II)

ions is established in the same model complex.

Reaction of **3** with triphenylphosphine in THF is sufficient to regioselectively

cleave the complex, affording the mononuclear copper(I)-NO_2^- adduct

[(iPr$_3$TACN)Cu((η^1-N)-NO$_2$)] (**5**) and an equivalent of [(iPr$_3$TACN)Cu(PPh$_3$)]PF$_6$.[39] **5** is

the first well-defined model complex that represents the proposed reduced CuNiR

catalytic site with bound substrate. X-ray quality crystals of **5** were obtained by

fractional crystallization directly from the reaction mixture. The crystal structure
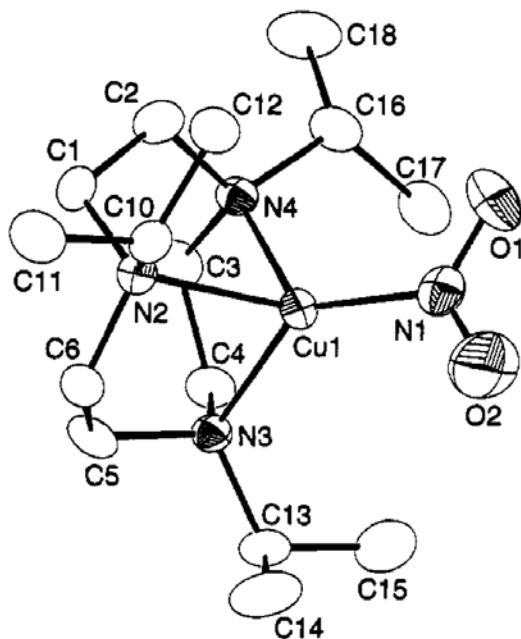
Figure 1-9. Representation of the X-ray crystal structure of [(iPr$_3$TACN)Cu((η^1-N)-NO$_2$)] (**5**), adapted from reference 38, showing 50% thermal ellipsoids. All hydrogen atoms have been omitted for clarity.

conclusively establishes the $\eta^1\text{-}N$ coordination of NO_2^- to the copper(I) ion and has essentially identical structural parameters as it did in the starting material, **3** (Figure 1-9).

Interestingly, the addition of 2 equivalents of glacial acetic acid to a solution of **5** in dichloromethane results in an instantaneous color change of the solution from yellow to blue with concomitant release of NO and, presumably, water. The blue product was identified as the copper(II) product $[(iPr_3TACN)Cu(CH_3CO_2)_2]$ by comparison of its UV-vis and EPR parameters to those of the independently synthesized material. The release of exactly one equivalent of NO from the complex upon addition of the acid was quantitatively established by GC. As both a structural and functional model, the ability of the copper(I)-NO_2^- complex, **5**, to cleanly produce gaseous NO and become oxidized to the corresponding copper(II) species provides strong support for the involvement of an initial copper(I)-NO_2^- species in the enzymatic mechanism.

Small-molecule model complexes, such as those described above, have provided much information about the structure and chemistry of NO_2^- and NO in mononuclear copper(I) and copper(II) complexes. This information is particularly relevant to the structure-function relationship of the Cu-II catalytic site of CuNiR. While analogies between these synthetic models and the proposed intermediates of the Hulse-Averill mechanism are obvious, the synthesis of model complexes that provide greater insight into the feasibility of the Adman mechanism or the influence of the Cu-I site on catalysis is far more challenging. Nonetheless, efforts are currently underway to develop advanced model complexes that more accurately represent the structure and reactivity of the CuNiR active site.

As an example, the recently published X-ray crystal structure of a unique mixed-valence CuNiR model complex, **6**, is shown in figure 1-10.[43] Here, two copper ions are connected by a pridyl-thiolate ligand, reminiscent of the His-Cys bridge of CuNiR. In addition to the pyridyl nitrogen or thiolate sulfur donor atoms, monoanionic bidentate β-diketiminate ligands cap each of the copper ions, forming a 3-coordinate trigonal planar coordination geometry at each. Thus, the copper(I) and copper(II) ions possess N_3 and N_2S donor sets, respectively, in this neutral complex. Although the authors compare the spectroscopic features of **6** to a previously reported Cu-I site model complex,[49] it is primarily presented as a proof-of-concept in the pursuit of yet more complex systems. Our concurrent efforts to also develop more advanced CuNiR model complexes using similar approaches are described in chapters 2 and 3 of this thesis.
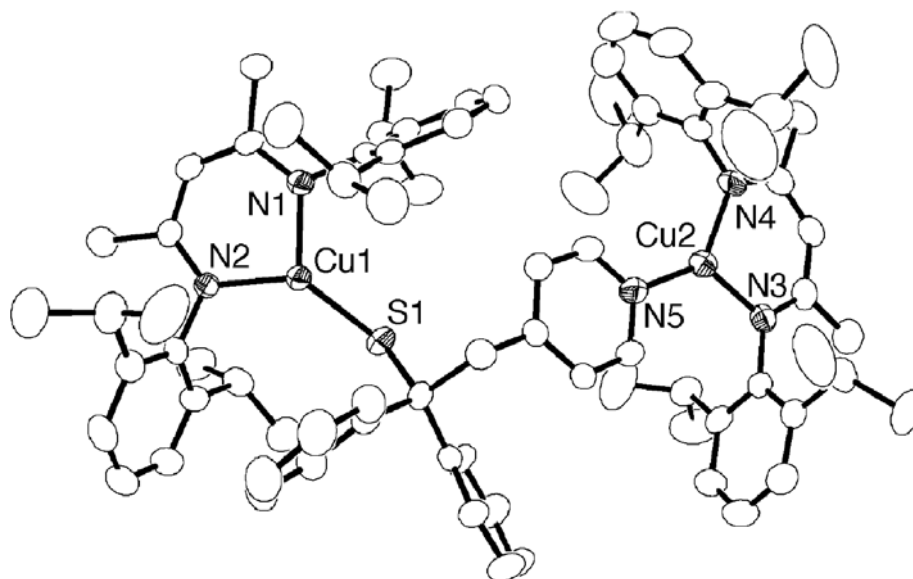
Figure 1-10. Representation of the X-ray crystal structure of **6**, adapted from reference 42, showing 50% thermal ellipsoids. All hydrogen atoms have been omitted for clarity.

1.3 Alzheimer's Disease

Alzheimer's Disease (AD) is a terminal disorder that is characterized by the formation of neurofibrillary tangles and the aggregation of insoluble amyloid-β (Aβ) plaques in the brain, accompanied by elevated levels of oxidative stress.[50] It is the most common form of dementia in people over 65 years of age and presents one of the largest health problems in industrialized countries, where life expectancies are comparatively high. The most recognizable symptoms of the disease include problems with memory, cognition, and, in its latter stages, language and general motor function. As the disease slowly progresses and the brain continues to be damaged, each of these symptoms gradually worsen and AD patients eventually become incapable of carrying out the simplest of daily tasks, functioning in society, or adequately caring for themselves.

Although the full course of the disease can span 20 years or more, the current average survival time for AD patients after diagnosis is about 4 to 6 years.[51] Its progression is so slow that behavioral differences are not readily noticeable until many years after its actual onset. Early diagnosis using current technologies is practically impossible and, as such, the time of onset is usually estimated from family members' recollections of when they first began to notice behavioral differences in the patient. Furthermore, because of the fact that most AD patients are bedridden in the latter stages of the disease, it is very common for them to develop secondary conditions that result in further deterioration of their health. Pneumonia, in fact, is the leading cause of death for AD patients.[52]

An estimated 4.5 million people currently suffer from AD worldwide, but this number is increasing with the number of people who are living into old age.[53] Without

the simultaneous development of new diagnostic methods and treatments to combat AD, estimates for the number of people who will have AD in 2050 are as high as 13.2 million in the United States alone. At the time of this writing, however, no effective methods exist to accurately predict AD onset and only a few drugs have been approved by the Food and Drug Administration (FDA) specifically for its treatment.[54] Regrettably, these drugs are currently directed toward the control of symptoms rather than root causes of the disease itself.

Two distinct types of AD have been identified to date. The first type, and less common of the two, is called Familial, or "early-onset", AD (FAD).[55] FAD occurs in a very small number of families and is related to known inheritable genetic mutations. In these cases, about half of the children of a parent with AD begin to show symptoms of the disease between 30 and 50 years of age. While the specific genes associated with FAD have been identified, the factors that lead to its expression in early mid-life remain unclear.

The second, and far more common type of AD, is called Sporadic, or "late-onset", AD (SAD).[56] SAD accounts for more than 90% of all known AD cases and appears indiscriminately in the general population in later life. Unlike FAD, the specific causes of SAD remain almost entirely unknown. It is widely believed, however, that environmental and lifestyle factors may play a large part in its onset because of the fact that no direct genetic links to it have conclusively been identified.[57]

Even though AD symptoms and many details of its pathology have now been well described, the specific biochemical events that trigger the onset of the disease are not understood and remain a major focus of AD research.[58] Through this work, it is

anticipated that new treatments can be developed that will either slow or altogether prevent the onset or progression of the disease. With the same goals, as much research is also centered on deconvoluting the complex chemistry that results in neurofibrillary tangles and Aβ plaque formation. Finally, efforts are also underway to determine the mechanism of neurotoxicity resulting from these species, Aβ peptides in particular, as they form and accumulates in the brain.[59]

Neurofibrillary tangles are abnormal groups of twisted protein threads that are located inside neurons.[60] The main component of the tangles is a protein called *tau*, which, in normal neurons, connects long structures called microtubes. These microtubes normally run the entire length of the neuron and serve the function of providing a route of nourishment delivery to the cell. In AD, however, *tau* becomes highly phosphorylated and the connections between it and the microtubes are disrupted. As a consequence, *tau* coagulates in the neurons, forming tangles, and the unbound microtubes begin to decompose. No longer capable of receiving adequate quantities of nutrients, the neuron eventually dies and communications to and from it and other neurons are disrupted. As more neurons continue to die in a particular area, function is lost and atrophy of that portion of the brain occurs.

In addition to the nerve damage that is indirectly caused by the phosphorylation of *tau*, postmortem analyses of AD brains consistently reveal the presence of insoluble deposits of Aβ peptides, which contain from 39 to 43 amino acid residues.[61] Aβ peptides are proteolytically derived from the larger transmembrane amyloid precursor glycoprotein (APP), the function of which is not yet fully known.[62] While the major form of Aβ peptide in the cerebrospinal fluid is Aβ(1-40), containing 40 amino acid

residues, the insoluble "senile" plaques found deposited on and between the neurons of an AD brain primarily consist of Aβ(1-42).[63] In the case of FAD, it is now known that the characteristic genetic mutations associated with that form of the disease result in a significant increase in the production of Aβ(1-42).[64] In addition to contributing to plaque formations, Aβ(1-42) peptide is also known to be neurotoxic in neuronal cultures at μM concentrations, generating reactive oxygen species (ROS) in the presence of copper ions, the concentration of which are also elevated in AD.[65]

Because of their high prevalence in AD brain tissues, the Aβ plaques themselves were originally presumed to be the primary source of neuronal damage. This notion has been increasingly challenged over the years, however, and theories about the deleterious effects of plaques in AD have evolved significantly. Based on a preponderance of evidence, it is now more widely accepted that the neurotoxicity associated with Aβ likely results from soluble oligomers of the Aβ peptide that cluster in the early stages of the disease before plaques begin to form.[66] Consequently, it has also been proposed that the process of plaque formation may, in fact, be a late-stage defense mechanism by the body aimed at segregating these harmful soluble forms of Aβ from intact neurons.[67] These remain areas of active research.

There are many interesting facets of AD pathology, of which only a few have briefly been mentioned here. The Aβ peptide chemistry, in particular, has attracted our attention because of the participation of copper ions in its neurotoxicity. Since copper(II) complexes are not capable of directly promoting ROS generation, *vide infra*, the copper must first be reduced to copper(I) for such reactivity to occur. Presently, the identity of the reducing agent that promotes this process remains unclear, but several hypotheses

have been reported with respect to this problem.[68, 69] One prevalent hypothesis suggests that the copper reduction and oxidative stress associated with Aβ neurotoxicity results from the one-electron oxidation of the unique methionine residue (Met-35) in Aβ(1-42).[70-72]

1.3.1 Proposed Role of Methionine in Amyloid-β Neurotoxicity

The solution structure of Aβ(1-42), the principal form of Aβ found in insoluble plaques of AD brains, is shown in Figure 1-11.[73] Aβ(1-42) is known to bind copper(II) with a high affinity through all three of its His residues (His-6, His-13, and His-14),
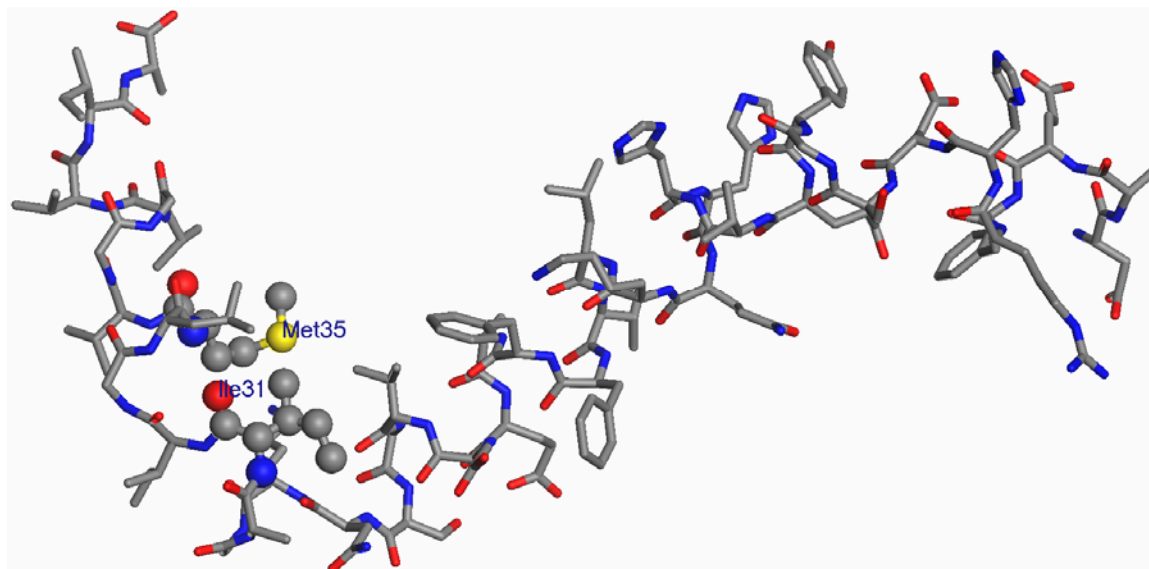
DAEFR⁵HDSGY¹⁰EVHHQ¹⁵KLVFF²⁰AEDVG²⁵SNKGA³⁰IIGLM³⁵VGGVV⁴⁰IA

Figure 1-11. *Representation of the solution structure of Aβ(1-42). Met-35 and Ile-31 are labeled and displayed as CPK spheres.*

located toward the N-terminus of the peptide.[74] The copper(II) binding site closely resembles that of CuZn superoxide dismutase (CuZn-SOD), an enzyme that, incidentally, catalyzes the conversion of superoxide anion radicals ($O_2^{\cdot-}$) to hydrogen peroxide (H_2O_2).[74, 75]

Reduction of the Aβ(1-42)-bound copper(II) ion has been directly linked to its neurotoxicity, where the resulting Aβ(1-42)-copper(I) species promotes Fenton chemistry, generating ROS in the oxygen-rich environment of the brain (reactions 1 – 4).[68, 75] Notably, both Aβ neurotoxicity and its ability to reduce copper(II) are dependent on the simultaneous presence of its three His residues and Met-35. While the full length peptide readily reduces copper(II), experiments have shown that neither the C-terminus truncated Aβ(1-28) peptide nor N-terminus truncated Aβ(25-35) peptide are capable of reducing copper(II). Additionally, substitution of Met-35 in the full length Aβ(1-42) peptide with either methionine sulfoxide (MetO) or norleucine (Nle) also renders the peptide redox inactive and the Aβ(1-42)-copper(II) adduct is stable.[70] These observations strongly support the possible role of the Met-35 sulfur as the copper(II) reductant, suggesting that it is also oxidized to a radical cation in the mechanism (reaction 5).[70, 72, 76]

$$O_2 + Cu^{I} \rightarrow Cu^{II} + O_2^{\cdot-} \tag{1}$$

$$O_2^{\cdot-} + O_2^{\cdot-} + 2\ H^{+} \rightarrow H_2O_2 \tag{2}$$

$$O_2^{\cdot-} + Cu^{II} \rightarrow O_2 + Cu^{I} \tag{3}$$

$$H_2O_2 + Cu^{I} \rightarrow {\cdot}OH + Cu^{II} + OH^{-} \tag{4}$$

$$(A\beta)Met(S) + Cu^{II} \rightarrow (A\beta)Met(S^{+\cdot}) + Cu^{I} \tag{5}$$
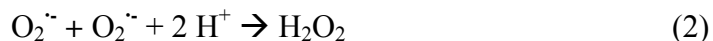
The reduction potentials for copper and Met(S), or more generally thioethers, however, are not conducive for a thermodynamically spontaneous redox reaction between these species.[77, 78] The Met(S$^{+\bullet}$)/Met(S) redox potential is between 1.2 to 1.5 V vs. Ag/AgCl,[77] and typical copper(II)/copper(I) redox potentials range from -0.6 to 0.6 V vs. Ag/AgCl, depending on solvent and ligand identity.[79] While the reduction potential of copper(II) in Aβ(1-42) (~0.5 V vs. Ag/AgCl)[68] is higher than it is in most other copper complexes, it is still too low to oxidize Met sulfur under normal circumstances. In order for spontaneous reduction of copper(II) to occur by the oxidation of the Met-35 thioether sulfur, as proposed, the oxidation potential of the Met sulfur must be decreased to a value near or below the reduction potential of the bound copper(II) ion.

In the same way that the copper redox potential is modulated by its ligand environment, the fact that the Met-35 sulfur is very closely oriented to the Ile-31 backbone carbonyl oxygen (~3.5 Å) in the Aβ(1-42) peptide (see figure 1-11) has led to a provocative proposal that its redox potential may be sufficiently modulated, allowing a thermodynamically favorable pathway for its unusually facile oxidation by copper(II).[80] In fact, thermochemical and theoretical studies have both revealed that the reduction potential of sulfides can be significantly modulated in two-center three-electron, so-called $\sigma\sigma^*$, interactions between the sulfur cation radical and an electronegative partner such as an amide carbonyl oxygen.[72, 77, 81] Aside from this proposal and the results of the Aβ(1-42) peptide reactivity studies, however, no examples of spontaneous methylthioether oxidation by copper(II) have been reported in the synthetic literature. Nonetheless, there is no doubt that copper(II) is reduced by Aβ(1-42) and that no reduction occurs without the Met-35 residue.

Chapter 4 of this thesis describes the synthesis and copper chemistry of a new family of ligands based on 2-Methyl-2-(2-pyridinyl)-1,3-propanediamine.[82] Preliminary experiments suggest that one of these ligands promotes the spontaneous reduction of bound copper(II) by its amide-activated methylthioether sulfur. The implication of this unprecedented reactivity on the proposed Met induced neurotoxicity of the Aβ(1-42) peptide is also addressed.

References

1. (a) Messerschmidt, A., *Handbook of Metalloproteins*. Wiley: Chichester ; New York, 2001. (b) Holm, R. H.; Kennepohl, P.; Solomon, E. I. *Chem. Rev.* **1996**, *96*, 2239-2314. (c) Cowan, J. A., *Inorganic Biochemistry : An Introduction*. 2nd ed.; Wiley-VCH: New York, 1997; p xiv, 440 p.

2. Solomon, E. I.; Szilagyi, R. K.; DeBeer George, S.; Basumallick, L. *Chem. Rev.* **2004**, *104*, 419-458.

3. (a) Gray, H. B.; Malmstrom, B. G.; Williams, R. J. P. *J. Biol. Inorg. Chem.* **2000**, *5*, 551-559. (b) Solomon, E. I.; Randall, D. W.; Glaser, T. *Coord. Chem. Rev.* **2000**, *200*, 595-632. (c) Kroneck, P. M. H., Binuclear copper A. In *Handbook of Metalloproteins*, Messerschmidt, A., Ed. John Wiley & Sons Ltd.: Chichester, UK, 2001; Vol. 2, pp 1333-1341.

4. Magnus, K. A., Hemocyanins from Arthropods and Molluscs. In *Handbook of Metalloproteins*, Messerschmidt, A., Ed. John Wiley & Sons Ltd.: Chichester, UK, 2001; Vol. 2, pp 1303-1318.

5. Suzuki, S.; Kataoka, K.; Yamaguchi, K. *Acc. Chem. Res.* **2000**, *33*, 728-735.

6. (a) Eicken, C.; Gerdemann, C.; Krebs, B., Catechol Oxidase. In *Handbook of Metalloproteins*, Messerschmidt, A., Ed. Wiley & Sons Ltd.: Chichester, UK, 2001; Vol. 2, pp 1319-1329. (b) Kannt, A.; Michel, H., Bacterial Cytochrome c Oxidase. In *Handbook of Metalloproteins*, Messerschmidt, A., Ed. John Wiley & Sons Ltd.: Chichester, UK, 2001; Vol. 1, pp 348-362.

7. (a) Massaro, E. J., *Handbook of Copper Pharmacology and Toxicology*. Humana Press: Totowa, N.J., 2002; p xvi, 608 p. (b) Fatemi, N.; Sarkar, B. *Inorg. Chim.*

Acta **2002**, *339*, 179-187. (c) Aoki, T. *Biomed. Res. Trace Elem.* **2004**, *15*, 307-315. (d) Brewer, G. J. *Curr. Op. Chem. Biol.* **2003**, *7*, 207-212.

8. (a) Valko, M.; Morris, H.; Cronin, M. T. D. *Curr. Med. Chem.* **2005**, *12*, 1161-1208. (b) Bush, A. I.; Masters, C. L.; Tanzi, R. E. *Proc. Natl. Acad. Sci. U.S.A.* **2003**, *100*, 11193-11194.

9. Greenwood, N. N.; Earnshaw, A., Copper, Silver and Gold. In *Chemistry of the Elements*, 2nd ed.; Butterworth-Heinemann: Oxford ; Boston, 1997; pp 1173-1199.

10. Jahn, H. A.; Teller, E. *Proc. R. Soc. London A* **1937**, *161*, 220-235.

11. Greenwood, N. N.; Earnshaw, A., Nitrogen. In *Chemistry of the Elements*, 2nd ed.; Butterworth-Heinemann: Oxford ; Boston, 1997; pp 406-472.

12. Rudolf, M.; Kroneck, P. M. H. *Met. Ions Biol. Sys.* **2004**, *43*, 75-103.

13. Postgate, J. R., *Nitrogen fixation*. 3rd ed.; Cambridge University Press: Cambridge, U.K. ; New York, NY, USA, 1998; p vi, 112 p.

14. Wray, J. L.; Kinghorn, J. R., *Molecular and Genetic Aspects of Nitrate Assimilation*. Oxford University Press: Oxford, 1989; p xv, 410 p.

15. Richardson, D. J.; Watmough, N. J. *Curr. Op. Chem. Biol.* **1999**, *3*, 207-219.

16. Travis, T. *Chem. Indust.* **1993**, 581-585.

17. (a) Kaiser, J. *Science* **2001**, *294*, 1268-1269. (b) Smil, V. *Sci. Am.* **1997**, *7*, 58-63.

18. Eady, R. R.; Hasnain, S. S. *Comp. Coord. Chem. II* **2004**, *8*, 759-786.

19. Zumft, W. G. *Microbiol. Mol. Biol. Rev.* **1997**, *61*, 533-616.

20. Hille, R. *Chem. Rev.* **1996**, *96*, 2757-2816.

21.   (a) Fulop, V.; Moir, J. W. B.; Ferguson, S. J.; Hajdu, J. *Cell* **1995**, *81*, 369-377. (b) Nurizzo, D.; Silvestrini, M. C.; Mathieu, M.; Cutruzzola, F.; Bourgeois, D.; Fulop, V.; Hajdu, J.; Brunori, M.; Tegoni, M.; Cambillau, C. *Structure* **1997**, *5*, 1157-1171. (c) Baker, S. C.; Saunders, N. F. W.; Willis, A. C.; Ferguson, S. J.; Hajdu, J.; Fulop, V. *J. Molec. Biol.* **1997**, *271*, 294-295.

22.   Adman, E. T.; Murphy, M. E. P., Copper Nitrite Reductase. In *Handbook of Metalloproteins*, Wiley: Chichester ; New York, 2001; Vol. 2, pp 1381-1390.

23.   Sakurai, N.; Sakurai, T. *Biochemistry* **1997**, *36*, 13809-13815.

24.   Averill, B. A. *Chem. Rev.* **1996**, *96*, 2951-2964.

25.   (a) Tsukihara, T.; Aoyama, H.; Yamashita, E.; Tomizaki, T.; Yamaguchi, H.; Shinzawaitoh, K.; Nakashima, R.; Yaono, R.; Yoshikawa, S. *Science* **1995**, *269*, 1069-1074. (b) Iwata, S.; Ostermeier, C.; Ludwig, B.; Michel, H. *Nature* **1995**, *376*, 660-669.

26.   Adman, E. T.; Godden, J. W.; Turley, S. *J. Biol. Chem.* **1995**, *270*, 27458-27474.

27.   Godden, J. W.; Turley, S.; Teller, D. C.; Adman, E. T.; Liu, M. Y.; Payne, W. J.; Legall, J. *Science* **1991**, *253*, 438-442.

28.   Antonyuk, S. V.; Strange, R. W.; Sawers, G.; Eady, R. R.; Hasnain, S. S. *PNAS* **2005**, *102*, 12041-12046.

29.   (a) Kukimoto, M.; Nishiyama, M.; Murphy, M. E.; Turley, S.; Adman, E. T.; Horinouchi, S.; Beppu, T. *Biochemistry* **1994**, *33*, 5246-5252. (b) Murphy, M. E. P.; Turley, S.; Kukimoto, M.; Nishiyama, M.; Horinouchi, S.; Sasaki, H.; Tanokura, M.; Adman, E. T. *Biochemistry* **1995**, *34*, 12107-12117.

30.   Murphy, M. E.; Turley, S.; Adman, E. T. *J. Biol. Chem.* **1997**, *272*, 28455-28460.

31. (a) Dodd, F. E.; Hasnain, S. S.; Abraham, Z. H.; Eady, R. R.; Smith, B. E. *Acta Cryst. Sec. D. Biol. Cryst.* **1997**, *53*, 406-418. (b) Dodd, F. E.; Van Beeumen, J.; Eady, R. R.; Hasnain, S. S. *J. Mol. Biol.* **1998**, *282*, 369-382. (c) Inoue, T.; Gotowda, M.; Deligeer; Kataoka, K.; Yamaguchi, K.; Suzuki, S.; Watanabe, H.; Gohow, M.; Kai, Y. *J. Biochem.* **1998**, *124*, 876-879.

32. (a) Suzuki, S.; Deligeer; Yamaguchi, K.; Kataoka, K.; Kobayashi, K.; Tagawa, S.; Kohzuma, T.; Shidara, S.; Iwasaki, H. *J. Biol. Inorg. Chem.* **1997**, *2*, 265-274. (b) Farver, O.; Eady, R. R.; Abraham, Z. H.; Pecht, I. *FEBS Lett.* **1998**, *436*, 239-242. (c) Hough, M. A.; Ellis, M. J.; Antonyuk, S.; Strange, R. W.; Sawers, G.; Eady, R. R.; Hasnain, S. S. *J. Mol. Biol.* **2005**, *350*, 300-309. (d) Kataoka, K.; Yamaguchi, K.; Sakai, S.; Takagi, K.; Suzuki, S. *Biochem. Biophys. Res. Comm.* **2003**, *303*, 519-524. (e) Suzuki, S.; Kohzuma, T.; Deligeer; Yamaguchi, K.; Nakamura, N.; Shidara, S.; Kobayashi, K.; Tagawa, S. *J. Am. Chem. Soc.* **1994**, *116*, 11145-11146. (f) Suzuki, S.; Maetani, T.; Yamaguchi, K.; Kobayashi, K.; Tagawa, S. *Chem. Lett.* **2005**, *34*, 36-37. (g) Yamaguchi, K.; Kataoka, K.; Kobayashi, M.; Itoh, K.; Fukui, A.; Suzuki, S. *Biochemistry* **2004**, *43*, 14180-14188.

33. Hulse, C. L.; Averill, B. A.; Tiedje, J. M. *J. Am. Chem. Soc.* **1989**, *111*, 2322-2323.

34. (a) Olesen, K.; Veselov, A.; Zhao, Y. W.; Wang, Y. S.; Danner, B.; Scholes, C. P.; Shapleigh, J. P. *Biochemistry* **1998**, *37*, 6086-6094. (b) Strange, R. W.; Murphy, L. M.; Dodd, F. E.; Abraham, Z. H. L.; Eady, R. R.; Smith, B. E.; Hasnain, S. S. *J. Mol. Biol.* **1999**, *287*, 1001-1009. (c) Veselov, A.; Olesen, K.;

Sienkiewicz, A.; Shapleigh, J. P.; Scholes, C. P. *Biochemistry* **1998**, *37*, 6095-6105.

35. Tocheva, E. I.; Rosell, F. I.; Mauk, A. G.; Murphy, M. E. P. *Science* **2004**, *304*, 867-870.

36. (a) Holland, P. L.; Tolman, W. B. *J. Am. Chem. Soc.* **2000**, *122*, 6331-6332. (b) Kim, Y. J.; Kim, S. O.; Kim, Y. I.; Choi, S. N. *Inorg. Chem.* **2001**, *40*, 4481-4484.

37. (a) Wasbotten, I. H.; Ghosh, A. *J. Am. Chem. Soc.* **2005**, *127*, 15384-15385. (b) Yokoyama, H.; Yamaguchi, K.; Sugimoto, M.; Suzuki, S. *Eur. J. Inorg. Chem.* **2005**, 1435-1441. (c) Scarpellini, M.; Neves, A.; Castellano, E. E.; Neves, E. F. D.; Franco, D. W. *Polyhedron* **2004**, *23*, 511-518. (d) Beretta, M.; Bouwman, E.; Casella, L.; Douziech, B.; Driessen, W. L.; Gutierrez-Soto, L.; Monzani, E.; Reedijk, J. *Inorg. Chim. Acta* **2000**, *310*, 41-50. (e) Casella, L.; Carugo, O.; Gullotti, M.; Doldi, S.; Frassoni, M. *Inorg. Chem.* **1996**, *35*, 1101-1113.

38. Tolman, W. B. *Inorg. Chem.* **1991**, *30*, 4877-4880.

39. Halfen, J. A.; Tolman, W. B. *J. Am. Chem. Soc.* **1994**, *116*, 5475-5476.

40. (a) Ruggiero, C. E.; Carrier, S. M.; Antholine, W. E.; Whittaker, J. W.; Cramer, C. J.; Tolman, W. B. *J. Am. Chem. Soc.* **1993**, *115*, 11285-11298. (b) Carrier, S. M.; Ruggiero, C. E.; Tolman, W. B.; Jameson, G. B. *J. Am. Chem. Soc.* **1992**, *114*, 4407-4408.

41. Halfen, J. A.; Mahapatra, S.; Olmstead, M. M.; Tolman, W. B. *J. Am. Chem. Soc.* **1994**, *116*, 2173-2174.

42. (a) Burg, A.; Lozinsky, E.; Cohen, H.; Meyerstein, D. *Eur. J. Inorg. Chem.* **2004**, 3675-3680. (b) Halfen, J. A.; Mahapatra, S.; Wilkinson, E. C.; Gengenbach, A.

J.; Young, V. G.; Que, L.; Tolman, W. B. *J. Am. Chem. Soc.* **1996**, *118*, 763-776. (c) Paul, P. P.; Karlin, K. D. *J. Am. Chem. Soc.* **1991**, *113*, 6331-6332.

43.   Lee, W. Z.; Tolman, W. B. *Inorg. Chem.* **2002**, *41*, 5656-5658.

44.   (a) Godwin, J. B.; Meyer, T. J. *Inorg. Chem.* **1971**, *10*, 2150-2153. (b) Rhodes, M. R.; Barley, M. H.; Meyer, T. J. *Inorg. Chem.* **1991**, *30*, 629-635. (c) Zang, V.; Vaneldik, R. *Inorg. Chem.* **1990**, *29*, 4462-4468. (d) Lancon, D.; Kadish, K. M. *J. Am. Chem. Soc.* **1983**, *105*, 5610-5617. (e) Barley, M. H.; Takeuchi, K. J.; Meyer, T. J. *J. Am. Chem. Soc.* **1986**, *108*, 5876-5885. (f) Barley, M. H.; Rhodes, M. R.; Meyer, T. J. *Inorg. Chem.* **1987**, *26*, 1746-1750. (g) Choi, I. K.; Liu, Y. M.; Feng, D.; Paeng, K. J.; Ryan, M. D. *Inorg. Chem.* **1991**, *30*, 1832-1839. (h) Finnegan, M. G.; Lappin, A. G.; Scheidt, W. R. *Inorg. Chem.* **1990**, *29*, 181-185. (i) Nasri, H.; Goodwin, J. A.; Scheidt, W. R. *Inorg. Chem.* **1990**, *29*, 185-191. (j) Nasri, H.; Wang, Y.; Huynh, B. H.; Scheidt, W. R. *J. Am. Chem. Soc.* **1991**, *113*, 717-719. (k) Nasri, H.; Wang, Y. N.; Huynh, B. H.; Walker, F. A.; Scheidt, W. R. *Inorg. Chem.* **1991**, *30*, 1483-1489.

45.   (a) Kitajima, N.; Fujisawa, K.; Morooka, Y.; Toriumi, K. *J. Am. Chem. Soc.* **1989**, *111*, 8975-8976. (b) Kitajima, N.; Koda, T.; Iwata, Y.; Morooka, Y. *J. Am. Chem. Soc.* **1990**, *112*, 8833-8839. (c) Kitajima, N.; Fujisawa, K.; Morooka, Y. *J. Am. Chem. Soc.* **1990**, *112*, 3210-3212. (d) Kitajima, N.; Fujisawa, K.; Morooka, Y. *Inorg. Chem.* **1990**, *29*, 357-358.

46.   Trofimenko, S.; Calabrese, J. C.; Thompson, J. S. *Inorg. Chem.* **1987**, *26*, 1507-1514.

47.   Haselhorst, G.; Stoetzel, S.; Strassburger, A.; Walz, W.; Wieghardt, K.; Nuber, B. *Dalt. Trans.* **1993**, 83-90.

48.   (a) Johnson, B. F. G.; Sieker, A.; Blake, A. J.; Winpenny, R. E. P. *Chem. Comm.* **1993**, 1345-1346. (b) Thewalt, U.; Marsh, R. E. *Inorg. Chem.* **1970**, *9*, 1604-1610. (c) Goodgame, D. M.; Hitchman, M. A.; Marsham, D. F.; Phavanan.P; Rogers, D. *Chem. Comm.* **1969**, 1383-1384.

49.   Holland, P. L.; Tolman, W. B. *J. Am. Chem. Soc.* **1999**, *121*, 7270-7271.

50.   Caughey, B.; Lansbury, P. T. *Annu. Rev. Neurosci.* **2003**, *26*, 267-298.

51.   Larson, E. B.; Shadlen, M. F.; Wang, L.; McCormick, W. C.; Bowen, J. D.; Teri, L.; Kukull, W. A. *Ann. Int. Med.* **2004**, *140*, 501-509.

52.   Kalia, M. *Metabolism* **2003**, *52*, 36-38.

53.   Herbert, L. E.; Scherr, P. A.; Bienias, J. L.; Bennett, D. A. *Arch. Neuro.* **2003**, *60*, 1119-1122.

54.   Suh, W. H.; Suslick, K. S.; Suh, Y.-H. *Curr. Med. Chem.* **2005**, *5*, 259-269.

55.   (a) Rademakers, R.; Cruts, M.; Van Broeckhoven, C. *Sci. World* **2003**, *3*, 497-519. (b) Lippa, C. F. *Int. J. Molec. Med.* **1999**, *4*, 529-536.

56.   Kamboh, M. I. *Ann. Hum. Genet.* **2004**, *68*, 381-404.

57.   Bertram, L.; Tanzi, R. E. *J. Mol. Neurosci.* **2001**, *17*, 127-136.

58.   (a) Uemura, K.; Kuzuya, A.; Shimohama, S. *Curr. Alz. Res.* **2004**, *1*, 1-10. (b) Stege, G. J.; Bosman, G. J. *Drugs Aging* **1999**, *14*, 437-446.

59.   (a) Roy, S.; Rauk, A. *Med. Hypotheses* **2005**, *65*, 123-137. (b) Lahiri, D. K.; Greig, N. H. *Neurobiol. Aging* **2004**, *25*, 581-587. (c) Bishop, G. M.; Robinson, S. R. *Drugs Aging* **2004**, *21*, 621-630.

60.   Gamblin, T. C.; Chen, F.; Zambrano, A.; Abraha, A.; Lagalwar, S.; Guillozet, A. L.; Lu, M.; Fu, Y.; Garcia-Sierra, F.; LaPointe, N.; Miller, R.; Berry, R. W.; Binder, L. I.; Cryns, V. L. *Proc. Natl. Acad. Sci. U.S.A.* **2003**, *100*, 10032-10037.

61.   (a) Delacourte, A. *Ann. Biol. Clin.* **1998**, *56*, 133-142. (b) Wengenack, T. M.; Curran, G. L.; Poduslo, J. F. *Nat. Biotechnol.* **2000**, *18*, 868-872.

62.   Mattson, M. P. *Physiol. Rev.* **1997**, *77*, 1081-1132.

63.   (a) Haass, C.; Schlossmacher, M. G.; Hung, A. Y.; Vigo-Pelfrey, C.; Mellon, A.; Ostaszewski, B. L.; Lieberburg, I.; Koo, E. H.; Schenk, D.; Teplow, D. B.; et al. *Nature* **1992**, *359*, 322-325. (b) Seubert, P.; Vigo-Pelfrey, C.; Esch, F.; Lee, M.; Dovey, H.; Davis, D.; Sinha, S.; Schlossmacher, M.; Whaley, J.; Swindlehurst, C.; et al. *Nature* **1992**, *359*, 325-327.

64.   Butterfield, D. A.; Boyd-Kimball, D. *Brain Pathol.* **2004**, *14*, 426-432.

65.   Yankner, B. A.; Duffy, L. K.; Kirschner, D. A. *Science* **1990**, *250*, 279-282.

66.   Cleary, J. P.; Walsh, D. M.; Hofmeister, J. J.; Shankar, G. M.; Kuskowski, M. A.; Selkoe, D. J.; Ashe, K. H. *Nat. Neurosci.* **2005**, *8*, 79-84.

67.   Stein, T. D.; Anders, N. J.; DeCarli, C.; Chan, S. L.; Mattson, M. P.; Johnson, J. A. *J. Neurosci.* **2004**, *24*, 7707-7717.

68.   Huang, X.; Cuajungco, M. P.; Atwood, C. S.; Hartshorn, M. A.; Tyndall, J. D.; Hanson, G. R.; Stokes, K. C.; Leopold, M.; Multhaup, G.; Goldstein, L. E.; Scarpa, R. C.; Saunders, A. J.; Lim, J.; Moir, R. D.; Glabe, C.; Bowden, E. F.; Masters, C. L.; Fairlie, D. P.; Tanzi, R. E.; Bush, A. I. *J. Biol. Chem.* **1999**, *274*, 37111-37116.

69. (a) Huang, X.; Atwood, C. S.; Hartshorn, M. A.; Multhaup, G.; Goldstein, L. E.; Scarpa, R. C.; Cuajungco, M. P.; Gray, D. N.; Lim, J.; Moir, R. D.; Tanzi, R. E.; Bush, A. I. *Biochemistry* **1999**, *38*, 7609-7616. (b) Cuajungco, M. P.; Goldstein, L. E.; Nunomura, A.; Smith, M. A.; Lim, J. T.; Atwood, C. S.; Huang, X.; Farrag, Y. W.; Perry, G.; Bush, A. I. *J. Biol. Chem.* **2000**, *275*, 19439-19442.

70. Varadarajan, S.; Kanski, J.; Aksenova, M.; Lauderback, C.; Butterfield, D. A. *J. Am. Chem. Soc.* **2001**, *123*, 5625-5631.

71. Butterfield, D. A.; Boyd-Kimball, D. *Biochim. Biophys. Acta* **2005**, *1703*, 149-156.

72. Rauk, A.; Armstrong, D. A.; Fairlie, D. P. *J. Am. Chem. Soc.* **2000**, *122*, 9761-9767.

73. Crescenzi, O.; Tomaselli, S.; Guerrini, R.; Salvadori, S.; D'Ursi, A. M.; Temussi, P. A.; Picone, D. *Eur. J. Biochem.* **2002**, *269*, 5642-5648.

74. (a) Atwood, C. S.; Moir, R. D.; Huang, X. D.; Scarpa, R. C.; Bacarra, N. M. E.; Romano, D. M.; Hartshorn, M. K.; Tanzi, R. E.; Bush, A. I. *J. Biol. Chem.* **1998**, *273*, 12817-12826. (b) Atwood, C. S.; Scarpa, R. C.; Huang, X. D.; Moir, R. D.; Jones, W. D.; Fairlie, D. P.; Tanzi, R. E.; Bush, A. I. *J. Neurochem.* **2000**, *75*, 1219-1233.

75. Curtain, C. C.; Ali, F.; Volitakis, I.; Cherny, R. A.; Norton, R. S.; Beyreuther, K.; Barrow, C. J.; Masters, C. L.; Bush, A. I.; Barnham, K. J. *J. Biol. Chem.* **2001**, *276*, 20466-20473.

76. Schoneich, C.; Pogocki, D.; Hug, G. L.; Bobrowski, K. *J. Am. Chem. Soc.* **2003**, *125*, 13700-13713.

77.   Armstrong, D. A., In *S-Centered Radicals*, Alfassi, Z. B., Ed. Wiley: New York, 1999; pp 27-61.

78.   Glass, R. S., In *Topics In Current Chemistry*, Page, P. C. B., Ed. Springer-Verlag: Berlin Heidelberg, 1999; Vol. 205, pp 1-87.

79.   Karlin, K. D.; Gultney, Y., In *Prog. Inorg. Chem.*, Lippard, S. J., Ed. 1987; Vol. 35, pp 219-328.

80.   (a) Butterfield, D. A.; Bush, A. I. *Neurobiol. Aging* **2004**, *25*, 563-568.   (b) Kanski, J.; Aksenova, M.; Schoneich, C.; Butterfield, D. A. *Free Radic. Biol. Med.* **2002**, *32*, 1205-1211.   (c) Pogocki, D.; Schoneich, C. *Chem. Res. Toxicol.* **2002**, *15*, 408-418.

81.   Bobrowski, K.; Pogocki, D.; Schoneich, C. *J. Phys. Chem. A* **1998**, *102*, 10512-10521.

82.   Friedrich, S.; Schubart, M.; Gade, L. H.; Scowen, I. J.; Edwards, A. J.; McPartlin, M. *Chem. Ber./Recueil* **1997**, *130*, 1751-1759.

CHAPTER 2.

MODELLING THE COPPER NITRITE REDUCTASE ACTIVE SITE: TACN-AMINO ACID CONJUGATES AND THEIR COPPER(II) COMPLEXES

2.1. Introduction

Copper-containing nitrite reductase (CuNiR) is an enzyme found in many terrestrial and aquatic bacteria and fungi that catalyzes the one electron reduction of nitrite (NO_2^-) to nitric oxide (NO).[1] This conversion is essential to such organisms as a terminal electron acceptor in their metabolic processes and represents the first committed step in the denitrification pathway, whereby nitrate (NO_3^-) and nitrite are ultimately reduced to inorganic nitrogen.[2] The active site of CuNiR from *Alcaligenes faecalis* has been shown by X-ray crystallography to contain a type 1 copper center (Cu-I) separated by 12.5 Å from a type 2 copper center (Cu-II) (Figure 2-1).[3] Connecting the Cu-I electron transfer center to the Cu-II catalytic center is a conserved His-Cys bridge, where His and Cys are immediate neighbors in the protein's primary structure. A thiolate sulfur from the bridging Cys residue coordinates the Cu-I copper ion and is complimented by two His and a Met residue. Likewise, a nitrogen donor from the bridging His residue imidazole side chain occupies a coordination site at the Cu-II copper ion. Two additional His residues (one from a neighboring subunit) and a single substrate or aqua ligand
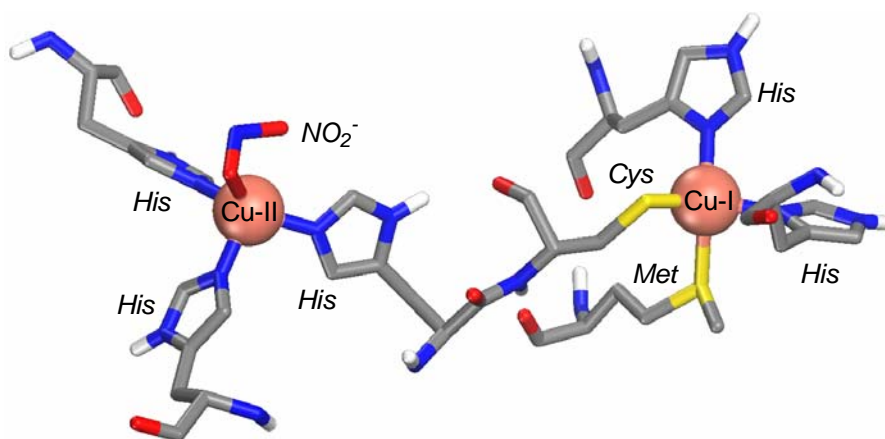
Figure 2-1. Representation of the NO_2^--bound CuNiR active site from *A. faecalis*.

complete the coordination sphere of the Cu-II copper.

Although the details of the CuNiR active site structure are now well understood, relatively little is known about the details of the enzyme's catalytic mechanism.[4, 5] Based on numerous structural[5, 6] and spectroscopic[7, 8] studies, however, it has become evident that an integral part of the mechanism involves an intramolecular electron transfer from Cu-I to Cu-II, presumably via the His-Cys bridge. This notion is particularly well supported by several site-directed mutagenesis[9] and pulse radiolysis[8, 10] experiments. Complementing these studies, several small molecule model complexes of proposed catalytic intermediates have also been prepared to help elucidate the likely coordination modes of copper(I)- and copper(II)-bound nitrite and nitric oxide and, by analogy, the specific reactivity of such intermediates in the enzyme.[11, 12] From these and other studies, it is generally accepted that the catalytic cycle proceeds by the reduction of an initial copper(II)-nitrite adduct to a short-lived copper(I)-nitrite species that rapidly reduces its
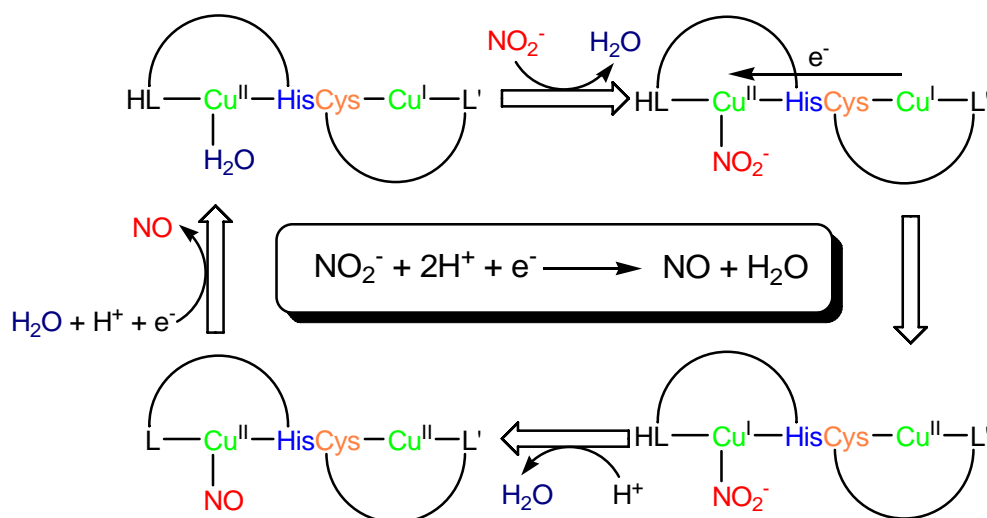
Figure 2-2. Schematic representation of the CuNiR catalytic cycle, emphasizing the important redox steps and key intermediates. L and L' represent the protein at Cu-II and Cu-I, respectively. The overall reaction is shown in the center.

bound nitrite to nitric oxide in the presence of protons. (Figure 2-2).

The CuNiR-related model complexes that had been reported at the inception of our work all used non-amino acid ligands to mimic various aspects of the ligand environment found in the enzyme and were almost all mononuclear. In an effort to develop next-generation models that could more accurately mimic the entire CuNiR active site structure and chemistry, we became interested in developing "ligand-peptide conjugates", where actual amino acids are coupled to traditional ligands (e.g. TACN). As a result of this effort, we hoped to eventually probe various aspects of the proposed catalytic cycle with greater accuracy. Specifically, we wished to gain a better understanding of the effect of nitrite binding at Cu-II on the subsequent electron transfer from Cu-I via the His-Cys bridge.

Section 2.2 of this chapter describes our initial synthetic strategy for synthesizing new ligands that contain a His-Cys bridge and our successes in coupling the normally tridentate ligand TACN with Gly, Ala, and Phe to afford ligand-amino acid conjugates. The synthesis and characterization of copper(II) complexes of these new ligands are discussed in section 2.3.

2.2.   *Ligands*

2.2.1. *General Ligand Design*

TACN was chosen as the supporting copper chelate in our synthetic strategy as a result of our previous experience with this ligand and its well precedented use by others in copper coordination and modeling chemistry.[12, 13] Ultimately, we envisioned the synthesis of a ligand containing two TACN moieties tethered to each end of a His-Cys peptide by linkers (Figure 2-3), where each TACN could accommodate a copper ion and
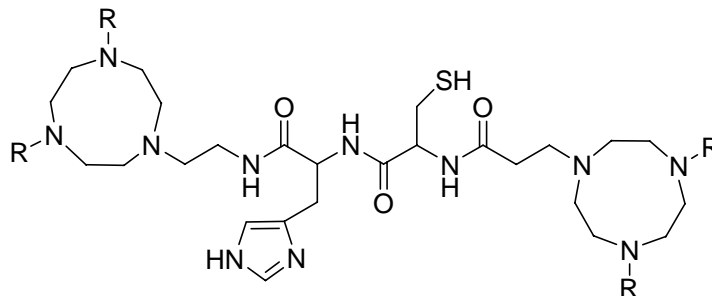
Figure 2-3. Ligand synthetic target containing two alkyl-protected TACN rings bridged by a His-Cys linker.

allow coordination of the His or Cys side chains to their nearest copper ion. Prior to this work, however, no copper complexes of TACN covalently coupled to any amino acid had been reported in the literature. To probe the synthetic feasibility of this approach and to gain an understanding of the effect(s) of covalently-bound amino acids on TACN-copper coordination, the ligand designs described in this chapter are primarily focused on the coupling of TACN by peptide bonds directly to simple amino acids (Gly, Ala, and Phe). The syntheses of these ligands and our preliminary attempts to synthesize a TACN-His ligand conjugate (i.e. the left half of the synthetic target in Figure 2-3) are described in the remainder of this section.

2.2.2.   (Boc)₂TACN Synthesis

In the first step of (Boc)$_2$TACN (**7**) synthesis, diethylenetriamine (**1**) and ethylene glycol (**2**) are reacted with *p*-toluenesulfonyl chloride (TsCl) to yield their N- and O-tosylated products, **3**[14] and **4**[15], respectively (Figure 2-4). **3** is then deprotonated at its terminal nitrogen atoms with sodium hydride (NaH) under an inert and dry atmosphere, thus greatly increasing the nucleophilicity. A DMF solution of **4** is slowly added to this mixture, resulting in the formation of the fully Ts-protected TACN (**5**) (Figure 2-5).[14]
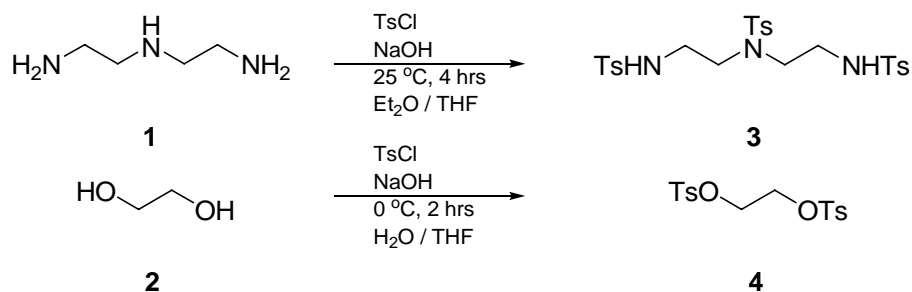
Figure 2-4. Tosylation of diethylenetriamine (**1**) and ethylene glycol (**2**) to yield N-and O-tosylated products, **3** and **4**, respectively.

Detosylation of **5** is achieved by high-temperature hydrolysis in concentrated sulfuric acid over three days to yield unprotected TACN (**6**) after basic workup.[14] Finally, in a method first described by A. Dean Sherry, *et al.*,[16] **6** is Boc-protected at two of its nitrogens by reaction with a two equivalents of BOC-ON,[17] giving **7** in high yield (Figure
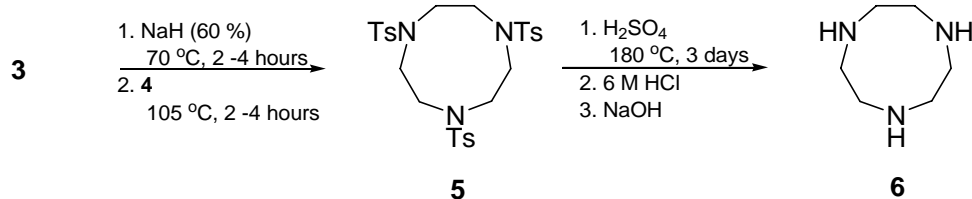
Figure 2-5. Reaction of **3** with **4** to yield Ts₃TACN (**5**), and detosylation of **5** in concentrated sulfuric acid to yield TACN (**6**).

2-6). Following alkylation of the unprotected nitrogen, the Boc protecting groups are easily removed by reaction with TFA, allowing successive alkylation at those positions.
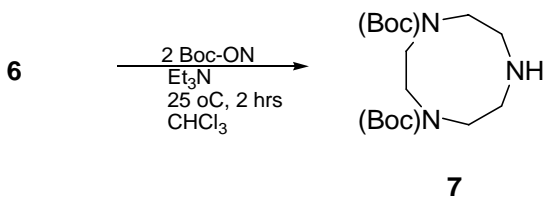
Figure 2-6. Synthesis of (Boc)₂TACN (**7**).

Because of the steric bulk of the His side chain and the consequently low reactivity of His with secondary amines (i.e. with **7** directly), we believed a linker with a primary amine would be required to couple His and TACN most efficiently. 1-(aminoethyl)-4,7-diisopropyl-TACN (**12**) was chosen for this purpose. The synthesis of **12** was first reported by Berreau, *et al*, by using the selective detosylated TACN method.[18] Figure 2-7 details our improved synthesis of **12** where Boc protecting groups
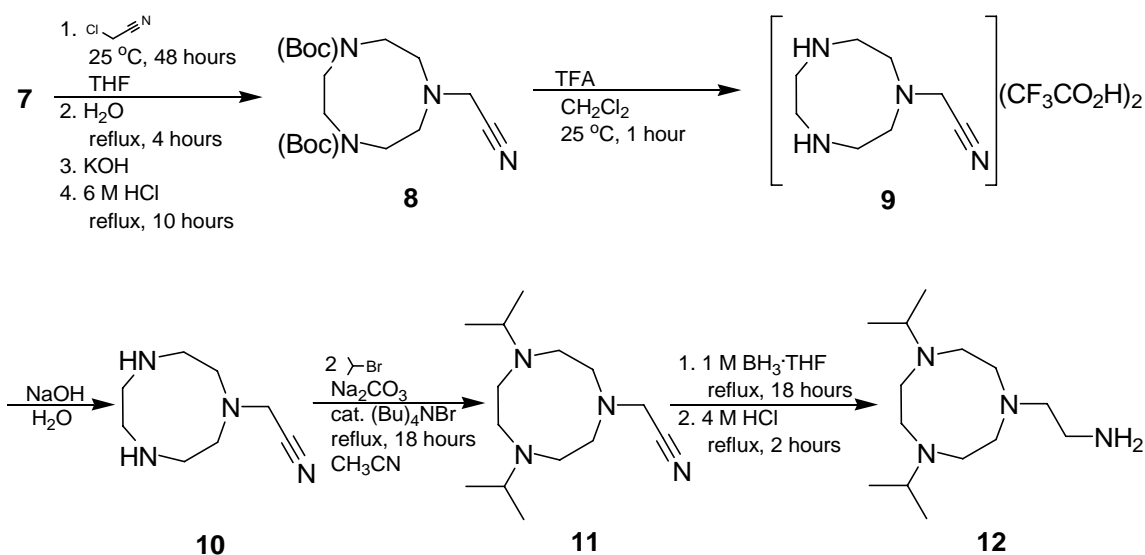
Figure 2-7. Synthesis of 1-(aminoethyl)-4,7-diisopropyl-TACN (**12**).

are employed rather than tosyl, requiring far milder conditions for deprotection. Compound **8** is obtained in high yield following reaction of **7** with a stoicheometric quantity of chloroacetonitrile. The Boc protecting groups are then removed in TFA at room temperature and **10** is isolated following basic workup and extraction. The resulting unprotected nitrogens are alkylated with isopropyl groups to give **11**. Finally, **12** is obtained by reduction of **11** in a 1.0 M borane/THF solution.

2.2.4.   *TACN-Histidine Conjugate (**L**^{His}) Synthesis and Characterization*

Standard peptide coupling techniques were applied to couple His to **12**.[19]   DCC

and HOBt hydrate were combined with a solution of **12** and Fmoc-His(Trt)-OH to afford

13 (Figure 2-8).   The low yield of this reaction (~5%) and loss of the Fmoc protecting
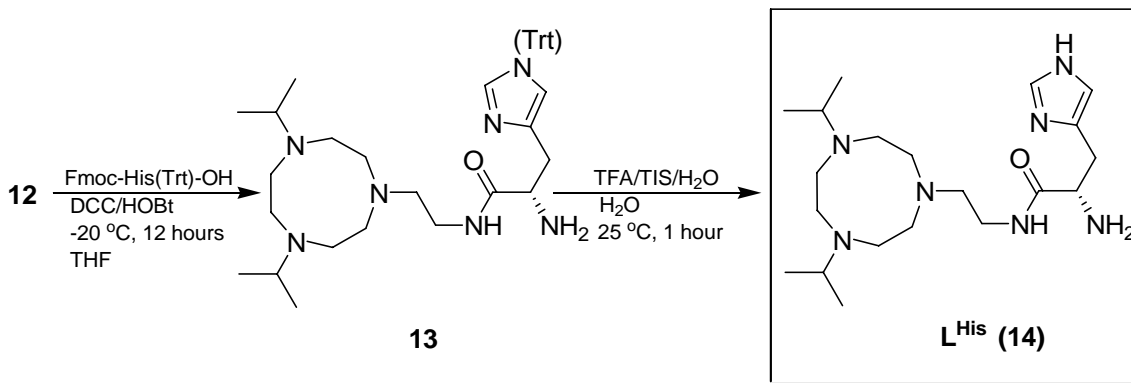
Figure 2-8. Synthesis of **L**^{His} (**14**).

group are both attributed to the complex workup necessitated by the difficulty of isolating

the desired product from dicyclohexylurea (DCU) byproduct and undesired side products.

Fmoc is cleaved from His upon basification of the reaction mixture with aqueous NaOH,

as evidenced by CO_2 gas evolution.[20]   The ^{1}H NMR spectrum of **13**, obtained in $CDCl_3$,

reveals characteristic Trt signals between 7.0 and 7.3 ppm, but shows no indication of

Fmoc.   **L**^{His} (**14**) was obtained in low yield (~5%) by direct addition of 95:5:5 %

TFA/TIS/H_2O to **13**.   The ^{1}H NMR spectrum of **14**, obtained in $CDCl_3$, clearly shows the

successful cleavage of Trt from the His imidazole side chain.   FTIR of **13** and **14** both

show a strong and sharp stretching frequency of ~1650 cm^{-1}, consistent with an amide

carbonyl.[21]

2.2.5. Glycine-, Alanine-, and Phenylalanine-TACN Conjugates

Because of the obvious synthetic difficulties, particularly the low yield, associated with the multistep synthesis of L^{His} as it was described above, we sought to investigate the possibility of coupling His directly to the secondary amine of **7**.[22] This, however, would require a better understanding of the effect that converting one of the TACN amine nitrogens to an amide would have on its ensuing ability to coordinate a copper(II) ion.[23] As a simple approach to eliminating synthetic problems with the steric bulk and/or reactivity of the His side chain in a direct reaction with **7**, Gly, Ala, and Phe were used in our initial attempts. The ligands L^{Gly} (**18**), L^{Ala} (**19**), and L^{Phe} (**20**) were synthesized by coupling the secondary amine nitrogen of **7** to the carboxylic acid of the Boc-protected amino acids, following Boc deprotection in TFA and purification (Figure 2-9).[24]
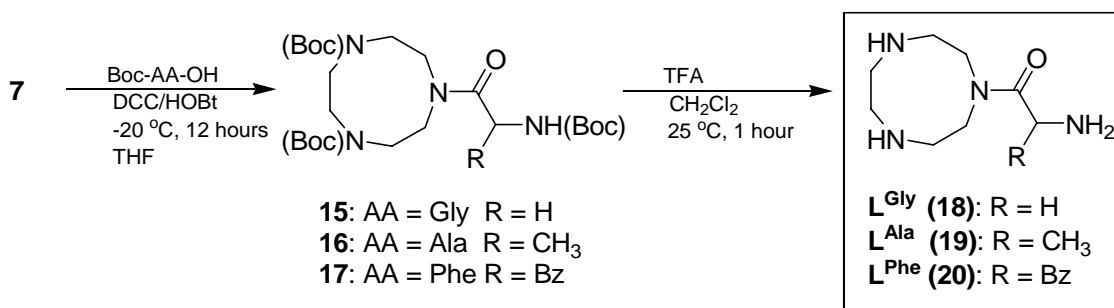
Figure 2-9. Synthesis of L^{Gly} (**18**), L^{Ala} (**19**), and L^{Phe} (**20**) from (Boc)2TACN (**7**).

2.3. Copper(II) Complexes

Copper(II) complexes of L^{Gly} (**18**), L^{Ala} (**19**), and L^{Phe} (**20**) were synthesized by reaction of the appropriate ligand with either $Cu(ClO_4)_2 \cdot 6H_2O$ or $CuCl_2 \cdot 2H_2O$ in

methanol. The specific reaction conditions, properties, and characterization of each complex are described in this section.

2.3.1. $[(CuL^{Gly})_2](ClO_4)_4$

Addition of a solution of **18** in methanol to a rapidly stirring solution of $Cu(ClO_4)_2 \cdot 6H_2O$ in the same solvent resulted in the immediate formation a blue solution (Figure 2-10). After stirring for some time, $[Cu(L^{Gly})]_2(ClO_4)_4$ (**21**) precipitated from the reaction mixture. This blue powder was filtered away from the reaction mixture and washed with fresh methanol. Despite repeated attempts, no X-ray quality crystals of **21** were obtained under any conditions. The dimeric structure and coordination mode of **21** as shown in Figure 2-10 was elucidated by analogy to the X-ray crystal structure obtained for **22** (see section 2.3.2.), as supported by Electrospray Ionization Mass Spectrometry (ESI-MS) and elemental analysis.
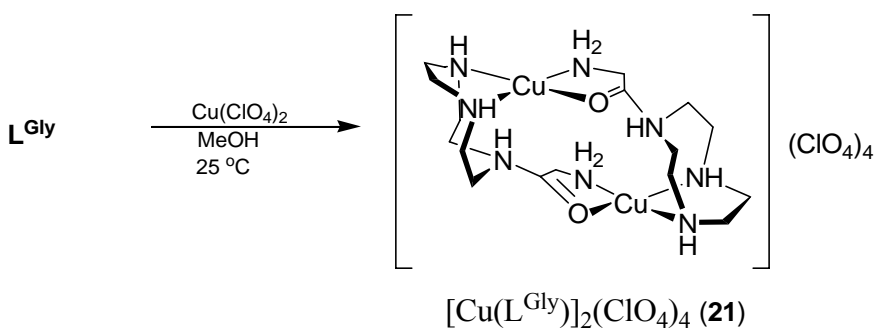
Figure 2-10. Synthesis of $[Cu(L^{Gly})]_2(ClO_4)_4$ (**21**).

The UV-vis spectrum of **21** (Figure 2-11) in acetonitrile exhibits a broad transition, or overlap of two transitions, at 589 nm with an extinction coefficient of 180 $M^{-1}cm^{-1}$. These parameters are typical for a copper(II) ion with nitrogen and oxygen donor atoms and are attributed predominantly to Ligand-to-Metal Charge Transfer transitions (LMCT) [N and/or O → Cu(II) d] mixed with less intense Cu(II) d-d transitions of lower energy.[25]
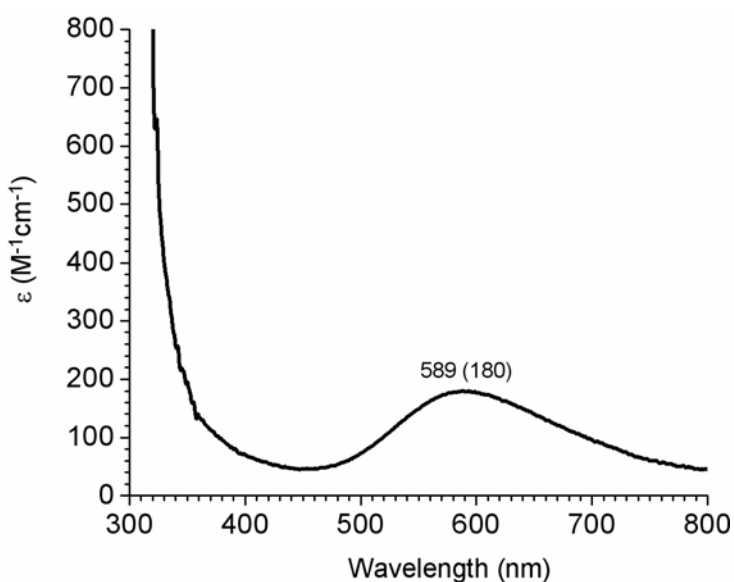
Figure 2-11. UV-vis spectrum of **21** dissolved in acetonitrile. Peak labels indicate the wavelength (nm) and extinction coefficient (ε) in parentheses ($M^{-1}cm^{-1}$).

ESI-MS strongly supports the dimeric structure assigned to **21**. The parent ion in the mass spectrum (Figure 2-12) at 797 *m/z* exactly matches the mass of **21** minus one perchlorate anion, $[M-ClO_4]^+$. A monomeric fragment of **21**, $[M-CuL^{Gly}-(ClO_4)_3]^+$, also appears in the mass spectrum at 348 *m/z*. The agreement of the experimental and calculated isotope patterns for these species further corroborate their assignments (Figure 2-12 inset).
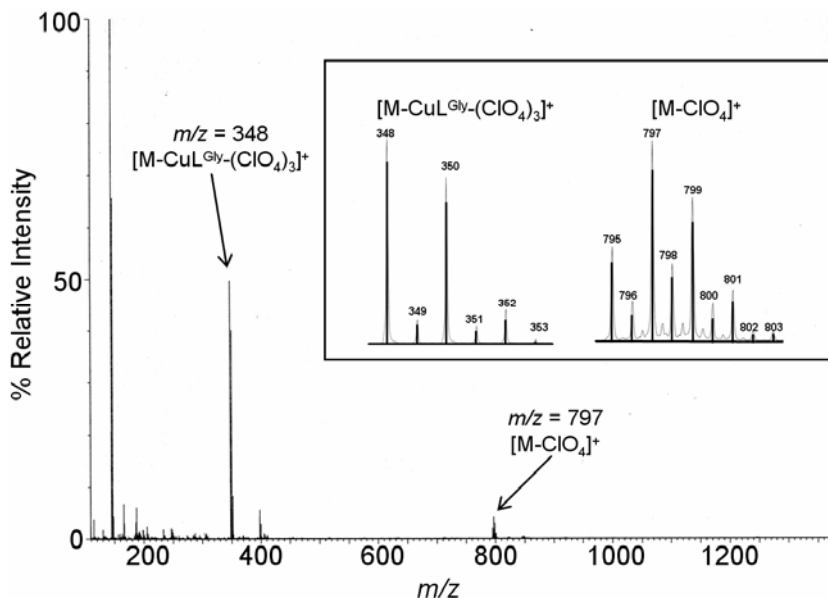
Figure 2-12. ESI-MS of **21** dissolved in acetonitrile. The inset shows expanded views of the dinuclear parent ion, $[M\text{-}ClO_4]^+$ ($m/z = 797$), and a mononuclear fragment, $[M\text{-}CuL^{Gly}\text{-}(ClO_4)_3]^+$ ($m/z = 348$). The overlaid solid black lines in the inset represent the calculated isotope patterns for each species.

2.3.2. $[(CuL^{Ala})_2Cl](ClO_4)_3$

$[(CuL^{Ala})_2Cl](ClO_4)_3$ (**22**) was synthesized and isolated in the same way as **21** (Figure 2-13). X-ray quality crystals of **22** were obtained by diffusing diethyl ether into a capped vial of the blue precipitate concentrated in methanol.
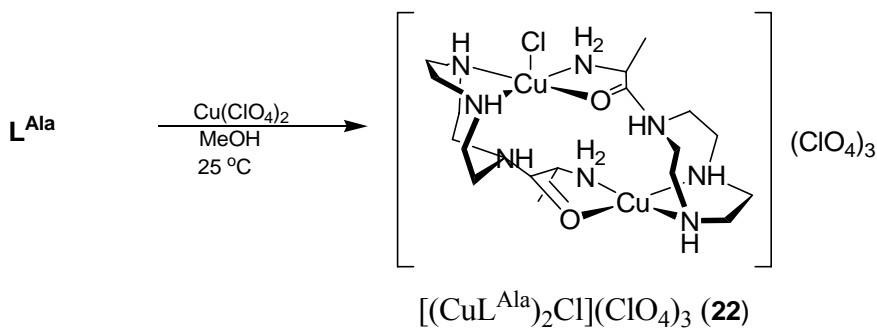
$[(CuL^{Ala})_2Cl](ClO_4)_3$ (**22**)

Figure 2-13. Synthesis of $[(CuL^{Ala})_2Cl](ClO_4)_3$ (**22**).

The crystal structure of **22** reveals a bimetallic complex, where two copper(II) ions are bridged by two $\mathbf{L^{Ala}}$ ligands, forming a 4^+ cation (Figure 2-14). The positive charge of this complex is balanced by one bridging chloride anion and three outer sphere perchlorate anions. The chloride links molecules of **22** in the crystal lattice by bridging between Cu1 from one dimer to Cu2 of an adjacent dimer. The TACN portion of the $\mathbf{L^{Ala}}$ ligand binds to Cu1 via two secondary amine nitrogens, but the amide nitrogen is not coordinated. The Cu1···N3 distance of 2.96 Å stands in contrast to the rare examples of copper complexes with coordinated tertiary amides (2.16 - 2.51 Å).[26] These amide-coordinated species are usually sensitive to C-N bond cleavage, while **22** is stable in methanol. The stability of the amide C-N bonds in **22** is most likely due to the fact that the metal is not coordinated by the amide nitrogen atom, but by the oxygen. The Ala portion of the ligand coordinates to the other copper atom, Cu2, by its terminal amine nitrogen and the carbonyl oxygen atom. This type of binding mode for amino acids is relatively common and has been reported for copper(II) amino acid species.[27] The second ligand in the bimetallic complex is related by a noncrystallographic pseudo-$C2$ axis to the first ligand; thus, two $\mathbf{L^{Ala}}$ ligands bridge between the copper atoms in **22**. The coordination geometry around each copper is closest to square pyramidal, with an N_3O ligand set in the equatorial plane and a chloride ligand in the axial position ($\tau = 0.16$ and 0.10 for Cu1 and Cu2, respectively).[28] The chloride anions bridge between bimetallic moieties [$\angle$Cu-Cl-Cu = 158.25(5)°] to create linear chains of molecules along the crystallographic b axis. The intra- and intermolecular Cu···Cu distances are long (> 4.9 Å), making any magnetic coupling between copper(II) ions unlikely, an assertion

corroborated by its axial EPR obtained in water/ethylene glycol glass at 77 K and a microwave frequency of 9.43 GHz ($g_\perp = 2.08$, $g_\parallel = 2.39$, $A^{Cu}_\parallel = 134 \times 10^{-4}$ cm^{-1}).
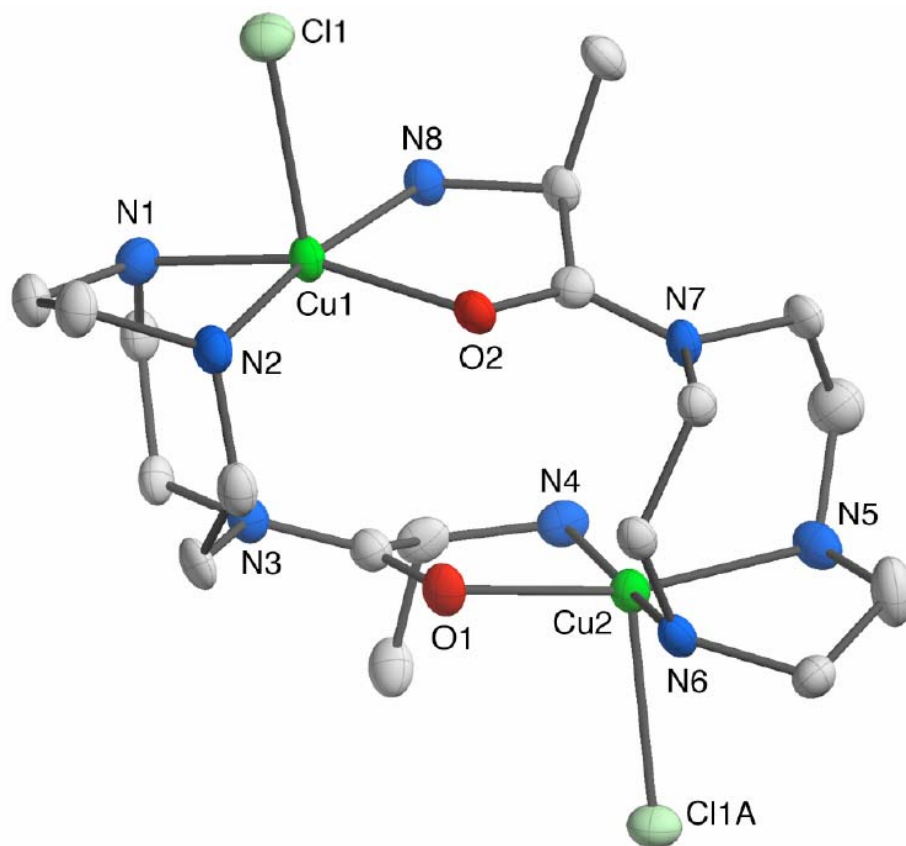
Bond Lengths (Å)		Angles (deg)			
Cu1–N1	2.031(3)	N1–Cu1–Cl1	100.1(2)	N4–Cu2–Cl1A	100.1(2)
Cu1–N2	1.999(3)	N2–Cu1–Cl1	94.5(1)	N5–Cu2–Cl1A	95.7(1)
Cu1–N8	2.057(3)	N8–Cu1–Cl1	90.3(1)	N6–Cu2–Cl1A	90.1(1)
Cu1–O2	1.998(3)	O2–Cu1–Cl1	104.6(1)	O1–Cu2–Cl1A	99.7(1)
Cu1–Cl1	2.508(1)	N1–Cu1–N2	85.5(1)	N5–Cu2–N4	99.4(1)
Cu2–N4	2.007(3)	N1–Cu1–N8	100.6(1)	N5–Cu2–N6	85.3(1)
Cu2–N5	2.025(3)	O2–Cu1–N2	90.5(1)	O1–Cu2–N4	82.3(1)
Cu2–N6	1.984(3)	O2–Cu1–N8	82.2(1)	O1–Cu2–N6	90.9(1)
Cu2–O1	1.999(3)	N1–Cu1–O2	162.5(1)	N5–Cu2–O1	164.2(1)
Cu2–Cl1A	2.526(1)	N2–Cu1–N8	172.1(1)	N4–Cu2–N6	170.2(1)

Figure 2-14. Representation of the X-ray crystal structure of [(CuL^{Ala})$_2$Cl](ClO$_4$)$_3$ (**22**) shoowing 50% thermal ellipsoids. H atoms have been omitted for clarity. Selected bond distances (Å) and angles (deg) relevant to copper coordination are tabulated.

The UV-vis spectrum of **22** (Figure 2-15) is nearly identical to that of **21**. Here, a predominant transition appears at 604 nm with an extinction coefficient of 242 $M^{-1}cm^{-1}$ and is attributed to ligand-to-metal charge transfer transitions (LMCT) [N and/or O $\rightarrow$ Cu(II) d] mixed with Cu(II) d-d transitions.[25]
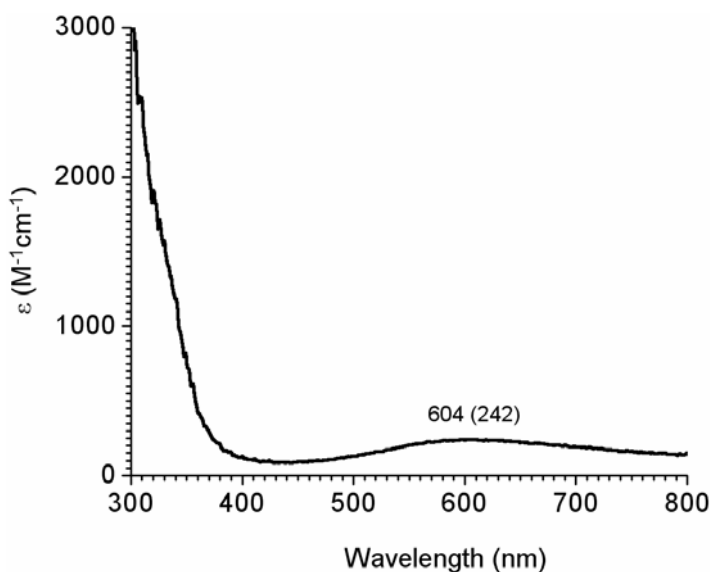
Figure 2-15. UV-vis spectrum of **22** dissolved in acetonitrile. Peak labels indicate the wavelength (nm) and extinction coefficient (ε) in parentheses ($M^{-1}cm^{-1}$).

ESI-MS of **22** confirms its bimetallic structure. The parent ion in the mass spectrum at 825 *m/z* exactly matches the mass of **22** minus one chloride anion, $[M-Cl]^+$ (Figure 2-16). Similarly, the mass of **22** with chloride, but without one perchlorate anion, is also observed at 761 *m/z*. A monomeric fragment, $[M-CuL^{Ala}Cl(ClO_4)_2]^+$, also appears in the mass spectrum at 362 *m/z*. The agreement of the experimental and calculated isotope patterns for the parent ion further corroborate the assignment (Figure 2-16 inset).
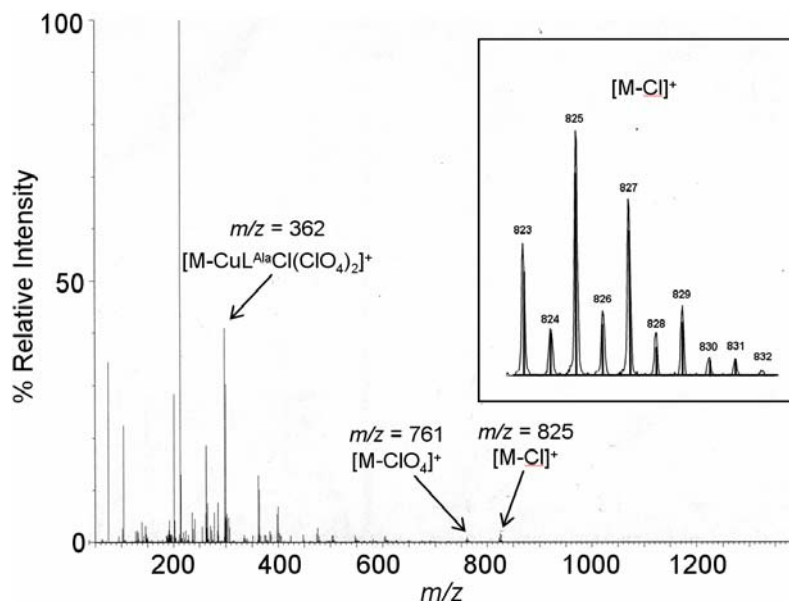
Figure 2-16. ESI-MS of **22** dissolved in acetonitrile. The inset shows the expanded view of the dinuclear parent ion, [M-Cl]$^+$ ($m/z = 825$). The overlaid solid black lines represent the calculated isotope pattern for the species.

2.3.3 [Cu$_2$L^{Phe}Cl$_4$]

[Cu$_2$L^{Phe}Cl$_4$] (**23**) was synthesized by combining a methanol solution of **L**^{Phe} with a methanol solution of cupric chloride (Figure 2-17). The product precipitated from this mixture as a pale blue powder. X-ray quality crystals were obtained by diffusing diethyl ether into a closed vial of the blue powder dissolved in concentrated methanol.
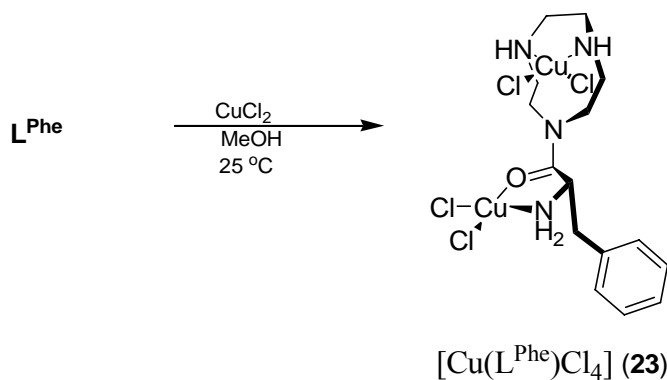
[Cu(L^{Phe})Cl$_4$] (**23**)

Figure 2-17. Synthesis of [Cu(L^{Phe})Cl$_4$] (**23**).

54
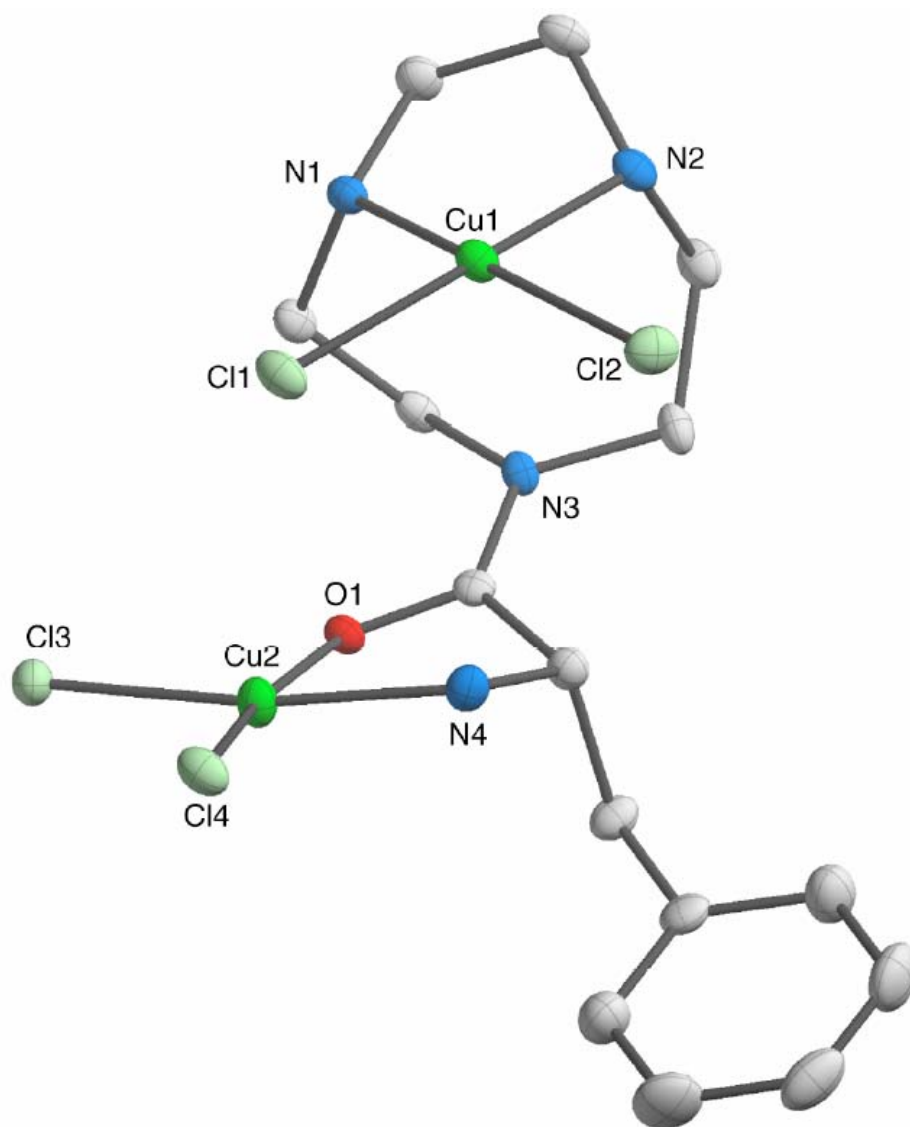
Bond Lengths (Å)		Angles (deg)			
Cu1–N1	2.039(2)	N1–Cu1–Cl1	89.6(1)	N4–Cu2–Cl4	87.8(1)
Cu1–N2	2.023(2)	N1–Cu1–N2	81.7(1)	N4–Cu2–O1	81.3(1)
Cu1–Cl1	2.273(1)	Cl2–Cu1–N2	90.7(1)	Cl3–Cu2–Cl4	101.4(1)
Cu1–Cl2	2.285(1)	Cl2–Cu1–Cl1	97.1(1)	Cl3–Cu2–O1	89.4(1)
Cu2–N4	2.004(2)	N1–Cu1–Cl2	169.3(1)	N4–Cu2–Cl3	169.1(1)
Cu2–O1	2.007(1)	N2–Cu1–Cl1	169.5(1)	O1–Cu2–Cl4	169.0(1)
Cu2–Cl3	2.250(1)				
Cu2–Cl4	2.239(1)				

Figure 2-18. Representation of the X-ray crystal structure of [Cu(L^Phe)Cl₄] (**23**) showing 50% thermal ellipsoids. H atoms have been omitted for clarity. Selected bond distances (Å) and angles (deg) relevant to copper coordination are tabulated.

The crystal structure of **23** reveals a bimetallic complex that is different than that of **22** (Figure 2-18). Here, $\mathbf{L^{Phe}}$ bridges between two copper(II) ions in a manner similar to **22**, with the TACN ring binding to Cu1 through the amine nitrogen atoms in a bidentate fashion and the Phe portion of the ligand binding to Cu2 through the terminal amine nitrogen and the carbonyl oxygen donor atoms. Unlike the pseudo-symmetric binding mode in **22**, however, the coordination sphere around each copper(II) ion in **23** is completed by two chloride ligands. The coordination geometry around both copper(II) ions is square planar with an N_2Cl_2 ligand set around Cu1 and a $NOCl_2$ ligand set around Cu2. If axial interactions are considered, however, the coordination geometry is closest to elongated octahedral. The axial distances involving Cu1 are shorter than the sum of their van der Waals radii [Cu1···N3 = 2.783(2) Å, intramolecular; Cu1A···Cl3 = 2.818(1) Å, intermolecular], suggesting weak Cu···ligand interactions. Likewise, the axial distances involving Cu2 are also shorter than the sum of their van der Waals radii [Cu2···Cl1 = 3.042(1) Å, intramolecular; Cu2···Cl2A = 3.087(1) Å, intermolecular]. The bimetallic complexes, loosely linked through weak intra- and intermolecular axial bonds, consequently form chains along the crystallographic *b* axis.

The UV-vis spectrum of **23** is similar to those of **21** and **22**, with a broad transition at 658 nm, but a significantly smaller extinction coefficient of 68 $M^{-1}cm^{-1}$ (Figure 2-19).
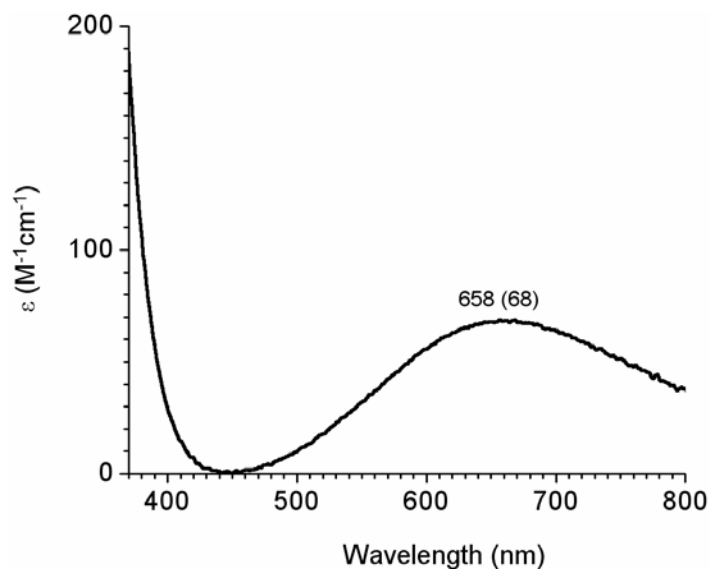
Figure 2-19. UV-vis spectrum of **23** dissolved in water. Peak labels indicate the wavelength (nm) and extinction coefficient (ε) in parentheses ($M^{-1}cm^{-1}$).
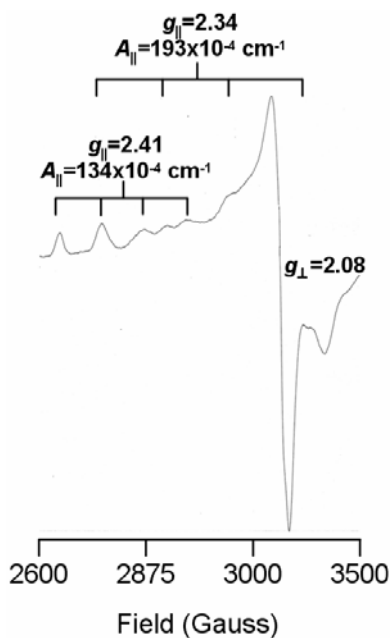
Figure 2-20. Experimental EPR spectrum spectrum of **23** dissolved in 50:50 water/ethylene glycol glass at 77 K and a microwave frequency of 9.43 GHz.

Evidence of two distinct copper coordination environments for **23** in solution was provided by EPR spectroscopy. The EPR spectrum of a frozen solution of **23** clearly shows two overlapping $g_\parallel$ signals (Cu1, $g_\parallel = 2.41$, $A^{Cu}{}_\parallel = 134$ cm^{-1}; Cu2, $g_\parallel = 2.24$, $A^{Cu} = 193 \times 10^{-4}$ cm^{-1}) (Figure 2-20).

No evidence of a bimetallic species was observed for copper(II) complexes of **L^{Phe}** by mass spectrometry. ESI-MS for **23** in acetonitrile shows a parent ion peak at 410 m/z, corresponding to the [M-CuCl$_2$+H]$^+$ cation (Figure 2-21). Furthermore, the [M-CuCl$_3$]$^+$ cation is observed at 374 m/z, suggesting that **3** dissociates into 1:1 L^{Phe}:Cu and solvated Cu^{2+} upon dissolution.
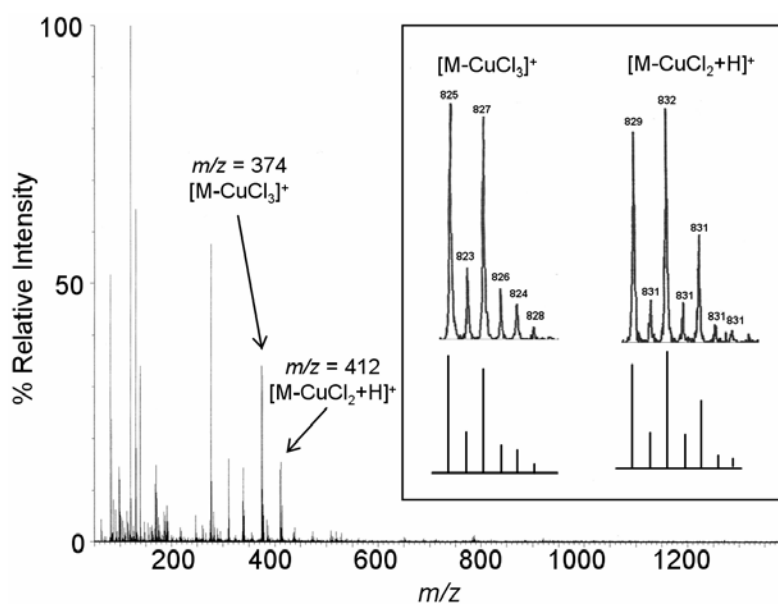
Figure 2-21. ESI-MS of **23** dissolved in acetonitrile. The inset shows expanded views of the parent ion, [M-CuCl$_2$+H]$^+$ ($m/z = 410$), and a related fragment, [M-CuCl$_3$]$^+$ ($m/z = 374$), with their respective calculated isotope patterns (bottom).

2.4. Conclusions

In summary, our original goal of synthesizing new TACN-amino acid conjugates that model the structure and/or reactivity of the CuNiR active site remains in its infancy.

Attempts to synthesize a covalently-linked TACN-His conjugate ($\mathbf{L^{His}}$) in the solution phase were met with unforeseen synthetic difficulties, particularly with undesired side reactions necessitating complex workup procedures to yield very small amounts of the desired product. The need to use multiple protecting groups (e.g. Fmoc, Boc, Trt, and Ts) in the synthesis of these ligands further complicates their chemistry and limits the synthetic scope using this approach.

Despite these problems, however, we successfully synthesized a new family of ligand-amino acid conjugates by coupling TACN directly to glycine, alanine, and phenylalanine. These simple ligands provided insight into the coordination chemistry of TACN to copper(II) where one of the TACN secondary amines is coupled directly to an amino acid. Each of these ligands ($\mathbf{L^{Gly}}$, $\mathbf{L^{Ala}}$, and $\mathbf{L^{Phe}}$) was obtained in high yield and without any complications using standard peptide coupling procedures. The copper(II) complexes of these ligands were synthesized in methanol and characterized by UV-vis, ESI-MS, FTIR, X-ray crystallography (for complexes of $\mathbf{L^{Ala}}$ and $\mathbf{L^{Phe}}$), and EPR. In the case of copper(II) complexes of $\mathbf{L^{Gly}}$ and $\mathbf{L^{Ala}}$, two ligands coordinate in a bridging mode between two copper ions, forming a pseudo-C_2 symmetric 1:1 copper-to-ligand complex. The TACN amines of each ligand coordinate different copper ions in the complex and the terminal amine and amide oxygen of the amino acid of the each ligand coordinate the other copper(II) ion. Although these complexes were synthesized using copper(II) perchlorate, the complex of $\mathbf{L^{Ala}}$ (**22**) features an axially-coordinated chloride as evidenced by its X-ray structure and ESI-MS. The source of this unanticipated chloride is likely the result of impurity in the ligand and/or copper salt, but this assertion has not been fully investigated. Reaction of copper(II) chloride with $\mathbf{L^{Phe}}$ gave a 2:1 copper-to-

ligand complex. In this case, the TACN secondary amines coordinate one copper(II) ion and the terminal amine and amide oxygen of the amino acid of the same ligand coordinate a second copper(II) ion. The copper(II) coordination spheres of both ions are completed with chloride ligands. In no case was the tertiary amide nitrogen of TACN in any of these complexes coordinated to or strongly interacting with a copper(II) ion. This observation reflects the poor ability of amides to coordinate copper(II), particularly where more favorable ligands are avaiable (e.g. the primary amine of the amino acids).

From this preliminary work, we conclude that it is possible for TACN to be covalently linked to amino acids and to obtain coordination complexes of these ligands. The normally tridentate TACN ligand, however, becomes bidentate as a result of converting its secondary amine to a tertiary amide, but the ligand still effectively coordinates copper(II). While **21** and **22** form cyclic dimers in both the solid and solution phases, **23** prefers coordination of two copper(II) ions per ligand. In addition to the presence of chloride ions, effectively blocking otherwise available coordination sites, the differing behavior of **23** is likely the result of the significantly higher steric bulk of its benzyl substituent over the much less bulky functional groups of **21** and **22**. Similar behavior to that of **23** may also be anticipated for an analogous TACN-His conjugate if competing ligands are available.

While this work could be continued to ultimately yield the target ligand or similar ligands, the synthetic challenges and complexity of this approach become greater as the complexity of the ligand increases. This allows for very limited design possibilities with few options for changing any aspect of the ligand without complete resynthesis. Because of these factors, we opted to simplify our approach and to try to achieve our goals by

creating a His-Cys analogue that could join two pre-formed copper complexes. By focusing on copper coordination chemistry instead of organic covalent bonds and complex ligand synthesis, we hoped to circumvent many synthetic difficulties and still produce dinuclear complexes that mimic the CuNiR active site structure more accurately than previous models. These efforts are described in Chapter 3.

2.5. *Experimental*

General. All reagents were purchased from commercial sources and used without additional purification unless otherwise noted. Solvents were dried and purified under nitrogen using standard methods.[29] Et$_2$O, THF, and pentane were distilled over NaK$_2$ alloy, CH$_3$CN and CH$_2$Cl$_2$ over CaH$_2$, MeOH over Mg(OMe)$_2$, and toluene over Na. Degassing of the dried solvents was achieved by triple freeze-pump-thaw degas cycles. Oxygen- and/or water-sensitive reactions were carried out using Schlenk vacuum line techniques and/or by using an M. Braun UNILab inert atmosphere glovebox with nitrogen as its working gas. Preparative procedures for the syntheses of **3**[14], **4**[15], **5**[14], **6**[14], and Boc$_2$TACN (**7**)[16] are published elsewhere and are briefly described in section 2.2.2. The synthesis of 1-(2-aminoethyl)-4,7-diisopropyl-TACN (**12**) by reduction of 1-cyanomethyl-4,7-diisopropyl-TACN (**11**) with 0.1 M Borane in THF is also published elsewhere,[18] but is included here for completeness.

Spectroscopy. Infrared (IR) spectra were prepared by pressing the sample into a KBr "glass" and were collected using a Nicolet NEXUS 470 FTIR spectrophotometer coupled to a computer running OMNIC E.S.P (version 5.1) software for spectrum display, background baseline correction, scaling, and automatic peak-picking. Unless otherwise stated, samples for electronic absorption (UV-vis) spectroscopy were prepared

at 5 mM concentrations in a 5 mL 1.00 cm path length quartz cuvette. UV-vis data were obtained using a Shimadzu UV2401PC UV-vis spectrophotometer capable of a 200 - 1100 nm scan range and having a dedicated variable temperature Neslab RTE-140 circulating heater/chiller and computer interface running Shimadzu UV Probe (v. 1.00) for instrument control and spectrum display. All UV-vis spectra were obtained at 298.0 K unless otherwise noted. ^{1}H and ^{13}C NMR spectra were measured at room temperature on a Varian 300 MHz (Mercury) spectrometer or a Varian 400 MHz spectrometer coupled to the Varian VNMR software package. Solvent was used as an internal chemical shift standard unless otherwise stated. All signals are reported in ppm relative to the reported value(s) for the solvent. X-band (~9.45 GHz) EPR spectra were obtained using a Bruker EMX spectrometer fitted with a either a liquid nitrogen finger dewer or a liquid nitrogen cryostat (BVT-3000). Temperature and *g* value calibrations were performed as described.[30]

Physical Methods. Capillary Gas Chromatography Mass Spectrometry (GC-MS) analyses were performed in a Trace GC 2000 and Thermoquest GCQ/Polaris mass spectrometer (ThermoQuest Finnigan, San Jose, CA). The software controlling the system was Xcalibur (version 1.1) from ThermoQuest Finnigan. Electron impact (EI) was the ionization source and the typical electron energy was set to 70 eV with the ion source temperature maintained at 200 ^{o}C. The instrument was calibrated with the perfluorotributyl amine FC-43 over a *m/z* range of 50-650 Da. Organic components were separated in an Alltech-ECCNO-OAP (30 m x 0.25 mm x 0.25 μm). The injector temperature was set at 210 ^{o}C and a splitless mode of injection was used in all analyses. The GC temperature gradient was set to 50 ^{o}C, holding for 5 minutes, then increased at

20 °C/minute to 250 °C holding for 20 minutes. The GC system was run at a constant flow rate of 1.0 mL/minute of helium gas (Minimum Purity 99.999%). ElectroSpray Ionization Mass Spectrometry (ESI-MS) data were recorded using a Q-TOF quadrupole time-of flight mass spectrometer (Micromass, Manchester, UK) equipped with a Z-spray electrospray ionization (ESI) source. The software controlling the instrument was MassLynx (version 4.0). A Harvard syringe pump (Harvard Apparatus, South Natick, MA, USA) was used to deliver the sample solution to the electrospray source at a flow rate of 5 μl/min. The electrospray capillary voltage was set at 3000 V and the cone voltage was typically set to 30 V. The temperature for desolvation and source was set to 90 °C. The desolvation gas (nitrogen, 99.99%) flow rate was set to 250 liters per hour. Nebuliser gas flow was set to 20 liters per hour. The mass spectrometer was calibrated over a mass range of 50-1500 Da using a 0.05 μg/μL CsI and 2 μg/μL NaI solution in methanol.

1-Cyanomethyl-4,7-di(*t*-butyloxycarbonyl)-1,4,7-triazacyclononane (**8**): To a solution of **7** (1.00 g, 3.03 mmol) in CH_3CN (20 mL) was added chloroacetonitrile (198 μL, 3.13 mmol), Na_2CO_3 (1.00 g), and tetrabutylammonium bromide (7 mg). The resulting mixture was heated at reflux under nitrogen for 3 hours and then cooled to room temperature. The solvent was removed *in vacuo*. To the remaining mixture was added benzene (20 mL). Following 15 minutes rapid stirring, the benzene solution was filtered and the solvent removed under reduced pressure, yielding the desired product as a yellow-orange oil (1.06 g, 95 %). ^{1}H NMR ($CDCl_3$, 300 MHz): δ 3.48 (d, J = 10.5 Hz, 2H), 3.34 (t, J = 12 Hz, 4H), 3.19 (m, 4H), 2.67 (m, 4H), 1.38 (s, 18H) ppm. [13]C{[1]H}

NMR (CDCl$_3$, 300 MHz); δ 155.2, 116.3, 79.7, 53.0, 51.2, 49.8, 44.4, 28.5 ppm. FTIR

(KBr, cm^{-1}): 3515 (w, br), 2975 (s), 2931 (s), 2866 (m), 2251 (w, C≡N), 1689 (s, C=O),

1463 (s), 1413 (s), 1366 (s), 1251 (s), 1153 (s), 1094 (m), 1030 (m), 1000 (m), 961(m),

921 (w), 860 (m), 776 (m), 733 (m). GC/MS: t$_R$ 18.87 min; m/z (relative intensity) 368 (3,

M$^+$), 168 (100). Anal. Calcd for C$_{18}$H$_{32}$N$_4$O$_4$: C, 58.67; H, 8.75; N, 15.21. Found: C,

59.63; H, 8.59; N, 14.75.

[1-Cyanomethyl-[1,4,7]-triazonan-1,4,7-ium]-bis(trifluoroacetate) (**9**): To a solution

of **8** (1.03 g, 2.80 mmol) in CH$_2$Cl$_2$ (3 mL) was added 80 v/v% CF$_3$CO$_2$H/CH$_2$Cl$_2$ (16

mL) at 0 ^{O}C. This solution was stirred at 0 ^{O}C for 1 hour and for an additional 24 hours at

room temperature. Removal of excess CF$_3$CO$_2$H was achieved by concentrating the

solution under reduced pressure followed by successive addition and evaporation of Et$_2$O

(2x) *in vacuo*. A final addition of Et$_2$O was allowed to evaporate slowly and resulted in a

pale tan precipitate that was filtered and washed with 50 v/v% Et$_2$O/*n*-pentane and dried

under reduced pressure to yield a fine, tan powder (0.83 g, 58 %). ^{1}H NMR (CD$_3$OD,

300 MHz): δ 3.79 (s, 2H), 3.55 (s, 4H), 3.33 (t, J = 6 Hz, 4H), 3.04 (t, J = 6 Hz, 4H) ppm.

^{13}C{^{1}H} NMR (CD$_3$OD, 300 MHz): δ 162.2, 162.0, 115.3, 48.1, 43.3, 43.0, 42.3 ppm.

^{19}F NMR (CD$_3$OD, 300 MHz): -77.46 ppm. FTIR (KBr, cm^{-1}): 2783 (m, br), 1667 (s,

C=O), 1440 (w), 1196 (s), 1129 (s), 796 (w), 722 (w). ESI-MS: m/z = 169 (M −

2(trifluoroacetic acid) + 1). Anal. Calcd for C$_{12}$H$_{18}$F$_6$N$_4$O$_4$: C, 37.49; H, 4.82; N, 14.10.

Found: C, 36.44; H, 4.64; N, 13.76.

1-cyanomethyl-1,4,7-triazacyclononane (**10**): To a solution of **9** (0.71 g, 1.39 mmol) in H_2O/CH_3OH (32 mL/8mL) was added 5 M NaOH (aq) dropwise until the pH was adjusted to 13. This mixture was then extracted with $CHCl_3$ (3 x 50 mL). The $CHCl_3$ solution was dried over anhydrous Na_2SO_4 and concentrated under reduced pressure to yield the desired product as a thick yellow-orange oil (0.22 g, 95%). ^{1}H NMR ($CDCl_3$, 300 MHz): δ 3.49 (s, 2H), 2.55-2.75 (m, 12H), 2.06 (s, 2H) ppm. ^{13}C{^{1}H} NMR ($CDCl_3$, 300 MHz); δ 116.51, 53.30, 47.85, 46.80, 45.73 ppm. FTIR (KBr, cm^{-1}): 3344 (s, br), 2925 (s), 2230 (w, C≡N), 1662 (s, C=O), 1550 (s) 1459 (s), 1360 (s), 1297(m), 1157 (s), 1119 (s), 915 (m), 54 (s). ESI-MS: m/z = 169 (M + 1).

1-cyanomethyl-4,7-diisopropyl-1,4,7-triazacyclononane (**11**): **10** (3.13 g, 18.6 mmol) was dissolved into 20 mL CH_3CN, to which was directly added Na_2CO_3 (8 g) and a catalytic amount of tetrabutylammonium bromide (10 mg). To this rapidly-stirring mixture was added 2-bromopropane (9.15 g, 74.4 mmol) via syringe. The reaction mixture was then refluxed under nitrogen for 18 hours after which the resulting orange-colored solution was filtered from excess Na_2CO_3. The filtrate was concentrated under reduced pressure and washed with 1 M NaOH (50 mL), then extracted with CH_2Cl_2 until the extract was colorless (3 x 100mL). The extract was dried over Na_2SO_4 and the solvent removed *in vacuo* to yield the desired product as a yellow-orange oil (4.23 g, 90%). ^{1}H NMR ($CDCl_3$, 300 MHz): δ 3.46 (s, 2H), 3.80 - 2.40 (m, 14H), 0.89 (s, 6H) 0.97 (s, 6H) ppm. ^{13}C{^{1}H} NMR ($CDCl_3$, 300 MHz); δ 117.01, 55.95, 54.81, 53.10, 56.25, 47.13, 18.73, 18.68 ppm.

1-(2-aminoethyl)-4,7-diisopropyl-1,4,7-triazacyclononane (12)[18]: **11** (4.23 g, 16.8 mmol) was dissolved in 1.0 M $BH_3 \cdot THF$ (46 mL) and the resulting solution refluxed for 18 hours. This clear solution was then cooled to room temperature and ethanol was carefully added dropwise while vigorously stirring under nitrogen to quench unreacted borane. The solvent was then removed *in vacuo* and the resulting white solid was redissolved in 4 M HCl in methanol (46 mL). This acidic solution was refluxed for 2 hours. Following cooling of the reaction mixture to room temperature, the methanol was removed *in vacuo* and the remaining aqueous solution was adjusted to pH >11 by addition of aqueous NaOH, then extracted with CH_2Cl_2 (3 x 50 mL). The combined extracts were dried over Na_2SO_4. Removal of the solvent under reduced pressure yielded the product as a pale yellow oil (3.45 g, 80%). ^{1}H NMR (CDCl$_3$, 300 MHz): δ 2.85 (heptet, J = 6.6 Hz, 2H), 2.76 (m, 4H), 2.71 (t, J = 6.0 Hz, 2H), 2.65 (m, 4H), 2.57 (s, 4H), 2.56 (t, J = 6.0 Hz, 2H), 0.95 (d, J = 6.6 Hz, 12H).

2-amino-N-(2-(4,7-diisopropyl-1,4,7-triazonan-1-yl)ethyl)-3-(1-trityl-1H-imidazol-4-yl)propanamide (13): A THF solution (100 mL) of Fmoc-His(Trt)-OH (2.42 g, 3.90 mmol), **12** (1.00 g, 3.90 mmol), and 1-hydroxybenzotriazole hydrate (HOBt·H$_2$O) (0.60 g, 3.90 mmol) was cooled to -20 °C in an ice/salt bath in air. To this solution was added dropwise N,N'-dicyclohexylcarbodiimide (DCC) (0.81 g, 3.90 mmol) in THF (10 mL). This solution was stirred at -20 °C for 1 hour and then removed from the ice bath and stirred at room temperature for 12 hours. The resulting white dicyclohexylurea (DCU) precipitate byproduct was filtered and the DCU washed with cold THF. THF was removed from the combined filtrate *in vacuo* and the residue was redissolved in CH_2Cl_2

(25 mL). This was washed with 0.05 M citric acid (3 x 40 mL), water (2 x 25 mL), NaHCO$_3$ (0.5 M, 3 x 40 mL), and finally with water (2 x 25 mL). The organic phase was then dried over MgSO$_4$, filtered, and its volume reduced by approximately one-half. This solution was cooled to -20 °C for 10 hours to facilitate additional DCU precipitation, after which the mixture was filtered and the solvent removed *in vacuo* to yield a yellow-red solid. This solid was then redissolved in methanol (100 mL) and filtered. The filtrate was concentrated to 5 mL and loaded onto a 30 g RediSep disposable flash column and sequentially eluted with hexanes and ethyl acetate (300 mL each). The Fmoc- and Trt-protected product remained on the column as an orange colored ring. The column was disassembled and the silica portion containing the orange ring was transferred to a 250 mL beaker. Water was added to saturate the silica then 4 M NaOH was added dropwise to adjust the pH to > 12. The pH increase resulted in CO$_2$ bubbling, resulting from removal of Fmoc under the highly basic conditions. The aqueous layer was extracted with chloroform (3 x 100 mL). The combined organic extracts were dried over sodium sulfate and filtered. Removal of the filtrate solvent revealed the desired product as a yellow oil (0.124 g, 5 %). ^{1}H NMR (CDCl$_3$, 300 MHz): δ 7.82-8.22 (s, 1H), 7.65 (s, 1H), 7.25 (s, 1H), 2.00 - 3.75 (m, 23H), 1.00 (m, 12H) ppm. FTIR (KBr, cm^{-1}): 3410 (s, br), 2950 (s), 2910 (m), 2880 (w), 1650 (s, amide C=O), 1450 (m), 1400 (m), 1380 (w), 1280 (w), 1200 (m), 1150 (m), 1100 (m), 900 (m), 730 (s).

2-amino-3-(1H-imidazol-4-yl)-N-(2-(4,7-diisopropyl-1,4,7-triazonan-1-yl)ethyl)propanamide (L^{His}, 14): To **13** was added 3 mL of TFA/TIS/H$_2$0 (95/2.5/2.5 v/v %). This mixture was stirred for 2 hours, after which the TFA and TIS were removed

in vacuo. The pH of the remaining aqueous solution was increased to pH > 9 with 4 M NaOH and this solution was then extracted with chloroform (3 x 100 mL). The combined organic extracts were dried over Na_2SO_4 and filtered. The filtrate solvent was removed *in vacuo* to yield the desired product as a yellow oil (0.062 g, 50 %). [^1]H NMR (CDCl₃, 300 MHz): δ 7.82-8.22 (s, 1H), 7.65 (s, 1H), 7.25 (s, 1H), 2.00 - 3.75 (m, 23H), 1.00 (m, 12H) ppm. FTIR (KBr, cm⁻¹): 3410 (s, br), 2950 (s), 2910 (m), 2880 (w), 1650 (s, amide C=O), 1450 (m), 1400 (m), 1380 (w), 1280 (w), 1200 (m), 1150 (m), 1100 (m), 900 (m), 730 (s). ESI-MS: *m/z* = 394 (M + 1).

Boc₂TACN(Boc-Gly) (**15**): A THF solution (80 mL) of Boc-Gly-OH, (1.48, 8.45 mmol), **7** (2.78 g, 8.45 mmol), and 1-hydroxybenzotriazole hydrate (HOBt·H₂O) (1.55 g, 10.12 mmol) was cooled to -20 °C in an ice/salt bath in air. To this solution was added dropwise N,N'-dicyclohexylcarbodiimide (DCC) (2.09 g, 10.12 mmol) in THF (10 mL). This solution was stirred at -20 °C for 1 hour and then removed from the ice bath and stirred at room temperature for 12 hours. The resulting white dicyclohexylurea (DCU) precipitate byproduct was filtered and the DCU washed with cold THF. THF was removed from the combined filtrate *in vacuo* and the residue was redissolved in CH₂Cl₂ (25 mL). This was washed with 0.05 M citric acid (3 x 40 mL), water (2 x 25 mL), NaHCO₃ (0.5 M, 3 x 40 mL), and finally with water (2 x 25 mL). The organic phase was then dried over MgSO₄, filtered, and its volume reduced by approximately one-half. This solution was cooled to -20 °C for 10 hours to facilitate additional DCU precipitation, after which the mixture was filtered and the solvent removed *in vacuo* to yield Boc₂TACN(Boc-Gly) as a pale-yellow solid (3.41 g, 83%). [^1]H NMR (500 MHz,

CD$_2$Cl$_2$): δ 7.53 (t, J = 12.0 Hz, 1H), 3.89 (s, 2H), 3.10 - 3.65 (m, 12H), 1.39 (s, 27H) ppm. ^{13}C{^{1}H} NMR (CDCl$_3$, 300 MHz); δ 170.08, 169.57, 155.76, 80.57, 46 - 54, 42.88, 28.84 ppm. Anal. Calcd for C$_{23}$H$_{42}$N$_4$O$_7$: C, 56.76; H, 8.63; N, 11.51. Found: C, 56.67; H, 8.58; N, 11.58.

Boc$_2$TACN(Boc-Ala) (**16**): A THF solution (80 mL) of Boc-Ala-OH, (1.60, 8.44 mmol), **7** (2.78 g, 8.44 mmol), and 1-hydroxybenzotriazole hydrate (HOBt·H$_2$O) (1.55 g, 10.12 mmol) was cooled to -20 °C in an ice/salt bath in air. To this solution was added dropwise N,N'-dicyclohexylcarbodiimide (DCC) (2.09 g, 10.12 mmol) in THF (10 mL). This solution was stirred at -20 °C for 1 hour and then removed from the ice bath and stirred at room temperature for 12 hours. The resulting white dicyclohexylurea (DCU) precipitate byproduct was filtered and the DCU washed with cold THF. THF was removed from the combined filtrate *in vacuo* and the residue was redissolved in CH$_2$Cl$_2$ (25 mL). This was washed with 0.05 M citric acid (3 x 40 mL), water (2 x 25 mL), NaHCO$_3$ (0.5 M, 3 x 40 mL), and finally with water (2 x 25 mL). The organic phase was then dried over MgSO$_4$, filtered, and its volume reduced by approximately one-half. This solution was cooled to -20 °C for 10 hours to facilitate additional DCU precipitation, after which the mixture was filtered and the solvent removed *in vacuo* to yield Boc$_2$TACN(Boc-Gly) as a yellow oil (3.72 g, 88 %). ^{1}H NMR (CDCl$_3$, 300 MHz): δ 3.00 - 3.85 (m, 12H); 1.65 (d, J = 7.2 Hz, 3H); 1.30 - 1.48 (m, 27H) ppm. ^{13}C{^{1}H} NMR (CDCl$_3$, 300 MHz); δ 174.28, 156.56, 81.08, 46.50 - 54.01, 29.23, 20.80 ppm. Anal. Calcd for C$_{24}$H$_{44}$N$_4$O$_7$: C, 57.58; H, 8.86; N, 11.19. Found: C, 57.23; H, 8.15; N, 10.92.

Boc$_2$TACN(Boc-Phe) (**17**):   A THF solution (80 mL) of Boc-Phe-OH, (1.63, 6.16 mmol), **7** (2.02 g, 6.16 mmol), and 1-hydroxybenzotriazole hydrate (HOBt·H$_2$O) (1.13 g, 7.39 mmol) was cooled to -20 °C in an ice/salt bath in air. To this solution was added dropwise N,N'-dicyclohexylcarbodiimide (DCC) (1.52 g, 7.39 mmol) in THF (10 mL). This solution was stirred at -20 °C for 1 hour and then removed from the ice bath and stirred at room temperature for 12 hours. The resulting white dicyclohexylurea (DCU) precipitate byproduct was filtered and the DCU washed with cold THF.   THF was removed from the combined filtrate *in vacuo* and the residue was redissolved in CH$_2$Cl$_2$ (25 mL). This was washed with 0.05 M citric acid (3 x 40 mL), water (2 x 25 mL), NaHCO$_3$ (0.5 M, 3 x 40 mL), and finally with water (2 x 25 mL). The organic phase was then dried over MgSO$_4$, filtered, and its volume reduced by approximately one-half. This solution was cooled to -20 °C for 10 hours to facilitate additional DCU precipitation, after which the mixture was filtered and the solvent removed *in vacuo* to yield Boc$_2$TACN(Boc-Phe) as a yellow oil (2.63 g, 74 %). ^{1}H NMR (CDCl$_3$, 300 MHz): δ 7.05 - 7.25 (m, 5H); 4.56 - 5.31 (m, 1H); 2.81-3.85 (br, 12H); 2.76 - 3.82 (m, 14H); 1.39 (m, 27H) ppm. Anal. Calcd for C$_{30}$H$_{48}$N$_4$O$_7$: C, 62.50; H, 8.33; N, 9.72. Found: C, 61.95; H, 8.41; N, 9.55.

TACN-Gly (L^{Gly}, 18): To **15** (3.04 g, 6.25 mmol) was added 10 mL of TFA/CH$_2$Cl$_2$ (50/50 v/v %). This mixture was stirred for one hour, after which the solvent was removed *in vacuo*. Cold Et$_2$O (200 mL) was then added to the resulting yellow oil residue resulting in yellow solid precipitate. This solid was filtered from Et$_2$O, triturated, and washed with fresh Et$_2$O.   Residual Et$_2$O was removed from the powder under

reduced pressure revealing white powder. This white solid was dissolved in 50 mL CH_2Cl_2 and stirred in the presence of crushed NaOH (10 g) for 15 hours. The CH_2Cl_2 solution was filtered from excess NaOH and the solvent removed *in vacuo* to give the desired product (0.75 g, 65 %). ^{1}H NMR (CDCl$_3$, 300 MHz): δ 3.43 (s, 2H), 3.37 -3.57 (m, 2H), 3.23 - 3.33 (m, 2H), 2.93 - 3.06 (m, 4H), 2.58 - 2.73 (m, 4H), 1.77 (s, 2H), 1.45 (s, 2H) ppm. FTIR (KBr, cm^{-1}): 3342 (m, br), 2926 (s), 2360 (s), 2334 (s), 1652 (s, C=O), 1478 (m), 1370 (m), 1294 (w), 1240 (w), 1198 (w), 1163 (w), 1120 (w), 1054 (m), 1013 (w), 942 (w), 887 (w), 667 (m). ESI-MS: m/z = 187 (M + 1). Anal. Calcd for $C_8H_{18}N_4O$: C, 51.59; H, 9.74; N, 30.08. Found: C, 50.93; H, 9.23; N, 30.54.

TACN-Ala (L^{Ala}, 19): To **16** (1.45 g, 2.90 mmol) was added 5 mL of TFA/CH_2Cl_2 (50/50 v/v %). This mixture was stirred for one hour, after which the solvent was removed *in vacuo*. Cold Et$_2$O (100 mL) was then added to the resulting yellow oil residue resulting in yellow solid precipitate. This solid was filtered from Et$_2$O, triturated, and washed with fresh Et$_2$O. Residual Et$_2$O was removed from the powder under reduced pressure revealing white powder. This white powder was dissolved in 25 mL CH_2Cl_2 and stirred in the presence of crushed NaOH (5 g) for 15 hours. The CH_2Cl_2 solution was filtered from excess NaOH and the solvent removed *in vacuo* to give the desired product (0.58 g, 45 %). ^{1}H NMR (CDCl$_3$, 300 MHz): δ 2.53 - 4.16 (m, 13H); 2.35 (s, 4H) 1.21 (d, J = 6.6 Hz, 3H) ppm. FTIR (KBr, cm^{-1}): 2928 (s), 2866 (s), 1649 (s, C=O), 1558 (w), 1473 (m), 1442 (m), 1424 (m), 1371 (s), 1288 (w), 1232 (m), 1194 (w), 1159 (m), 1104 (m), 1057 (m), 1013 (m), 944 (w), 909 (w), 748 (w), 667 (w). Anal. Calcd for $C_9H_{20}N_4O$: C, 53.97; H, 10.06; N, 27.97. Found: C, 53.40; H, 9.12; N, 28.99.

TACN-Phe (**L^{Phe}, 20**): To **17** (3.21 g, 5.57 mmol) was added 10 mL of TFA/CH$_2$Cl$_2$ (50/50 v/v %). This mixture was stirred for one hour, after which the solvent was removed *in vacuo*. Cold Et$_2$O (200 mL) was then added to the resulting yellow oil residue resulting in yellow solid precipitate. This solid was filtered from Et$_2$O, triturated, and washed with fresh Et$_2$O. Residual Et$_2$O was removed from the powder under reduced pressure revealing white powder. This white powder was dissolved in 50 mL CH$_2$Cl$_2$ and stirred in the presence of crushed NaOH (10 g) for 15 hours. The CH$_2$Cl$_2$ solution was filtered from excess NaOH and the solvent removed *in vacuo* to give the desired product (0.77 g, 50 %). ^{1}H NMR (CD$_2$Cl$_2$, 300 MHz): δ 7.02 - 7.27 (m, 5H); 2.45 - 3.97 (m, 15H); 2.02 (s, 4H) ppm. FTIR (KBr, cm^{-1}): 3261 (s, br), 3025 (s), 2924 (s), 1641 (s, C=O), 1493 (m), 1453 (m), 1369 (w), 1340 (m), 1287 (m), 1236 (w), 1195 (m), 1157 (m), 1120 (w), 1105 (m), 1065 (m), 1010 (m), 939 (w), 906 (w), 881 (w), 861 (m), 751 (w), 702 (w), 668 (w), 621 (w), 595 (w), 530 (w). Anal. Calcd for C$_{15}$H$_{24}$N$_4$O: C, 65.21; H, 8.70; N, 20.28. Found: C, 65.46; H, 8.17; N, 19.09.

[(CuL^{Gly})$_2$](ClO$_4$)$_4$ (21): L^{Gly} (0.187 g, 1.00 mmol) was dissolved in 5 mL of methanol. To this rapidly-stirring solution was added a solution of Cu(ClO$_4$)$_2$·6H$_2$O (0.371 g, 1.00 mmol) in 5 mL of methanol via syringe. Stirring was continued for 5 hours, during which time a blue precipitate formed. The blue precipitate was filtered from the reaction mixture, washed with a minimal volume of fresh methanol, and transferred to a vacuum flask. The desired product was obtained as a blue powder following complete removal of residual solvent *in vacuo* (0.18 g, 40 %). UV/vis (CH$_3$CN) [λ_{max} (ε, M^{-1}cm^{-1})] 330 (sh,

630), 593 (180) nm. EPR (CH$_3$CN, 9.431 GHz, 90 K) $g_\perp$ = 2.09, $g_\parallel$ = 2.34, $A_\parallel$ Cu = 200 G. FTIR (KBr) 3430, 3215, 1591, 1457, 1367, 1085, 1002, 626 cm^{-1}. ESI-MS (CH$_3$CN): 797 [M - ClO$_4$]$^+$; 348 [M - CuLGly (ClO$_4$)$_3$]$^+$ m/z. Anal. Calcd for C$_{16}$H$_{36}$Cl$_4$Cu$_2$N$_8$O$_{18}$: C, 21.41; H, 4.04; N, 12.49. Found: C, 20.04; H, 4.33; N, 11.08.

[(CuL^{Ala})$_2$Cl](ClO$_4$)$_3$ (22): L^{Ala} (0.217 g, 1.08 mmol) was dissolved in methanol (5 mL). To this rapidly-stirring solution was added a solution of Cu(ClO$_4$)$_2$·6H$_2$O (0.684 g, 1.08 mmol) in methanol (5 mL) via syringe. Stirring was continued for 5 hours, during which time a blue precipitate formed. The blue precipitate was filtered from the reaction mixture, washed with a minimal volume of fresh methanol, and transferred to a vacuum flask. The desired product was obtained as a blue powder following complete removal of residual solvent *in vacuo*. X-ray quality crystals were obtained by dissolving the crystalline powder into a minimal volume of methanol and diffusing ether into this solution at room temperature (0.28 g, 60 %). UV-vis (CH$_3$CN) [λ_{max} (ε, M^{-1}cm^{-1})] 331 (sh, 1850), 600 (300) nm. EPR (CH$_3$CN, 9.4341 GHz, 90 K) $g_\perp$= 2.08, $g_\parallel$ = 2.39, $A_\parallel$ Cu = 120 G. FTIR (KBr, cm^{-1}): 3427, 3225, 3124, 2925, 1583, 1139, 1112, 1088, 625. ESI-MS (CH$_3$CH): 825 [M - Cl]$^+$; 761 [M - ClO$_4$]$^+$; 362 [M - CuL^{Ala}Cl(ClO$_4$)$_2$]$^+$ m/z. Anal. Calcd for C$_{18}$H$_{40}$Cl$_4$Cu$_2$N$_8$O$_{14}$·CH$_3$NO$_2$·H$_2$O: C, 24.26; H, 4.82; N, 13.51. Found: C, 23.53; H, 4.88; N, 12.53.

[Cu$_2$L^{Phe}Cl$_4$] (23): L^{Phe} (0.138 g, 0.499 mmol) was dissolved in 5 mL of methanol. To this rapidly-stirring solution was added a solution of CuCl$_2$ (0.134 g, 0.998 mmol) in 5 mL of methanol via syringe. Stirring was continued for 5 hours, during which time a

blue precipitate formed. The blue precipitate was filtered from the reaction mixture, washed with a minimal volume of fresh methanol, and transferred to a vacuum flask. The desired product was obtained as a blue powder following complete removal of residual solvent *in vacuo*. X-ray quality crystals were obtained by dissolving the crystalline powder into a minimal volume of methanol and diffusing ether into this solution at room temperature (0.136 g, 50 %). UV/vis (CH_3CN) [λ_{max} (ε, $M^{-1}cm^{-1}$))] 366 (sh, 210), 655 (74) nm. EPR (H_2O/ethylene glycol 50/50 v/v %, 9.44 GHz, 100 K) $g_\perp$ = 2.080, $g_\parallel$(1) = 2.239, $A_\parallel$ Cu(1) = 190.2 x 10-4 cm-1, $g_\parallel$(2) = 2.410, $A_\parallel$ Cu(2) = 133.9 x 10-4 cm-1. FTIR (KBr, cm^{-1}): 3438, 3325, 3271, 1573, 1433, 1338, 1073, 1022, 977, 816, 751, 706, 629, 572. ESI-MS (H_2O): 410, [M - $CuCl_2$]$^+$; 374, [M - $CuCl_3$]$^+$ *m/z*. Anal. Calcd for $C_{15}H_{24}Cl_4Cu_2N_4O$: C, 33.04; H, 4.44; N, 10.27. Found: C, 32.78; H, 4.91; N, 10.71.

X-ray Crystalloraphy. **[(CuL^{Ala})$_2$Cl](ClO$_4$)$_3$ (22):** A green crystal of the complex, having approximate dimensions 0.42 x 0.26 x 0.24 mm, was mounted on a glass capillary with heavy-weight oil and quickly placed under a cold stream of nitrogen on the diffractometer. The data were collected at 143(1) K on a Bruker Apex diffractometer using Mo Kα (λ = 0.71073 Å) radiation.[31] Important crystallographic information is summarized in table 2-1. Intensity data, which approximately covered the full sphere of the reciprocal space, were measured as a series of ω oscillation frames each 0.3° for 24 seconds per frame. The detector was operated in 512 x 512 mode and was positioned 6.00 cm from the crystal. Coverage of unique data was 99.6 % complete to 52° (2θ). Cell parameters were determined from a non-linear least squares fit of 6818

reflections in the range of 2.27 < θ < 26.4°. A total of 36607 reflections were measured. The data were corrected for absorption by multi-scan method form equivalent reflections giving minimum and maximum transmission of 0.5549 and 0.7015. The data were merged to form a set of 6919 unique data with R(int) = 0.049.

The structure was solved by the direct method using SHELXTL system and refined by full-matrix least squares on F^2 using all reflections.[32] All the non-hydrogen atoms were refined anisotropically. All the hydrogen atoms were included with idealized parameters except the hydrogen atoms on N(l), N(2), N(4), N(5), N(6), N(8) and O(17) atoms, which were located and refined with fixed temperature factors. The asymmetric unit contains one $C_{18}H_{38}C1Cu_2N_8O_2$ cation, three $C1O_4^-$ anions and $CH_3NO_2 \cdot H_2O$ solvent molecules. The cations form polymeric chains along the b-axis. Final $R1$ = 0.051 is based on 6548 "observed reflections" [$I > 2\sigma(I)$] and wR^2 = 0.135 is based on all reflections (6919 unique data). The final structure was graphically presented using the Accelrys Materials Studio software package.[33]

[Cu$_2$L^{Phe}Cl$_4$] (**23**): A green crystal of the complex, having approximate dimensions 0.10 x 0.08 x 0.04 mm, was mounted on a glass capillary with heavy-weight oil and quickly placed under a cold stream of nitrogen on the diffractometer. The data were collected at 120(1) K on a Bruker Apex diffractometer using Mo Kα (λ = 0.71073 Å) radiation.[31] Important crystallographic information is summarized in table 2-1. Intensity data, which approximately covered the full sphere of the reciprocal space, were measured as a series of co oscillation frames each 0.4° for 31 seconds per frame. The detector was operated in 512 x 512 mode and was positioned 6.00 cm from the crystal. Coverage of unique data

was 98.7 % complete to 53°(2θ). Cell parameters were determined from a non-linear least squares fit of 6679 reflections in the range of $3.20 < 0 < 25.92°$. A total of 8025 reflections were measured. The data were corrected for absorption by multi-scan method form equivalent reflections giving minimum and maximum transmission of 0.7758 and 0.9006. The data were merged to form a set of 3795 unique data with $R(\text{int}) = 0.021$.

The structure was solved by the direct method using SHELXTL system and refined by full-matrix least squares on F^2 using all reflections.[32] All the non-hydrogen atoms were refined anisotropically. All the hydrogen atoms were included with idealized parameters. Final $R1 = 0.022$ is based on 3634 "observed reflections" [$I > 2\sigma(I)$] and $wR^2 = 0.050$ is based on all reflections (3795 unique data). The final structure was graphically presented using the Accelrys Materials Studio software package.[33]

Table 2-1. Summary of crystallographic data for compounds **22** and **23**.

	22	23
empirical formula	$C_{19}H_{45}C_{14}Cu_2N_9O_{17}$	$C_{15}H_{24}C_{14}Cu_2N_4O$
formula weight	940.52	545.26
crystal system	orthorhombic	monoclinic
space group	P2(1)2(1)2(1)	P2(1)
a (Å)	9.9962(11)	7.5158(6)
b (Å)	17.432(2)	7.5207(6)
c (Å)	20.285(2)	17.9669(15)
α (deg)	90	90
β (deg)	90	100.012(1)
γ (deg)	90	90
V (Å^{-3})	3534.7(7)	1000.10(14)
Z	4	2
density (calcd)	1.767 g/cm^3	1.811 g/cm^3
temperature (K)	143(2)	120(2)
crystal size (mm)	0.42 x 0.26 x 0.24	0.10 x 0.08 x 0.04
diffractometer	Bruker Apex	Bruker Apex
absorption coefficient	1.590 mm^{-1}	2.674 mm^{-1}
radiation, λ (Å)	Mo Kα, $\lambda = 0.71073$	Mo Kα, $\lambda = 0.71073$
2θ max (deg)	52.0	53.0
reflections collected	36607	8025
independent reflections	6919	3795
observed reflections	6548	3634
variable parameters	1936	552
$R1$ [$I > 2\sigma(I)$]	0.0505	0.0221
w$R2$ [$I > 2\sigma(I)$]	0.1334	0.0492
$R1$ (all data)	0.0535	0.0238
w$R2$ (all data)	0.1353	0.0497
goodness-of-fit	1.051	1.005
largest diff. peak and hole (e^{-1} Å^{-3})	1.779, -0.721	0.665, -0.271

2.6. References

1. (a) Adman, E. T.; Murphy, M. E. P., Copper Nitrite Reductase. In *Handbook of Metalloproteins*, Wiley: Chichester ; New York, 2001; Vol. 2, pp 1381-1390. (b) Suzuki, S.; Kataoka, K.; Yamaguchi, K.; Inoue, T.; Kai, Y. *Coord. Chem. Rev.* **1999**, *192*, 245-265. (c) Averill, B. A. *Chem. Rev.* **1996**, *96*, 2951-2964. (d) Inokuchi, R.; Kuma, K.; Miyata, T.; Okada, M. *Phys. Plant.* **2002**, *116*, 1-11. (e) Takaya, N. *J. Biosc. Bioeng.* **2002**, *94*, 506-510. (f) Suzuki, S.; Kataoka, K.; Yamaguchi, K. *Acc. Chem. Res.* **2000**, *33*, 728-735.

2. (a) Galloway, J. N.; Dentener, F. J.; Capone, D. G.; Boyer, E. W.; Howarth, R. W.; Seitzinger, S. P.; Asner, G. P.; Cleveland, C. C.; Green, P. A.; Holland, E. A.; Karl, D. M.; Michaels, A. F.; Porter, J. H.; Townsend, A. R.; Vorosmarty, C. J. *Biogeochemistry* **2004**, *70*, 153-226. (b) Van de Pas-Schoonen, K. T.; Schalk-Otte, S.; Haaijer, S.; Schmid, M.; den Camp, H. O.; Strous, M.; Kuenen, J. G.; Jetten, M. S. M. *Biochem. Soc. Trans.* **2005**, *33*, 205-209. (c) Eady, R. R.; Hasnain, S. S. *Comp. Coord. Chem. II* **2004**, *8*, 759-786. (d) Wasser, I. M.; de Vries, S.; Moenne-Loccoz, P.; Schroder, I.; Karlin, K. D. *Chem. Rev.* **2002**, *102*, 1201-1234. (e) Moura, I.; Moura, J. J. G. *Curr. Op. Chem. Biol.* **2001**, *5*, 168-175.

3. Murphy, M. E.; Turley, S.; Adman, E. T. *J. Biol. Chem.* **1997**, *272*, 28455-28460.

4. (a) Dodd, F. E.; Hasnain, S. S.; Abraham, Z. H.; Eady, R. R.; Smith, B. E. *Acta Cryst. Sec. D. Biol. Cryst.* **1997**, *53*, 406-418. (b) Dodd, F. E.; Van Beeumen, J.; Eady, R. R.; Hasnain, S. S. *J. Mol. Biol.* **1998**, *282*, 369-382. (c) Ellis, M. J.; Dodd, F. E.; Strange, R. W.; Prudencio, M.; Sawers, G.; Eady, R. R.; Hasnain, S.

S. *Acta Cryst. Sec. D Biol. Cryst.* **2001**, *57*, 1110-1118. (d) Godden, J. W.; Turley, S.; Teller, D. C.; Adman, E. T.; Liu, M. Y.; Payne, W. J.; LeGall, J. *Science* **1991**, *253*, 438-442. (e) Jacobson, F.; Guo, H.; Olesen, K.; Okvist, M.; Neutze, R.; Sjolin, L. *Acta Cryst. Sec. D Biol. Cryst.* **2005**, *61*, 1190-1198.

5. Xie, Y.; Inoue, T.; Seike, N.; Matsumura, H.; Kanbayashi, K.; Itoh, K.; Kataoka, K.; Yamaguchi, K.; Suzuki, S.; Kai, Y. *Acta Cryst. Sec. D Biol. Cryst.* **2004**, *60*, 2383-2386.

6. (a) Ellis, M. J.; Prudencio, M.; Dodd, F. E.; Strange, R. W.; Sawers, G.; Eady, R. R.; Hasnain, S. S. *J. Mol. Biol.* **2002**, *316*, 51-64. (b) Farver, O.; Eady, R. R.; Sawers, G.; Prudencio, M.; Pecht, I. *FEBS Lett.* **2004**, *561*, 173-176. (c) Wijma, H. J.; Boulanger, M. J.; Molon, A.; Fittipaldi, M.; Huber, M.; Murphy, M. E. P.; Verbeet, M. P.; Canters, G. W. *Biochemistry* **2003**, *42*, 4075-4083. (d) Wherland, S.; Farver, O.; Pecht, I. *Chemphyschem* **2005**, *6*, 1440.

7. (a) Basumallick, L.; Szilagyi, R. K.; Zhao, Y.; Shapleigh, J. P.; Scholes, C. P.; Solomon, E. I. *J. Am. Chem. Soc.* **2003**, *125*, 14784-14792. (b) Deligeer; Fukunaga, R.; Kataoka, K.; Yamaguchi, K.; Kobayashi, K.; Tagawa, S.; Suzuki, S. *J. Inorg. Biochem.* **2002**, *91*, 132-138. (c) Prudencio, M.; Eady, R. R.; Sawers, G. *Biochem. J.* **2001**, *353*, 259-266. (d) LaCroix, L. B.; Shadle, S. E.; Wang, Y. N.; Averill, B. A.; Hedman, B.; Hodgson, K. O.; Solomon, E. I. *J. Am. Chem. Soc.* **1996**, *118*, 7755-7768.

8. Suzuki, S.; Deligeer; Yamaguchi, K.; Kataoka, K.; Kobayashi, K.; Tagawa, S.; Kohzuma, T.; Shidara, S.; Iwasaki, H. *J. Biol. Inorg. Chem.* **1997**, *2*, 265-274.

9.   (a) Hough, M. A.; Ellis, M. J.; Antonyuk, S.; Strange, R. W.; Sawers, G.; Eady, R. R.; Hasnain, S. S. *J. Mol. Biol.* **2005**, *350*, 300-309. (b) Yamaguchi, K.; Kataoka, K.; Kobayashi, M.; Itoh, K.; Fukui, A.; Suzuki, S. *Biochemistry* **2004**, *43*, 14180-14188. (c) Kataoka, K.; Yamaguchi, K.; Sakai, S.; Takagi, K.; Suzuki, S. *Biochem. Biophys. Res. Comm.* **2003**, *303*, 519-524.

10.   (a) Suzuki, S.; Maetani, T.; Yamaguchi, K.; Kobayashi, K.; Tagawa, S. *Chem. Lett.* **2005**, *34*, 36-37. (b) Farver, O.; Eady, R. R.; Abraham, Z. H.; Pecht, I. *FEBS Lett.* **1998**, *436*, 239-242. (c) Suzuki, S.; Kohzuma, T.; Deligeer; Yamaguchi, K.; Nakamura, N.; Shidara, S.; Kobayashi, K.; Tagawa, S. *J. Am. Chem. Soc.* **1994**, *116*, 11145-11146.

11.   (a) Richards, R. L.; Durrant, M. C. *J. Chem. Res.* **2002**, 95-98. (b) Beretta, M.; Bouwman, E.; Casella, L.; Douziech, B.; Driessen, W. L.; Gutierrez-Soto, L.; Monzani, E.; Reedijk, J. *Inorg. Chim. Acta* **2000**, *310*, 41-50. (c) Casella, L.; Carugo, O.; Gullotti, M.; Doldi, S.; Frassoni, M. *Inorg. Chem.* **1996**, *35*, 1101-1113. (d) Wasbotten, I. H.; Ghosh, A., Modeling Side-On NO Coordination to Type 2 Copper in Nitrite Reductase: Structures, Energetics, and Bonding. *J. Am. Chem. Soc.*, 2005. (e) Scarpellini, M.; Neves, A.; Castellano, E. E.; Neves, E. F. D.; Franco, D. W. *Polyhedron* **2004**, *23*, 511-518. (f) Holland, P. L.; Tolman, W. B. *J. Am. Chem. Soc.* **2000**, *122*, 6331-6332. (g) Monzani, E.; Koolhaas, G. J. A. A.; Spandre, A.; Leggieri, E.; Casella, L.; Gullotti, M.; Nardin, G.; Randaccio, L.; Fontani, M.; Zanello, P.; Reedijk, J. *J. Biol. Inorg. Chemistry.* **2000**, *5*, 251-261. (h) Halfen, J. A.; Mahapatra, S.; Wilkinson, E. C.; Gengenbach, A. J.; Young, V. G.; Que, L.; Tolman, W. B. *J. Am. Chem. Soc.* **1996**, *118*, 763-776. (i) Tolman,

W. B. *Mech. Bioinorg. Chem.* **1995**, *246*, 195-217. (j) Averill, B. A. *Angew.Chem. Int. Ed. Engl.* **1994**, *33*, 2057-2058. (k) Ruggiero, C. E.; Carrier, S. M.; Antholine, W. E.; Whittaker, J. W.; Cramer, C. J.; Tolman, W. B. *J. Am. Chem. Soc.* **1993**, *115*, 11285-11298. (l) Tolman, W. B. *Inorg. Chem.* **1991**, *30*, 4877-4880. (m) Paul, P. P.; Karlin, K. D. *J. Am. Chem. Soc.* **1991**, *113*, 6331-6332. (n) Lee, W. Z.; Tolman, W. B. *Inorg. Chem.* **2002**, *41*, 5656-5658.

12. (a) Halfen, J. A.; Tolman, W. B. *J. Am. Chem. Soc.* **1994**, *116*, 5475-5476. (b) Carrier, S. M.; Ruggiero, C. E.; Tolman, W. B.; Jameson, G. B. *J. Am. Chem. Soc.* **1992**, *114*, 4407-4408.

13. (a) Berreau, L. M.; Mahapatra, S.; Halfen, J. A.; Houser, R. P.; Young, V. G.; Tolman, W. B. *Angew. Chem. Int. Ed. Engl.* **1999**, *38*, 207-210. (b) Houser, R. P.; Halfen, J. A.; Young, V. G.; Blackburn, N. J.; Tolman, W. B. *J. Am. Chem. Soc.* **1995**, *117*, 10745-10746. (c) Chaudhuri, P.; Wieghardt, K. *Prog. Inorg. Chem.* **1987**, *35*, 329-436. (d) Jia, G. C.; Lau, C. P. *Coord. Chem. Rev.* **1999**, *192*, 83-108. (e) Fry, F. H.; Fischmann, A. J.; Belousoff, M. J.; Spiccia, L.; Brugger, J. *Inorg. Chem.* **2005**, *44*, 941-950. (f) Jazdzewski, B. A.; Reynolds, A. M.; Holland, P. L. Y., Victor G.; Kaderli, S.; Zuberbuehler, A. D.; Tolman, W. B. *J. Biol. Inorg. Chem.* **2003**, *8*, 381-393.

14. Searle, G. H.; Geue, R. J. *Aust. J. Chem.* **1984**, *37*, 959-970.

15. Halfen, J. A., Unpublished work. 1999.

16. Kovacs, Z.; Sherry, A. D. *Tet. Lett.* **1995**, *36*, 9269-9272.

17. Itoh, M.; Hagiwara, D.; Kamiya, T. *Bull. Chem. Soc. Jap.* **1977**, *50*, 718-721.

18. Berreau, L. M.; Halfen, J. A.; Young, V. G.; Tolman, W. B. *Inorg. Chem.* **1998**, *37*, 1091-1098.

19. Elmore, D. T. *Amino Acids, Peptides, and Proteins* **2003**, *34*, 1-53.

20. Shute, R. E.; Rich, D. H. *Tet. Lett.* **1987**, *28*, 3419-3422.

21. Silverstein, R. M.; Webster, F. X.; Kiemle, D. J., *Spectrometric identification of organic compounds*. 7th ed.; John Wiley & Sons: Hoboken, NJ, 2005; p x, 502 p.

22. Mondal, A.; Klein, E. L.; Khan, M. A.; Houser, R. P. *Inorg. Chem.* **2003**, *42*, 5462-5464.

23. Greenberg, A.; Breneman, C. M.; Liebman, J. F., *The amide linkage : selected structural aspects in chemistry, biochemistry, and materials science*. Wiley-Interscience: New York, 2000; p xii, 653 p.

24. (a) Geisser, B.; Konig, B.; Alsfasser, R. *Eur. J. Inorg. Chem.* **2001**, 1543-1549. (b) Schmidt, B.; Ehlert, D. K. *Tet. Lett.* **1998**, *39*, 3999-4002.

25. (a) Garg, B. S.; Nandan Kumar, D.; Sarbhai, M.; Reddy, M. J. *Spectrochim. Acta Sec. A Mol. Biomol. Spectrosc.* **2003**, *59*, 2775-2783. (b) Haidar, R.; Ipek, M.; DasGupta, B.; Yousaf, M.; Zompa, L. J. *Inorg. Chem.* **1997**, *36*, 3125-3132.

26. (a) Cox, C.; Ferraris, D.; Murthy, N. N.; Lectka, T. *J. Am. Chem. Soc.* **1996**, *118*, 5332-5333. (b) Niklas, N.; Heinemann, F. W.; Hampel, F.; Alsfasser, R. *Angew. Chem. Int. Ed. Engl.* **2002**, *41*, 3386-3388. (c) Niklas, N.; Hampel, F.; Liehr, G.; Zahl, A.; Alsfasser, R. *Chem. Eur. J.* **2001**, *7*, 5135-5138. (d) Sibbons, K. F.; Al-Hashimi, M.; Motevalli, M.; Wolowska, J.; Watkinson, M. *Dalt. Trans.* **2004**, 3163-3165.

27. (a) Castellano, E. E.; Piro, O. E.; Casado, N. M. C.; Brondino, C. D.; Calvo, R. *J. Chem. Cryst.* **1998**, *28*, 61-68. (b) Tan, X. S.; Fujii, Y.; Sato, T.; Nakano, Y.; Yashiro, M. *Chem. Comm.* **1999**, 881-882.

28. Addison, A. W.; Rao, T. N.; Reedijk, J.; Vanrijn, J.; Verschoor, G. C. *Dalt. Trans.* **1984**, 1349-1356.

29. Armarego, W. L. F.; Chai, C. L. L., *Purification of laboratory chemicals*. 5th ed.; Butterworth-Heinemann: Amsterdam ; Boston, 2003; p xv, 609 p.

30. Lipscomb, J. D. *Biochemistry* **1980**, *19*, 3590-3599.

31. (a) *X-ray data collection and cell refinement: SMART*, version 5.625; Bruker AXS, Inc.: Madison, WI, 2002. (b) *X-ray data reduction program: SAINT-plus*, version 6.28A; Bruker AXS, Inc.: Madison, WI, 2002.

32. *X-ray structure solution and refinement program: SHELXTL*, version 6.12; Bruker AXS, Inc.: Madison, WI, 1997.

33. *X-ray structure presentation software: Materials Studio*, version 2.1; Accelrys, Inc.: San Diego, CA, 2001.

CHAPTER 3.

SYNTHESIS AND THIOLATE REACTIVITY OF NEW THIOETHER-CONTAINING PYRIDINE AMIDE COPPER(II) COMPLEXES

3.1. *Introduction*

Modelling the active site structure of copper-containing nitrite reductase (CuNiR) through the synthesis of ligands that are covalently linked to His and Cys residues presents difficult synthetic challenges and allows little room for ligand alteration without complete resynthesis (see chapter 2). In an attempt to circumvent such difficulties while simultaneously increasing the overall synthetic potential of our designs, we sought to investigate the possibility of achieving next-generation dinuclear CuNiR model complexes by synthesizing discrete nitrogen- and sulfur-containing ligands that each mimic a certain aspect of the active site structure. These ligand units would join in their coordination to copper ions to form complex structures that could be easily tuned. Thus, instead of first designing and synthesizing a singular covalently-linked ligand and subsequently reacting that ligand with copper, we proposed that our goals could be achieved in a far more elegant manner by minimizing our reliance on covalent linkages altogether.

Beyond CuNiR, the coordination chemistry of copper with sulfur-containing ligands has attracted considerable interest because of its relevance to bioinorganic chemistry in general.[1, 2] Copper thiolate and thioether complexes are of particular interest because of their key roles in a number of ubiquitous metalloproteins such as the type 1 copper (Cu-I) electron transfer sites found in cupredoxins.[1] Cu-I centers contain a copper ion coordinated by a distorted tetrahedral arrangement of $His_2CysMet$ (e.g., plastocyanin[3]), an axially elongated trigonal bipyramidal array of $His_2CysMetGly$ (e.g., azurin[4]), or a distorted trigonal planar array of His_2Cys (e.g., azurin mutants[4]). The cysteine residue donates a thiolate sulfur atom to copper in each case and methionine

donates a thioether sulfur atom in the first two cases. In what can be described as a binuclear version of the Cu-I center, the CuA electron transfer site, found in both cytochrome c oxidase (CcO)[4] and nitrous oxide reductase (N$_2$OR)[5], contains two copper ions bridged by two cysteine thiolates.[6] Copper metallothioneins contain copper(I) ions coordinated exclusively by cysteine thiolate ligands.[7] A methionine thioether sulfur atom and two histidines coordinate to the copper ion in Cu$_B$ from the peptidylglycine α-hydroxylating monooxygenase (PHM) domain of peptidylglycine α-amidating monooxygenase (PAM).[8] Finally, inorganic sulfide is found in the unprecedented catalytic CuZ site from N$_2$OR.[9]

This chapter describes our initial efforts to produce dinuclear CuNiR model complexes by focusing on copper(II) coordination chemistry with new thioether-containing pyridine amide ligands. As an unanticipated consequence of this effort, our investigation into new mixed thiolate/thioether copper(II) complexes with pyridyl, amide, and thioether supporting ligands is also presented along with an unprecedented copper(II)-thiolate redox decomposition mode. Section 3.2 of this chapter describes the ligand syntheses. Copper and zinc complexes are described in sections 3.3 and 3.4, respectively. Finally, thiolate reactions with the copper(II) complexes are described in section 3.5.

3.2.   Ligand Syntheses

The new ligands N-(pyridin-2-ylmethyl)-(methylthio)acetamide (**2-HL^{N2S}**, **1**), N-(pyridin-3-ylmethyl)-(methylthio)acetamide (**3-HL^{N2S}**, **2**), and N-(pyridin-4-ylmethyl)-(methylthio)acetamide (**4-HL^{N2S}**, **3**) were synthesized by DCC-mediated coupling of methylthioacetic acid to 2-, 3-, and 4-picolylamine, respectively (Figure 3-1).[10] The

design of these ligands was modeled after the His-Cys bridge portion of the CuNiR active site that connects the Cu-I and type 2 copper (Cu-II) centers, where the His imidazole and Cys thiolate are substituted with less reactive pyridyl and thioether functionalities to circumvent undesired side reactions in their syntheses and reactions with copper. These His-Cys analogues were envisioned to coordinate between two preformed copper(II) complexes in a similar mode as the actual His-Cys bridge of CuNiR. A similar approach using a pyridyl thiolate ligand bridging between two substituted β-diketiminate copper complexes was independently proposed by the Lee and Tolman.[11] Ideally, one copper ion would coordinate to the pyridyl nitrogen while another would be available for coordination via the methyl thioether sulfur atom and possibly the amide oxygen. Eventually, the thioether and pyridyl groups would be replaced with thiolate and imidizole to more closely match the properties of His and Cys as found in the enzyme.
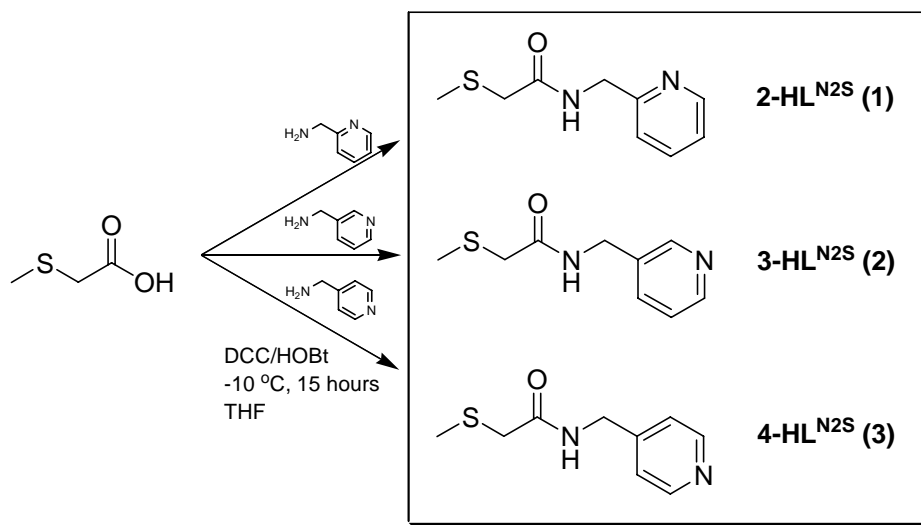
Figure 3-1. Synthesis of 2- HL^{N2S} (**1**), 3- HL^{N2S} (**2**), and 4-HL^{N2S} (**3**).

Ligand 2-HL^{N2S} is nearly identical to ligand ptgH,[12] reported by Nonoyama, *et al.*, differing only in its thioether substituent (methyl vs. ethyl). Although spectroscopic data

for copper(II) complexes of ptgH have been reported, no structural information for complexes of this ligand exist. 2-HL^{N2S} is also related to the N$_3$S(thioether) tetradentate ligand, pygeH, for which structures have been reported,[13, 14] and contains pyridyl and thioether functional groups connected by an amide linkage, providing up to four potential donor atoms: N(pyridine), N(amide), O(amide), and S(thioether). In the case of the closely related *N*-(2-pyridylmethyl)acetamide (2-HL^{N2}), previously reported in our group, copper(II) coordination through all of its potential donor atoms, N(pyridine), N(amide), and O(amide), is observed.[15] 3- and 4-HL^{N2S} differ from 2-HL^{N2S} only in the relative position of their pyridyl nitrogen atoms. Since the position of the nitrogen in the pyridyl ring would likely affect the favored copper coordination mode of each ligand, predictions of their coordination chemistry with copper were difficult to make. Clearly 3- and 4-HL^{N2S} were anticipated to favor a bridging coordination mode more than 2-HL^{N2S} because of their more outward-oriented nitrogens. In addition to these, ligand 2-MeL^{N2S} was synthesized in an attempt to disfavor possible amide nitrogen coordination in copper complexes of 2-HL^{N2S} and to promote a linear coordination mode. With the exception of its tertiary methyl amide, it is identical to 2-HL^{N2S} in all respects. The synthesis of 2-MeL^{N2S} was accomplished in a similar manner as that of **1**, **2**, and **3** by DCC-mediated coupling of (methylthio)acetic acid to *N*-methyl(2-pyridyl)methaneamine[16] (Figure 3-2).
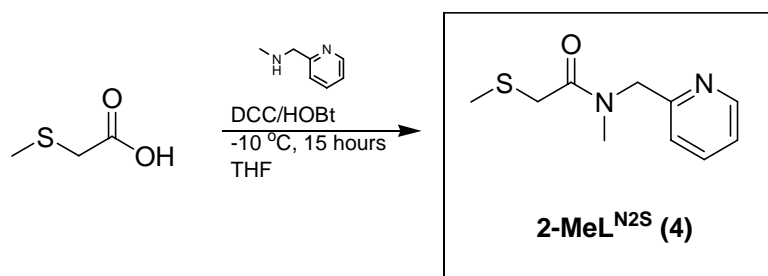
Figure 3-2. Synthesis of 2-MeL^{N2S} (**4**).

3.3. Copper(II) Complexes of 2-HL^{N2S}

3.3.1. [Cu(2-HL^{N2S}*)Cl$_2$]

Prior to using 2-, 3-, or 4-HL^{N2S} in reactions with preformed copper complexes to produce dinuclear bridging species, we sought to first investigate the coordination chemistry of these new ligands directly with copper(II). The reaction of 2-HL^{N2S} with CuCl$_2$·2H$_2$O in methanol results in the immediate formation of a deep blue solution (Figure 3-3). X-ray quality crystals of the product were obtained in good yield by
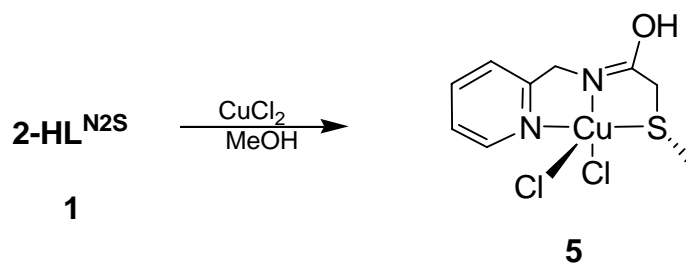
Figure 3-3. Synthesis of [Cu(2-HL^{N2S}*)Cl$_2$] (**5**).

diffusing diethyl ether into the concentrated reaction mixture in a tightly capped vial. The X-ray crystal structure of **5** clearly reveals that the copper(II) ion is coordinated by the tautomeric form of 2-HL^{N2S}, designated 2-HL^{N2S}*, via its N(pyridine), N(imidic acid), and S(thioether) donors in three basal plane positions of the square pyramidal complex (τ = 0.02) (Figure 3-4).[17, 18] The fourth basal position and one axial position are occupied by chloride ligands. The imidic acid form of 2-HL^{N2S} is evident in its relatively short C7-N2 and long C7-O1 bond distances as well as in the presence of the hydrogen atom, H1, that is covalently bonded to O1. The imidic acid proton of each molecule forms hydrogen bonds to chloride ligands of neighboring monomeric units in the crystal structure.
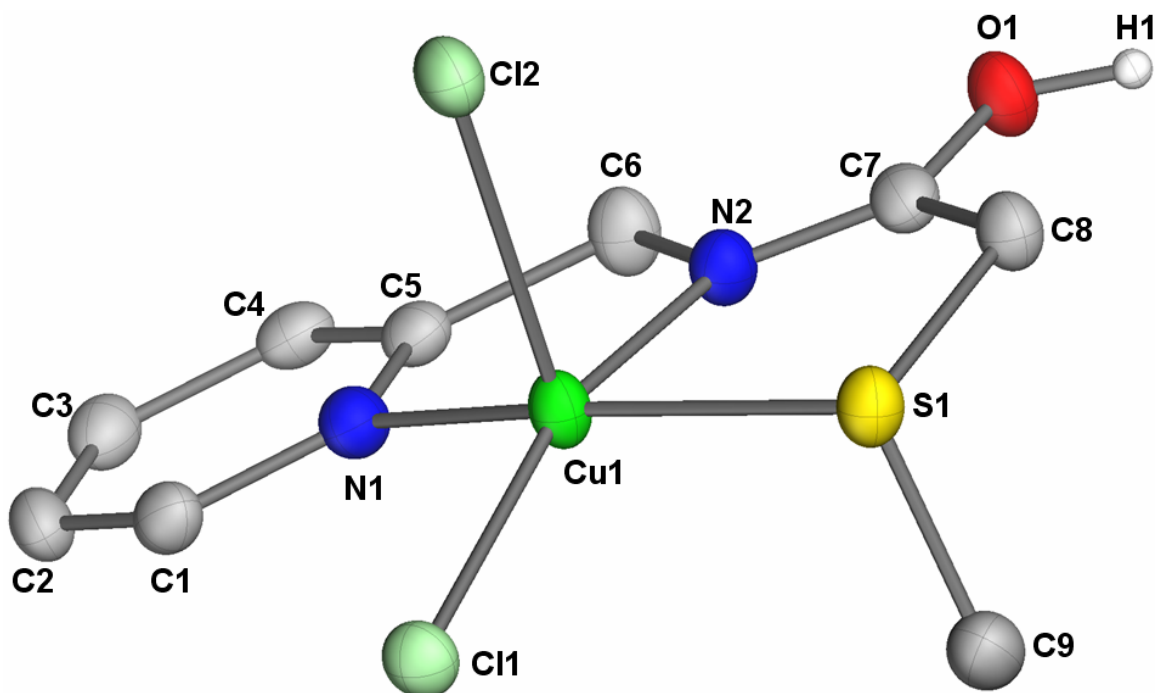
Bond Lengths (Å)		Angles (deg)	
Cu1–N1	2.015(3)	N1–Cu1–N2	82.0(1)
Cu1–N2	1.950(3)	N1–Cu1–Cl1	96.9(1)
Cu1–S1	2.367(1)	S1–Cu1–N2	84.1(1)
Cu1–Cl1	2.237(1)	S1–Cu1–Cl1	93.3(3)
Cu1–Cl2	2.648(1)	N1–Cu1–Cl2	103.9(1)
N2–C7	1.277(4)	N2–Cu1–Cl2	97.1(1)
C7–O1	1.318(4)	S1–Cu1–Cl2	97.4(3)
		Cl1–Cu1–Cl2	100.9(3)
		N1–Cu1–S1	163.1(1)
		N2–Cu1–Cl1	161.7(1)

Figure 3-4. Representation of the X-ray crystal structure of [Cu(2-HL^{N2S}*)Cl$_2$] (**5**) as 50% thermal ellipsoids. H atoms other than the imidic acid H1 have been omitted for clarity. Selected bond distances (Å) and angles (deg) relevant to copper coordination and amide group are tabulated.

The UV-vis spectrum of **5** is typical for a copper(II) complex with nitrogen, chloride, and thioether sulfur ligands in a square pyramidal geometry (Figure 3-5).[19] The spectrum exhibits a characteristic Ligand-to-Metal-Charge Transfer (LMCT) transition at 655 nm with an extinction coefficient of 140 $M^{-1}cm^{-1}$.
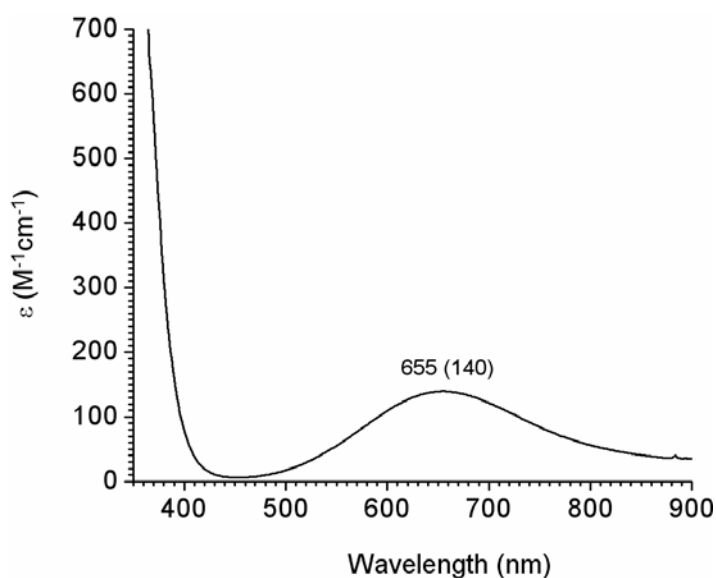
Figure 3-5. UV-vis spectrum of $[Cu(2-HL^{N2S}*)Cl_2]$ in H_2O.

The X-band EPR spectrum of **5** provides more information about its nature in the solution phase (Figure 3-6). The sample for this experiment was prepared by dissolving clean X-ray quality crystals of **5** in 1:1 CH_2Cl_2/MeOH and was measured at 120 K. Interestingly, two overlapping axial copper(II) hyperfine signals are observed, suggesting the presence of two unique copper(II) species in solution. The more intense signal, centered at $g = 2.19$, shows a copper(II) hyperfine splitting of 170×10^{-4} cm^{-1}. The other signal, centered at $g = 2.42$ has a slightly smaller copper(II) hyperfine splitting of 121×10^{-4} cm^{-1}. The parameters for the latter signal exactly match that of a pure solvated

cupric chloride solution under identical conditions, indicating significant dissociation of copper(II) from the ligand upon dissolution. This observation was rationalized by considering the acidic nature of the ligand itself, especially in the imidic acid form, and the low binding affinity of pyridyl for copper(II) ions under acidic conditions. Indeed, the pH of this solution was measured to be 3.71, favoring equilibrium toward pyridyl protonation and ligand dissociation.
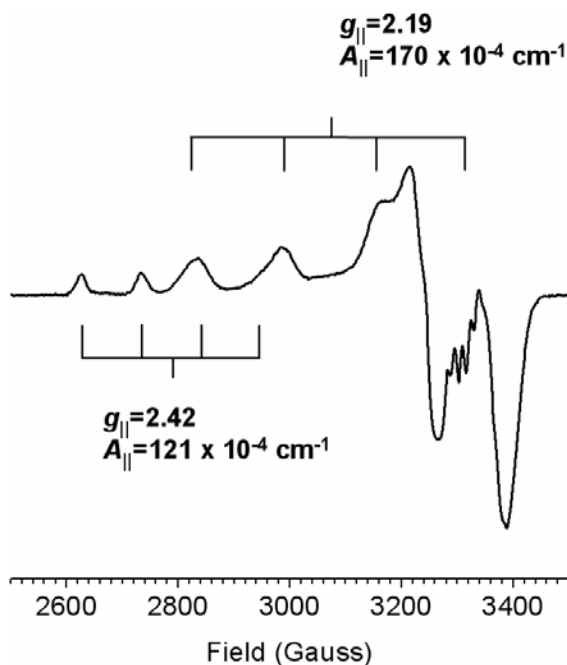
Figure 3-6. Experimental EPR spectrum of [Cu(2-HL^{N2S}*)Cl$_2$] in 1:1 CH$_2$Cl$_2$/MeOH at 120 K and a microwave frequency of 9.43 GHz.

3.3.2. [Cu(2-L^{N2S})Cl(CH$_3$OH)]

Despite the observation that 2-HL^{N2S} readily tautomerizes upon coordination to free copper(II) ions, its original design function as a His-Cys analogue bridging unit

remained our primary interest. As an initial test of its ability to perform in this role, a methanol solution of 2-HL^{N2S} was combined with two equivalents of a rapidly stirring solution of [Cu(iPr$_3$TACN)Cl$_2$]^{20} in the same solvent (Figure 3-7). The reaction mixture changed from the bright green color of pure [Cu(iPr$_3$TACN)Cl$_2$] to a very dark shade of blue similar to that of **5** over the course of 30 minutes. Slow evaporation of the solvent from the reaction mixture afforded deep blue X-ray quality crystals and a small amount of pale yellow residue on the vial walls. ^{1}H NMR and COSY of the pale yellow residue were sufficient to identify that substance as containing iPr$_3$TACN. The blue crystals were submitted for X-ray analysis.
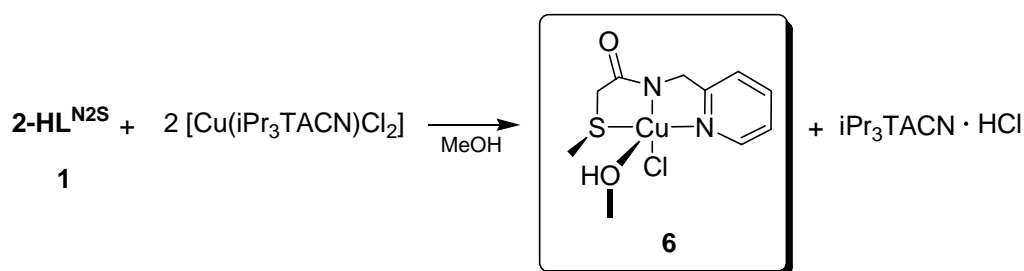
Figure 3-7. Synthesis of [Cu(2-L^{N2S})Cl(CH$_3$OH)] (**6**) by reaction of 2-HL^{N2S} with [Cu(iPr$_3$TACN)Cl$_2$].

The X-ray crystal structure of the blue product, [Cu(2-L^{N2S})Cl(MeOH)] (**6**), is similar to that of **5** in that the ligand coordinates to copper(II) in the three basal plane positions of the distorted square pyramidal complex via its N(pyridyl), N(amidate), and S(thioether) donors (Figure 3-8). Instead of 2-HL^{N2S} acting in a bridging coordination motif between the two [Cu(iPr$_3$TACN)Cl$_2$] complexes, however, it surprisingly abstracts the copper(II) ion from [Cu(iPr$_3$TACN)Cl$_2$]. Moreover, 2-HL^{N2S} becomes deprotonated

at its amide nitrogen, converting the liberated iPr$_3$TACN to its monohydrochloride salt. The charge of the copper(II) ion in **6** is balanced by the anionic 2-L^{N2S} ligand and a single equatorial chloride ligand. Unlike **5**, where the ligand is neutral and two chloride ligands are coordinated, methanol solvent serves as the axial ligand in **6**. The same product can be obtained with much higher efficiency by reaction of a stoicheometric quantity of 2-HL^{N2S} with CuCl$_2$·2H$_2$O in the presence of excess triethylamine.

With the exception of the axial ligands, the bond distances and angles around the copper atoms in **5** and **6** are very similar. The axial Cu1-O1 bond distance in **6** is more than 0.3 Å shorter than the Cu1-Cl2 distance in **5**. This shorter axial bond length in **6** is accompanied by a shifting of the copper atom out of the basal plane, giving rise to a larger τ value of 0.21.[17] The tautomeric relationship of the ligands in **5** and **6** is illustrated quantitatively by their C-N and C-O bond distances, which support the assignment of the imidic acid form of the ligand in **5** and the amidate form of the ligand in **6**. Although no structural data has been reported for the copper(II) complexes of the very similar ptgH ligand reported by Nonoyama, IR studies of those complexes also support the assignment of amidate and imidic acid ligand tautomers and the relationship between [Cu(ptgH)Cl$_2$] and [Cu(ptg)Cl] is proposed.[12] The spectroscopic features reported for the ptgH complexes mirror those of **5** and **6**. It is also noteworthy that **6** is structurally and spectroscopically similar to [Cu(pyge)Br].[14] With the exception of the axial Cu(II)-ligand bond and the Cu(II)-halide bonds, the solid state structural parameters for **6** and [Cu(pyge)Br] are nearly identical. While the structure of **6** is a slightly distorted square pyramid (τ = 0.21), [Cu(pyge)Br] has a τ value of 0.01,[14] making it a nearly ideal square pyramid.
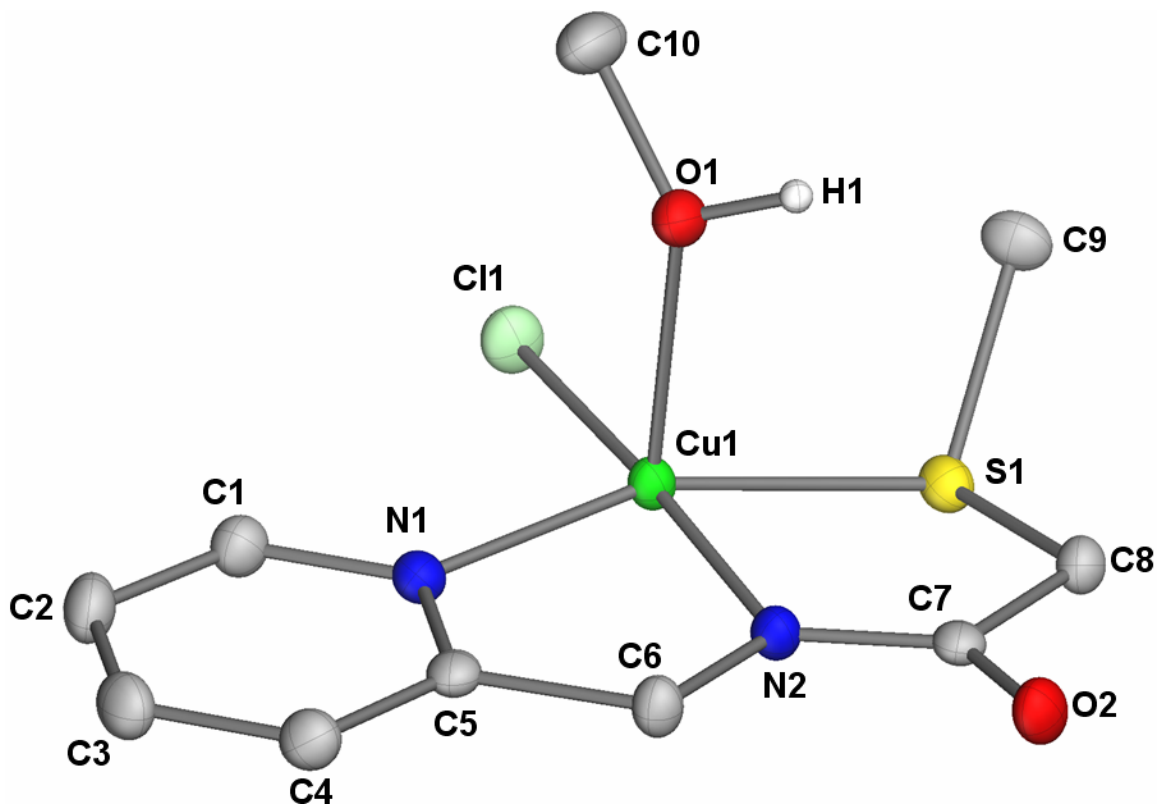
Bond Lengths (Å)		Angles (deg)	
Cu1–N1	2.019(1)	N1–Cu1–N2	82.3(1)
Cu1–N2	1.932(1)	N1–Cu1–Cl1	98.4(1)
Cu1–S1	2.332(1)	S1–Cu1–N2	84.1(1)
Cu1–Cl1	2.238(1)	S1–Cu1–Cl1	93.4(1)
Cu1–O1	2.329(1)	N1–Cu1–O1	93.7(4)
N2–C7	1.318(2)	N2–Cu1–O1	90.0(4)
C7–O2	1.252(2)	S1–Cu1–O1	100.5(1)
		Cl1–Cu1–O1	96.7(1)
		N1–Cu1–S1	160.3(1)
		N2–Cu1–Cl1	173.2(1)

Figure 3-8. Representation of the X-ray crystal structure of [Cu(2-L^{N2S})Cl(MeOH)] (**6**) as 50% thermal ellipsoids. H atoms other than methanol H1 have been omitted for clarity. Selected bond distances (Å) and angles (deg) relevant to copper coordination and the amide group are tabulated.

The UV-vis spectrum of **6** in methanol is nearly identical to that of **5** (Figure 3-9). A distinctive LMCT transition appears at 642 nm with an extinction coefficient of 236 $M^{-1}cm^{-1}$. While the UV-vis of **5** arguably shows the equilibrium with solvated copper(II) in its low energy shoulder, there is no indication of more than a single chromophore in the UV-vis spectrum of **6**.
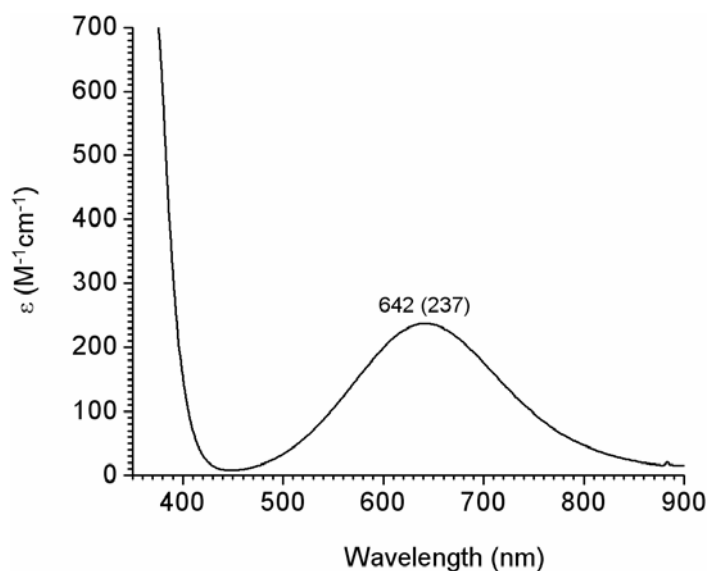
Figure 3-9. UV-vis spectrum of [Cu(2-L^{N2S})Cl(MeOH)] in MeOH.

Corroborating these observations, the X-band EPR spectrum of **6**, also prepared from X-ray quality crystals of the compound dissolved in 1:1 CH_2Cl_2/MeOH, shows a single axial signal (Figure 3-10). The $g_{\parallel}$ and $A_{\parallel}$ values for **6** ($g_{\parallel}$ = 2.19 and $A_{\parallel}$ = 170 x 10^{-4} cm^{-1}) are identical to those of the higher intensity signal in the EPR spectrum of **5** under the same conditions, suggesting that **5** and **6** are identical in solution. In contrast to **5**, no additional copper(II) signal is observed in the spectrum of **6** due to its higher pH of 6.43. Lending further credence to this argument, direct addition of triethylamine to solutions of **5** results in spectroscopic features that are identical to those of **6** without any
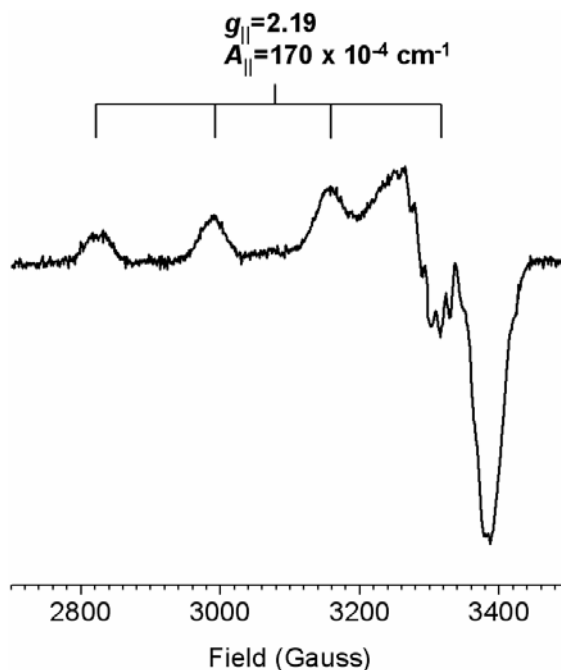
Figure 3-10. Experimental EPR Spectrum of $[Cu(2\text{-}L^{N2S})Cl(MeOH)]$ in 1:1 $CH_2Cl_2/MeOH$ at 120 K and a microwave frequency of 9.43 GHz.

detectable signal for solvated copper(II). Conversely, addition of dilute hydrochloric acid solutions to either **5** or **6** results in concomitant ligand dissociation and release of copper(II), as evidenced by the resulting EPR and UV-vis spectra where only solvated copper(II) is detected. Based on this evidence, it is clear that **5** and **6** are identical in solution and that the imidic acid form of the ligand, as in **5**, is stabilized only in the solid state.

Reactions of ligands 3- and 4-HL^{N2S} with cupric chloride or cupric triflate gave very different results than the reactions described above with 2-HL^{N2S}. In both cases, an insoluble green powder was obtained, regardless of the presence of base. Despite repeated efforts, we were neither able to obtain X-ray quality crystals of these products

nor conclusively characterize their structures due to their very low solubility. Reactions of 3- and 4-HL^{N2S} with [Cu(iPr$_3$TACN)Cl$_2$] were fraught with similar difficulties.

3.3.   Synthesis and Characterization of [Zn(2-MeL^{N2S})Cl$_2$]

Ligand 2-MeL^{N2S} was designed and synthesized as an analogue of 2-HL^{N2S} that would be physically incapable of amidate or imidic acid nitrogen coordination. With its tertiary methyl amide, it was hoped that 2-MeL^{N2S} would favor a bridging copper(II) coordination mode rather than a 1:1 square pyramidal complex like **5** or **6**. Unlike 2-HL^{N2S}, 2-MeL^{N2S} proved to be a poor copper(II) ligand and no structural information was obtained for comparison of its copper coordination chemistry with that of the other ligands. The reaction of 2-MeL^{N2S} with ZnCl$_2$ in methanol, however, gave X-ray quality crystals of [Zn(2-MeL^{N2S})Cl$_2$] (**7**) (Figure 3-11). As anticipated, the X-ray crystal structure of **7** confirmed the complete inability of the amide nitrogen to coordinate the metal ion (Figure 3-12). Instead, the amide is rotated 180° and coordinates via its carbonyl oxygen, forcing the thioether sulfur away from the metal ion and hindering its ability to coordinate. In addition to the N(pyridyl) and O(amide) donor atoms from 2-MeL^{N2S}, the coordination sphere of the tetrahedral zinc(II) ion is completed by two chloride anions.
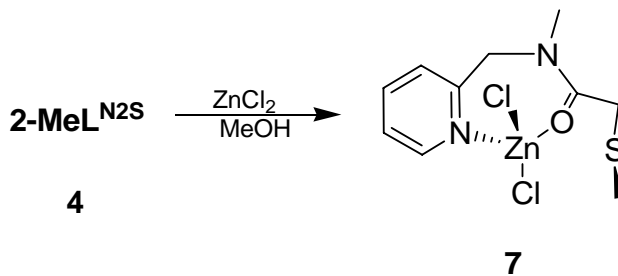
Figure 3-11. Synthesis of [Zn(2-MeL^{N2S})Cl$_2$] (**7**).
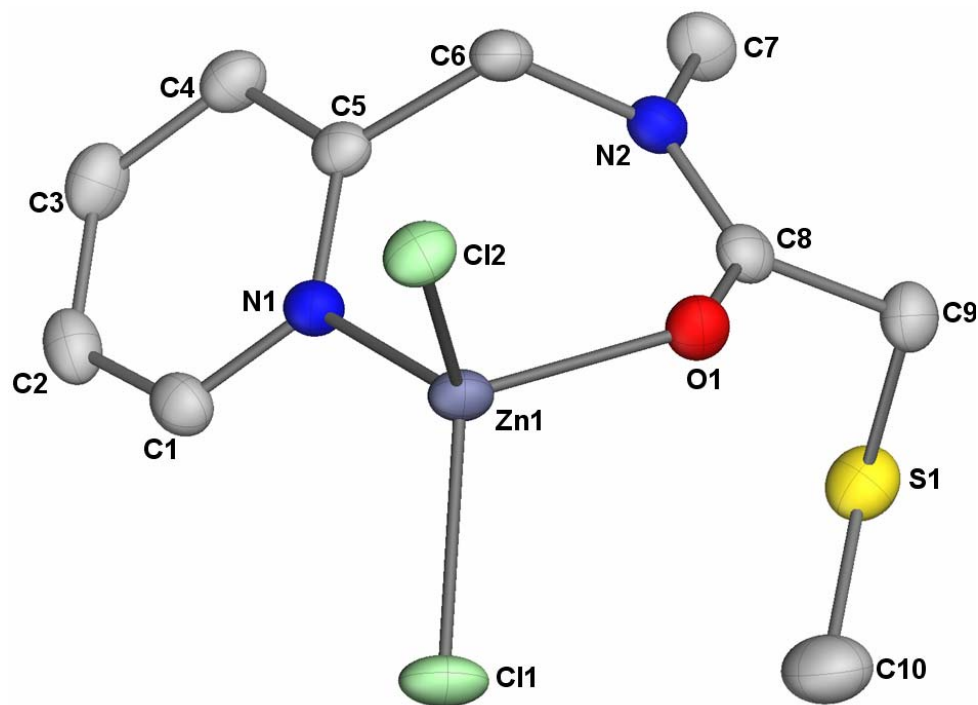
Bond Lengths (Å)		Angles (deg)	
Zn1–N1	2.039(1)	N1–Zn1–Cl1	82.0(1)
Zn1–O1	2.013(1)	N1–Zn1–Cl2	96.9(1)
Zn1–Cl1	2.212(1)	N1–Zn1–O1	84.1(1)
Zn1–Cl2	2.209(1)	O1–Zn1–Cl1	93.3(3)
		O1–Zn1–Cl2	103.9(1)
		Cl1–Cu1–Cl2	97.1(1)

Figure 3-12. Representation of the X-ray crystal structure of [Zn(2-MeL^{N2S})Cl$_2$] (**7**) as 50% thermal ellipsoids. H atoms have been omitted for clarity. Selected bond distances (Å) and angles (deg) relevant to zinc coordination are tabulated.

3.5. *[Cu(2-L^{N2S})Cl(CH$_3$OH)] Thiolate Reactivity*

Despite our difficulties with these ligands with respect to their intended purposes, the similarity of the N$_2$S(thioether) ligand set in **6** to the His$_2$Met ligand set of the Cu-I site in azurin, for example, prompted us to attempt the synthesis of thiolate complexes of **6**. Success with this approach would potentially lead to the development of new neutral

models of the Cu-I electron transfer center. To this end, methanol solutions of **6** were treated with thiols 2,6-dimethylthiophenol (HSAr) or tritylthiol (HSCPh$_3$) at -80 °C in the presence of triethylamine for *in situ* thiol deprotonation.[21] Alternatively, **6** could also be treated using the sodium thiolate salts of HSAr[22] and HSCPh$_3$[23] without addition of triethylamine to give the same results (Figure 3-13). These reactions all occur spontaneously and are accompanied by dramatic color changes of their respective solutions from the deep blue of **6** to scarlet red for **6**(SAr) and to dark green for **6**(SCPh$_3$).
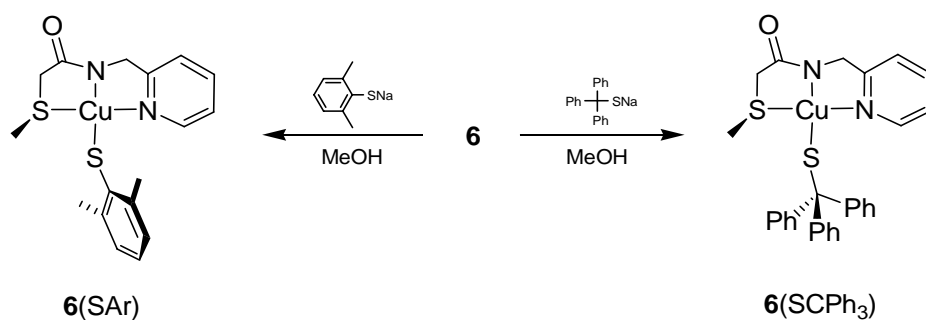
Figure 3-13. Syntheses of **6**(SAr) and **6**(SCPh$_3$).

Rather than forming stable complexes, **6**(SAr) and **6**(SCPh$_3$) both undergo spontaneous redox decomposition at room temperature. In this process, the thiolate sulfur is oxidized to disulfide, reducing copper(II) to copper(I) in the process. The redox decomposition of **6**(SCPh$_3$) also produces a white powder precipitate during the course of its decomposition, *vide infra*.

The redox decomposition of copper(II)-thiolates is well precedented in the literature and results in the complete bleaching of intensely colored copper(II) solutions as the reaction proceeds.[24, 25] Interestingly, reactions of **6**(SAr) and **6**(SCPh₃) appear to progress to only one-half completion and return half of **6** unreacted. Addition of a full second equivalent of thiolate is required to completely bleach these solutions. Since only one equivalent of thiolate per copper(II) should be sufficient to reduce all of the copper(II) ion in a normal redox decomposition, the requirement for two thiolate equivalents per copper(II) in our reactions was puzzling and unprecedented, demanding further investigation. While **6**(SCPh₃) has a half-life of about 90 minutes at room temperature, **6**(SAr) decomposes within one minute under the same conditions. In either case, the high instability of these complexes at room temperature renders them undesirable candidates as potential Cu-I models. Because of its higher relative stability, however, the decomposition of **6**(SCPh₃) was chosen for a more thorough investigation of its interesting redox behavior described above.

The UV-vis spectrum of **6**(SCPh₃), obtained in THF immediately after thiolate addition to **6**, shows a high intensity transition at 428 nm (Figure 3-14). The extinction coefficient of this transition is 2618 $M^{-1}cm^{-1}$ and lies in the characteristic range for a typical thiolate-copper(II) LMCT transition, strongly supporting its assignment as such.[22] A second transition at 555 nm is also evident in this spectrum with an extinction coefficient of 460 $M^{-1}cm^{-1}$ and is attributed to a second thiolate-copper(II) LMCT and/or a N(pyridine) $\rightarrow$ Cu(II) LMCT as observed for pure **6**.[1]

The redox decomposition of **6**(SCPh₃), followed in the same UV-vis spectrum, was observed to proceed cleanly as per the isosbestic point at 338 nm. While the

S(thiolate) → Cu(II) LMCT band at 428 nm completely diminishes, the 555 nm transition undergoes a red shift of about 50 nm with the final spectrum corresponding exactly to the spectrum of **6** in the same solvent. Additionally, the amount of **6** remaining after the redox decomposition was quantified by its extinction coefficient as exactly half of the original amount of **6** introduced into the reaction originally. Conclusive identification was achieved by X-ray crystallographic analysis of remaining **6** recrystalized from the decomposition mixture.
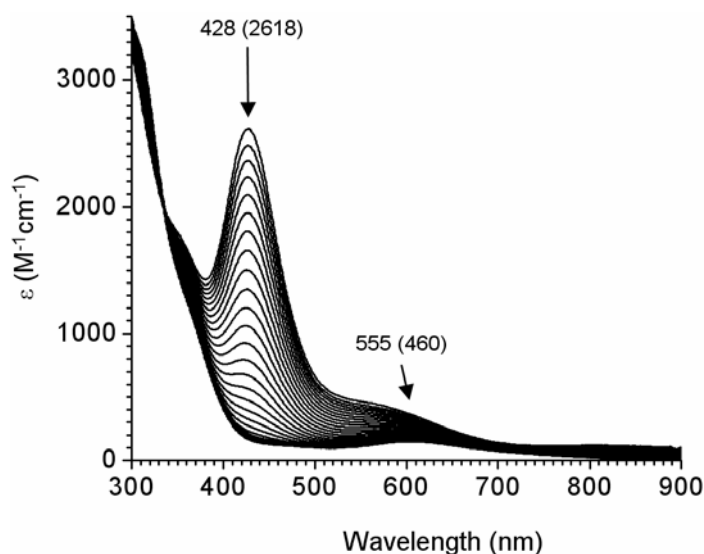
Figure 3-14. UV-vis spectrum of **6**(SCPh$_3$) in methanol at 25 $^{\circ}$C. Individual scans showing the redox decomposition were measured at 10 minute intervals.

Characterization of the white precipitate that formed during the reaction was also performed. Unfortunately, all efforts to dissolve this powder result in its rapid decomposition to an insoluble brown solid within minutes. Ultimately, the empirical formula of the white powder was determined by elemental analysis to be [Cu(SCPh$_3$)] (Anal calcd for C$_{19}$H$_{15}$CuS: C, 67.33; H, 4.46, N, 0.00; S, 9.46. Found: C, 67.58; H, 4.85;

N, 0.17; S, 9.43). ^{1}H NMR of the powder in d_8-THF, obtained immediately after dissolving the sample, confirmed this assignment. Additionally, gravimetric analysis of the collected powder accounts for exactly 50% of the original copper ions and half of the HSCPh$_3$. A mixture of organic products, including the remaining half of the HSCPh$_3$ in the form of disulfide, was separated from the decomposition solution by flash column chromatography and characterized by NMR and GC-MS. When a second equivalent of thiolate is titrated into the remaining **6** in the decomposition mixture, all of the Cu(II) is reduced as indicated by the complete bleaching of the solution and formation of more [Cu(SCPh$_3$)]. In this case, the excess thiolate added to the solution is sequestered by copper(I) instead of from unreacted **6**(SCPh$_3$). The absence of any observable features in the UV-vis or EPR after this decomposition confirms the nonexistence of any detectable quantities of Cu(II).

3.6. Conclusions

The new ligands 2-, 3-, and 4-HL^{N2S} were prepared by DCC-mediated coupling of (methylthio)acetic acid to 2-, 3-, or 4-picolylamine. 2-HL^{N2S} tautomerizes to its imidic acid form upon coordination to cupric chloride in methanol. Under basic conditions, 2-HL^{N2S} becomes deprotonated and mono-anionic with a high affinity for copper(II) as evidenced by its ability to sequester copper(II) directly from normally robust [Cu(iPr$_3$TACN)Cl$_2$] complexes. The formation of the amidate is facilitated by the thioether coordination, forcing the amide nitrogen to strongly interact with the copper(II) ion. The methylated amide variant of this ligand, 2-MeL^{N2S}, does not have a high affinity for copper(II), but readily complexes zinc(II). X-ray structural analysis of this complex reveals amide carbonyl and pyridyl coordination to the metal ion. The orientation of the

amide, however, forces the thioether away from the metal center, preventing sulfur coordination. Reactions of 3- and 4-HL^{N2S} with cupric chloride or cupric triflate form insoluble green products. Although no structural information for these products has been determined to date, their known properties, particularly their low solubility, lend credence to the notion that they are highly stable coordination polymers.

With the notable exceptions of several stable copper(II) and mixed valence copper thiolate complexes,[23, 26] copper(II) thiolates are readily reduced to copper(I) with concomitant oxidation of thiolate to disulfide.[25] Our preliminary experiments, however, show that the decompositions of **6**(SAr) and **6**(SCPh$_3$) proceed by an alternate pathway. When solutions of **6**(SCPh$_3$) or **6**(SAr) are allowed to equilibrate at room temperature, their color does not fully bleach, but remains the blue color of the starting material, **6**. From extensive spectroscopic, X-ray crystallographic, and gravimetric analysis studies, it is apparent that only half of the copper(II) is reduced per equivalent of thiolate, leaving the remainder unchanged as **6**. Furthermore, only half of the thiolate is oxidized to disulfide. These data are consistent with the reactions illustrated in equations 1 and 2, where the relatively slow redox formation of copper(I) is followed by a fast step where the copper(I) sequesters the thiolate from remaining **6**(SCPh$_3$), producing [Cu(SCPh$_3$)] and liberated **6**. Consequently, these one-electron reactions require two full equivalents of thiolate to reduce all of the copper(II) since one equivalent of thiolate is rapidly sequestered by generated copper(I).

$$Cu^{II}(2\text{-}L^{N2S})(SCPh_3) \xrightarrow{\text{slow}} Cu^{I} + (SCPh_3)_2 + 2\text{-}HL^{N2S} \qquad (1)$$

$$Cu^{I} + Cu^{II}(2\text{-}L^{N2S})(SCPh_3) \xrightarrow{\text{fast}} Cu^{I}(SCPh_3) + Cu^{II}(2\text{-}L^{N2S}) \qquad (2)$$
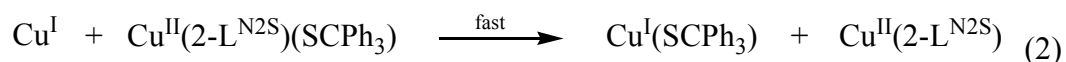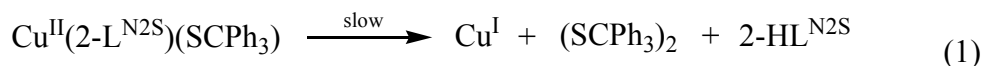
In summary, although the ligands described in this work did not adequately perform their intended design roles as His-Cys bridge analogues to yield dinuclear models of the CuNiR active site, interesting copper(II) and zinc(II) complexes were synthesized and characterized that may have relevance to various biological sites. Finally, a new mode of copper(II)-thiolate redox decomposition has been discovered where two equivalents of thiolate are required to fully reduce a single equivalent of copper(II).

3.7. *Experimental*

General. All reagents were purchased from commercial sources and used without additional purification unless otherwise noted. Solvents were dried and purified under nitrogen using standard methods. Et$_2$O, THF, and pentane were distilled over NaK$_2$ alloy, CH$_3$CN and CH$_2$Cl$_2$ over CaH$_2$, MeOH over Mg(OMe)$_2$, and toluene over Na. Degassing of the dried solvents was achieved by triple freeze-pump-thaw degas cycles. Oxygen- and/or water-sensitive reactions were carried out using Schlenk vacuum line techniques and/or by using an M. Braun UNILab inert atmosphere glovebox with nitrogen as its working gas. Preparative procedures for the syntheses of [Cu(iPr$_3$TACN)Cl$_2$] and *N*-methyl(2-pyridyl)methaneamine are published elsewhere.[16, 27]

Spectroscopy. Infrared (IR) spectra were prepared by pressing the sample into a KBr "glass" and were collected using a Nicolet NEXUS 470 FTIR spectrophotometer coupled to a computer running OMNIC E.S.P (version 5.1) software for spectrum display, background baseline correction, scaling, and automatic peak-picking. Unless otherwise stated, samples for electronic absorption (UV-vis) spectroscopy were prepared at 5 mM concentrations in a 5 mL 1.00 cm path length quartz cuvette. UV-vis data were

obtained using a Shimadzu UV2401PC UV-vis spectrophotometer capable of a 200 - 1100 nm scan range and having a dedicated variable temperature Neslab RTE-140 circulating heater/chiller and computer interface running Shimadzu UV Probe (v. 1.00) for instrument control and spectrum display. All UV-vis spectra were obtained at 298.0 K unless otherwise noted. ^{1}H and ^{13}C NMR spectra were measured at room temperature on a Varian 300 MHz (Mercury) spectrometer or a Varian 400 MHz spectrometer coupled to the Varian VNMR software package. Solvent was used as an internal chemical shift standard unless otherwise stated. All signals are reported in ppm relative to the reported value(s) for the solvent. X-band (~9.45 GHz) EPR spectra were obtained using a Bruker EMX spectrometer fitted with a either a liquid nitrogen finger dewer or a liquid nitrogen cryostat (BVT-3000). Temperature and *g* value calibrations were performed as described.[28]

Physical Methods. Capillary Gas Chromatography Mass Spectrometry (GC-MS) analyses were performed in a Trace GC 2000 and Thermoquest GCQ/Polaris mass spectrometer (ThermoQuest Finnigan, San Jose, CA). The software controlling the system was Xcalibur (version 1.1) from ThermoQuest Finnigan. Electron impact (EI) was the ionization source and the typical electron energy was set to 70 eV with the ion source temperature maintained at 200 °C. The instrument was calibrated with the perfluorotributyl amine FC-43 over a *m/z* range of 50-650 Da. Organic components were separated in an Alltech-ECCNO-OAP (30 m x 0.25 mm x 0.25 μm). The injector temperature was set at 210 °C and a splitless mode of injection was used in all analyses. The GC temperature gradient was set to 50 °C, holding for 5 minutes, then increased at 20 °C/minute to 250 °C holding for 20 minutes. The GC system was run at a constant

flow rate of 1.0 mL/minute of helium gas (Minimum Purity 99.999%). ElectroSpray Ionization Mass Spectrometry (ESI-MS) data were recorded using a Q-TOF quadrupole time-of flight mass spectrometer (Micromass, Manchester, UK) equipped with a Z-spray electrospray ionization (ESI) source. The software controlling the instrument was MassLynx (version 4.0). A Harvard syringe pump (Harvard Apparatus, South Natick, MA, USA) was used to deliver the sample solution to the electrospray source at a flow rate of 5 μl/min. The electrospray capillary voltage was set at 3000 V and the cone voltage was typically set to 30 V. The temperature for desolvation and source was set to 90 ^{o}C. The desolvation gas (nitrogen, 99.99%) flow rate was set to 250 liters per hour. Nebuliser gas flow was set to 20 liters per hour. The mass spectrometer was calibrated over a mass range of 50-1500 Da using a 0.05 μg/μL CsI and 2 μg/μL NaI solution in methanol.

N-(pyridin-2-ylmethyl)-(methylthio)acetamide (2-HL^{N2S}, 1). A solution of (methylthio)-acetic acid (1.00 g, 9.42 mmol), HOBt (1.53 g, 11.3 mmol), and 2-(aminomethyl)-pyridine (1.02 g, 9.43 mmol) in 20 mL THF was cooled to -10 °C in an ice/salt bath. *N,N*-Dicyclohexylcarbodiimide monohydrate (DCC·H$_2$O) (2.33 g, 11.3 mmol) was dissolved in a minimal volume of THF, cooled to -10 °C, and added in one portion to the (methylthio)acetic acid solution. The resulting mixture was stirred at -10 °C for 1 hour and then allowed to warm to room temperature. Stirring was continued at room temperature for 15 hours. The reaction mixture was then cooled to -40 °C and the DCU suspension was filtered off. The filtrate was concentrated *in vacuo* and the desired product was distilled from the reaction byproducts using a Kugelrohr distillation

apparatus (170 °C, 0.18 torr). The product was stored at -45 °C (1.64 g, 90 %). ^{1}H NMR

(CDCl$_3$, 300 MHz): δ 8.48 (d, J = 4.7 Hz, 1H), 7.96 (s, 1H), 7.56 - 7.66 (m, 1H), 7.10 -

7.26 (m, 2H), 4.55 (d, J = 5.22 Hz, 2H), 3.22 (s, 2H), 2.11 (s, 3H) ppm. ^{13}C{^{1}H} NMR: δ

168.47, 156.02, 148.78, 136.48, 122.13, 121.66, 44.53, 37.95, 16.29 ppm. FTIR (KBr,

cm^{-1}): 3063, 2927, 2854, 1652 (υ_{CO}), 1221, 757. GC/MS: t$_R$ 14.14 min; m/z (relative

intensity) 196 (1, M$^+$), 92 (100). Anal. Calcd for C$_9$H$_{12}$N$_2$OS: C, 55.08; H, 6.16; N,

14.27. Found: C, 54.85; H, 6.54; N, 13.71.

N-(pyridin-3-ylmethyl)-(methylthio)acetamide (3-HL^{N2S}, 2).   A   solution   of

(methylthio)-acetic acid (2.00 g, 18.8 mmol), HOBt (3.06 g, 22.6 mmol), and 3-

(aminomethyl)-pyridine (2.04 g, 18.8 mmol) in 20 mL THF was cooled to -10 °C in an

ice/salt bath. N,N-Dicyclohexylcarbodiimide monohydrate (DCC·H$_2$O) (2.66 g, 22.6

mmol) was dissolved in a minimal volume of THF, cooled to -10 °C and added in one

portion to the (methylthio)acetic acid solution. The resulting mixture was stirred at -10

°C for 1 hour and then allowed to warm to room temperature. Stirring was continued at

room temperature for 15 hours. The reaction mixture was then cooled to -40 °C and the

DCU suspension was filtered off.   The filtrate was concentrated in $vacuo$ and the

remaining oil-solid mixture was separated by Kugelrohr distillation (170 C, 0.05 torr).

The desired product was obtained as a yellow oil in the Kugelrohr collection flask (2.58

g, 70 %). ^{1}H NMR (CDCl$_3$, 300 MHz): δ 7.10 – 8.42 (m, 5H), 4.35 (d, J=6.00 Hz, 2H)

3.19 (s, 2H), 1.98 (s, 3H) ppm. ^{13}C{^{1}H} NMR: δ 169.52, 148.95, 148.64, 135.88, 134.42,

123.86, 41.23, 37.97, 16.48 ppm. Anal. Calcd for C$_9$H$_{12}$N$_2$OS: C, 55.08; H, 6.16; N,

14.27. Found: C, 55.88; H, 6.22; N, 15.34.

***N*-(pyridin-4-ylmethyl)-(methylthio)acetamide** **(4-HL^{N2S}**, **3**). A solution of (methylthio)acetic acid (2.00 g, 18.8 mmol), HOBt (3.06 g, 22.6 mmol), and 4-(aminomethyl)-pyridine (2.04 g, 18.8 mmol) in 20 mL THF was cooled to -10 °C in an ice/salt bath. *N,N*-Dicyclohexylcarbodiimide monohydrate (DCC·H$_2$O) (2.66 g, 22.6 mmol) was dissolved in a minimal volume of THF, cooled to -10 °C and added in one portion to the (methylthio)acetic acid solution. The resulting mixture was stirred at -10 °C for 1 hour and then allowed to warm to room temperature. Stirring was continued at room temperature for 15 hours. The reaction mixture was then cooled to -40 °C and the DCU suspension was filtered off. The filtrate was concentrated *in vacuo* and the remaining oil-solid mixture was separated by Kugelrohr distillation (170 C, 0.05 torr). The desired product was obtained as a yellow oil in the Kugelrohr collection flask (2.50 g, 68 %). ^{1}H NMR (CDCl$_3$, 300 MHz): δ 7.18 – 8.38 (m, 5H), 4.41 (d, *J*=6.15 Hz, 2H) 3.17 (s, 2H), 2.02 (s, 3H) ppm. ^{13}C{^{1}H} NMR: δ 170.24, 150.83, 147.77, 123.24, 42.59, 37.92, 16.60 ppm. GC/MS: t$_R$ 15.0 min; m/z (relative intensity) 196 (5, M+), 150 (100).

***N*-Methyl-2-methylsulfanyl-*N*-pyridin-2-ylmethyl-acetamide** **(2-MeL^{N2S}**, **4**). A solution of (methylthio)acetic acid (0.43 g, 4.09 mmol), HOBt (0.75 g, 4.91 mmol), and *N*-methyl(2-pyridyl)methaneamine (0.50 g, 4.09 mmol) in THF (10 mL) was cooled to -10 °C in an ice/salt bath. *N,N*-Dicyclohexylcarbodiimide monohydrate (DCC·H$_2$O) (1.01 g, 4.91 mmol) was dissolved in a minimal volume of THF, cooled to -10 °C and added in one portion to the (methylthio)acetic acid solution. The mixture was stirred at -10 °C for 1 hour and then allowed to warm to room temperature. Stirring was continued at room

temperature for 30 hours. The reaction mixture was then cooled to -40 °C and the DCU suspension was filtered off. The filtrate was concentrated *in vacuo* and then dissolved in 6 mL of chloroform. This solution was loaded onto a RediSep (35 gr) flash column. Impurities were eluted from the column with chloroform and the desired product was obtained in high purity as an orange oil following subsequent elution with methanol and removal of the solvent *in vacuo* (0.86 g, 100 %). ^{1}H NMR (CDCl$_3$, 300 MHz): δ 8.47 (m, 1H), 7.60 (m, 1H), 7.08 - 7.22 (m, 2H), 4.62 – 4.66 (s, 2H), 3.27 - 3.32 (s, 2H), 2.91 - 3.06 (s, 3H), 2.13 - 2.17 (s, 3H) ppm. ^{13}C$\{^1$H$\}$ NMR: δ 169.25, 157.22, 149.28, 137.30, 122.43, 121.90, 55.93, 53.43, 35.51, 16.16 ppm. FTIR (KBr, cm^{-1}): 3062, 2920, 2855, 1717, 1645 (υ_{CO}), 1590, 1571, 1476, 1435, 1397, 1300, 1257, 1151, 1099, 1049, 993, 939, 783, 753, 607. GC/MS: t$_R$ 14.15 min; *m/z* (relative intensity) 210 (4, M$^+$), 93 (100).

[Cu(2-HL^{N2S}*)Cl$_2$] (**5**). CuCl$_2$·2H$_2$O (197 mg, 1.15 mmol) was weighed into a 50 mL Erlenmeyer flask and dissolved in 15 mL methanol. 2-HL^{N2S} (250 mg, 1.27 mmol) was weighed into another 50 ml Erlenmeyer flask and dissolved in 15 mL methanol. This solution was added to the CuCl$_2$ mixture in a single portion, yielding an dark blue solution after several minutes. The reaction mixture was stirred for 5 hours at room temperature then cooled to -40 °C, resulting in the formation of a blue precipitate. The blue precipitate was filtered from the solution onto a fritted glass filter, redissolved from the frit in water, and transferred to a 50 mL round bottom flask. The water was then removed under reduced pressure and the remaining solid was redissolved into a minimal amount of warm methanol. Recrystallization from MeOH/Et$_2$O yielded X-ray-quality, dark blue crystals of the desired product (187 mg, 49.2 %). UV-vis (methanol) [λ_{max}, nm

110

(ϵ, M^{-1} cm^{-1})]: 656 (140). FTIR (KBr, cm^{-1}): 3107, 3068, 3045, 2956, 2914, 2749, 2661, 2463, 2295, 1685, 1642, 1608, 1570, 1493, 1480, 1437, 1441, 1426, 1397, 1374, 1360, 1326, 1282, 1228, 1160, 1084, 1054, 1026, 993, 966, 844, 786, 719, 646. Anal. Calcd for $C_9H_{12}Cl_2CuN_2OS$: C, 32.69; H, 3.66; Cl, 21.44; N, 8.47. Found: C, 32.38; H, 3.72; Cl, 21.57; N, 8.36.

[Cu(2-L^{N2S})Cl(MeOH)] (**6**). $CuCl_2 \cdot 2H_2O$ (197 mg, 1.15 mmol) was weighed into a 50 mL Erlenmeyer flask and dissolved into 15 mL of methanol. To this stirring solution was added Et$_3$N (349 mg, 3.45 mmol) via syringe, resulting in the immediate formation of a green precipitate. 2-HL^{N2S} (250 mg, 1.27 mmol) was weighed into another 50 ml Erlenmeyer flask and dissolved in 15 mL of methanol. This solution was added to the CuCl$_2$ mixture in a single portion, yielding an dark blue solution after several minutes. The reaction mixture was stirred for 5 hours at room temperature and then cooled to -40 °C. The crude product precipitated as a blue solid and was filtered away from the solution. The filtrate was collected in a 50 mL round bottom flask, concentrated, and again cooled to -40 °C. The precipitation/filtration process was repeated until no additional solid could be collected. The combined crude product was combined and dissolved in a minimal amount of methanol. Recrystallization from MeOH/Et$_2$O yielded X-ray-quality, dark blue crystals of the desired product (127 mg, 38.8 %). UV-vis (methanol) [λ_{max}, nm (ϵ, M^{-1} cm^{-1})]: 642 (240). EPR (9.433 GHz, 1:1 CH$_2$Cl$_2$/toluene, 77 K) $g_{\parallel}$ = 2.30, $A_{\parallel}^{Cu}$ = 87 x 10^{-4} cm^{-1}, $g_{\perp}$ = 2.08. FTIR (KBr, cm^{-1}): 3144, 2871, 2806,1593,1564,1483, 1409, 1382, 1345, 1315, 1283, 1227, 1212, 1162, 1089, 1051, 1026, 968, 881, 764, 719, 673, 646, 469, 418, 352, 310, 251, 216, 205. Anal. Calcd for

$C_{10}H_{15}ClCuN_2O_2S$: C, 36.81; H, 4.63; Cl, 10.87; N, 8.59. Found: C, 36.92; H, 4.42; Cl, 11.11; N, 8.82.

[Zn(2-MeL^{N2S})Cl$_2$] (**7**). 2-MeL^{N2S} (250 mg, 1.19 mmol) was weighed into a 50 ml Erlenmeyer flask and dissolved in 10 mL of methanol. ZnCl$_2$ (162 mg, 1.07 mmol) was weighed into a separate 50 mL Erlenmeyer flask and dissolved into 10 mL methanol which was then added to the 2-MeL^{N2S} solution in a single portion. The reaction mixture was stirred for 5 hours at room temperature and the solvent then removed *in vacuo*. To the remaining solid was added 10 mL of chloroform. The desired product was obtained in high purity as a light tan powder after filtering this solution and removing the filtrate solvent *in vacuo*. X-ray-quality crystals were obtained by slow evaporation of a concentrated solution of the tan powder (347 mg, 93 %). FTIR (KBr, cm^{-1}): 3435, 3106, 3054, 3031, 2991, 2959, 2916, 2829, 1587 (s, C=O), 1486, 1459, 1442, 1406, 1352, 1323, 1280, 1225, 1150, 1123, 1095, 1059, 1029, 1001, 986, 874, 836, 797, 775, 707, 660, 652, 618, 571, 534, 480, 464, 422. Anal. Calcd for $C_{10}H_{14}Cl_2N_2OSZn$: C, 34.65; H, 4.07; N, 8.08. Found: C, 34.72; H, 4.07; N, 8.09.

X-ray Crystallography: **[Cu(2-HL^{N2S}*)Cl$_2$]** (**5**): A blue crystal of the complex, having approximate dimensions 0.24 x 0.22 x 0.16 mm, was mounted on a glass capillary with heavy-weight oil and quickly placed under a cold stream of nitrogen on the diffractometer. The data were collected at 153(2) K on a Bruker Apex diffractometer using Mo Kα (λ =0.71073 Å) radiation.[29] Important crystallographic information is summarized in table 3-1. Intensity data, which approximately covered the

full sphere of the reciprocal space, were measured as a series of ω oscillation frames each 0.3° for 21 seconds per frame. The detector was operated in 512 x 512 mode and was positioned 6.12 cm from the crystal. Coverage of unique data was 98.2 % complete to 52° (2θ). Cell parameters were determined from a non-linear least squares fit of 3248 reflections in the range of $4.3 < \theta < 25.4°$. A total of 4330 reflections were measured. The data were corrected for absorption by multi-scan method form equivalent reflections giving minimum and maximum transmission of 0.5987 and 0.7018. The data were merged to form a set of 2189 unique reflections with R(int) = 0.026.

The structure was solved by the direct method using SHELXTL system and refined by full-matrix least squares on F^2 using all reflections.[30] All the non-hydrogen atoms were refined anisotropically. All the hydrogen atoms were included with idealized parameters except the hydrogen atom on O1 atom, which was located and refined isotropically. The asymmetric unit contains a $C_9H_{12}N_2OSCl_2Cu$ moiety that forms H-bonds with another $C_9H_{12}N_2OSCl_2Cu$ molecule in the unit cell. Final $R1 = 0.025$ is based on 2137 "observed reflections" [$I > 2\sigma(I)$] and $wR^2 = 0.062$ is based on all reflections (2189 unique reflections). The final structure was graphically presented using the Accelrys Materials Studio software package.[31]

[Cu(2-L^{N2S})Cl(MeOH)] (6): A deep blue crystal of the complex, having approximate dimensions 0.56 x 0.52 x 0.48 mm, was mounted on a glass capillary with heavy-weight oil and quickly placed under a cold stream of nitrogen on the diffractometer. The data were collected at 120(2) K on a Bruker Apex diffractometer using Mo Kα (λ =0.71073 Å) radiation.[29] Important crystallographic information is summarized in table 3-1.

Intensity data, which approximately covered the full sphere of the reciprocal space, were measured as a series of ω oscillation frames each 0.3° for 10 sec / frame. The detector was operated in 512 x 512 mode and was positioned 6.12 cm from the crystal. Coverage of unique data was 98.0 % complete to 54° (2θ). Cell parameters were determined from a non-linear least squares fit of 4921 reflections in the range of 4.2 < θ < 26.4°. A total of 7396 reflections were measured. The data were corrected for absorption by multi-scan method form equivalent reflections giving minimum and maximum transmission of 0.3850 and 0.4312. The data were merged to form a set of 2694 unique reflections with R(int) = 0.016.

The structure was solved by the direct method using SHELXTL system and refined by full-matrix least squares on F^2 using all reflections.[30] All the non-hydrogen atoms were refined anisotropically. All the hydrogen atoms were included with idealized parameters except the hydrogen atoms on O1 atom, which was located and refined isotropically. The asymmetric unit contains a $C_{10}H_{15}N_2O_2SClCu$ moiety that forms H-bonds with another $C_9H_{12}N_2OSCl_2Cu$ molecule in the unit cell. Final $R1 = 0.0270$ is based on 2673 "observed reflections" [$I > 2\sigma(I)$] and $wR^2 = 0.050$ is based on all reflections (2673 unique reflections). The final structure was graphically presented using the Accelrys Materials Studio software package.[31]

[Zn(2-MeL^{N2S})Cl$_2$] (7): A colorless crystal of the complex, having approximate dimensions 0.22 x 0.20 x 0.16 mm, was mounted on a glass capillary with heavy-weight oil and quickly placed under a cold stream of nitrogen on the diffractometer. The data were collected at 120(2) K on a Bruker Apex diffractometer using Mo Kα (λ =0.71073

Å) radiation.[29]   Important crystallographic information is summarized in table 3-2. Intensity data, which approximately covered the full sphere of the reciprocal space, were measured as a series of ω oscillation frames each 0.3° for 25 seconds per frame. The detector was operated in 512 x 512 mode and was positioned 6.12 cm from the crystal. Coverage of unique data was 95.6 % complete to 56.6° (2θ). Cell parameters were determined from a non-linear least squares fit of 6136 reflections in the range of $2.2 < \theta <$ 28.3°. A total of 15507 reflections were measured.

The structure was solved by the direct method using SHELXTL system and refined by full-matrix least squares on F^2 using all reflections.[30]   All the non-hydrogen atoms were refined anisotropically. All the hydrogen atoms were included with idealized parameters. There are four molecules in the unit cell. Final $R1 = 0.0178$ is based on 3220 "observed reflections" $[I > 2\sigma(I)]$ and w$R^2 = 0.0478$ is based on all reflections (3295 unique reflections). The final structure was graphically presented using the Accelrys Materials Studio software package.[31]

Table 3-1. Summary of crystallographic data for compounds **5** and **6**.

	5	6
empirical formula	$C_9H_{12}Cl_2CuN_2OS$	$C_{10}H_{15}ClCuN_2O_2S$
formula weight	330.71	326.29
crystal system	trigonal	triclinic
space group	P3(1)	P-1
a (Å)	6.9560(8)	7.3002(3)
b (Å)	6.9560(8)	8.2461(4)
c (Å)	21.791(5)	10.8430(5)
α (deg)	90	78.059(1)
β (deg)	90	80.354(1)
γ (deg)	120	84.568(1)
V ($Å^{-3}$)	913.1(3)	628.36(5)
Z	3	2
density (calcd)	1.804 g/cm^3	1.725 g/cm^3
temperature (K)	153(2)	120(2)
crystal size (mm)	0.24 x 0.22 x 0.16	0.56 x 0.52 x 0.48
diffractometer	Bruker Apex	Bruker Apex
absorption coefficient	2.382 mm^{-1}	2.107 mm^{-1}
radiation, λ (Å)	Mo Kα, $\lambda = 0.71073$	Mo Kα, $\lambda = 0.71073$
2θ max (deg)	52.0	54.0
reflections collected	4330	7396
independent reflections	2189	2694
observed reflections	2137	2673
variable parameters	501	334
$R1$ [$I > 2\sigma(I)$]	0.0251	0.0197
w$R2$ [$I > 2\sigma(I)$]	0.0617	0.0506
$R1$ (all data)	0.0257	0.0199
w$R2$ (all data)	0.0620	0.0508
goodness-of-fit	1.023	1.051
largest diff. peak and hole (e^{-1} $Å^{-3}$)	0.492, -0.262	0.364, -0.437

Table 3-2. Summary of crystallographic data for compound **7**.

	7
empirical formula	$C_{10}H_{14}Cl_2N_2OSZn$
formula weight	346.56
crystal system	monoclinic
space group	P2(1)/n
a (Å)	10.5046(5)
b (Å)	8.6334(4)
c (Å)	15.4007(8)
α (deg)	90
β (deg)	97.0570(10)
γ (deg)	90
V (Å^{-3})	1386.11(12)
Z	4
density (calcd)	1.661 g/cm^3
temperature (K)	120(2)
crystal size (mm)	0.22 x 0.20 x 0.16
diffractometer	Bruker Apex
absorption coefficient	2.292 mm^{-1}
radiation, λ (Å)	Mo Kα, $\lambda = 0.71073$
2θ max (deg)	56.6
reflections collected	15507
independent reflections	3295
observed reflections	3220
variable parameters	704
$R1$ [$I > 2\sigma(I)$]	0.0178
w$R2$ [$I > 2\sigma(I)$]	0.0476
$R1$ (all data)	0.0183
w$R2$ (all data)	0.0478
goodness-of-fit	1.083
largest diff. peak and hole (e^{-1} Å^{-3})	0.381, -0.213

3.8.   References

1.   Solomon, E. I.; Szilagyi, R. K.; DeBeer George, S.; Basumallick, L. *Chem. Rev.* **2004**, *104*, 419-458.

2.   (a) Gray, H. B.; Malmstrom, B. G.; Williams, R. J. P. *J. Biol. Inorg. Chem.* **2000**, *5*, 551-559. (b) Belle, C.; Rammal, W.; Pierre, J. L. *J. Inorg. Biochem.* **2005**, *99*, 1929-1936.

3.   Freeman, H. C.; Guss, J. M., In *Handbook of Metalloproteins*, Wieghardt, K., Ed. Wiley: Chichester, 2001; Vol. 2, pp 1153-1169.

4.   Kolczak, U.; Dennison, C.; Messerschmidt, A.; Canters, G. W., In *Handbook of Metalloproteins*, Messerschmidt, A.; Huber, R.; Poulos, T.; Wieghardt, K., Eds. Wiley: Chichester, 2001; Vol. 2, pp 1170-1194.

5.   Brown, K.; Tegoni, M.; Prudencio, M.; Pereira, A. S.; Besson, S.; Moura, J. J.; Moura, I.; Cambillau, C. *Nat. Struct. Biol.* **2000**, *7*, 191-195.

6.   Farrar, J. A.; Neese, F.; Lappalainen, P.; Kroneck, P. M. H.; Saraste, M.; Zumft, W. G.; Thomson, A. J. *J. Am. Chem. Soc.* **1996**, *118*, 11501-11514.

7.   Henkel, G.; Krebs, B. *Chem. Rev.* **2004**, *104*, 801-824.

8.   Prigge, S. T.; Eipper, B. A.; Mains, R. E.; Amzel, L. M. *Science* **2004**, *304*, 864-867.

9.   (a) Alvarez, M. L.; Ai, J. Y.; Zumft, W.; Sanders-Loehr, J.; Dooley, D. M. *J. Am. Chem. Soc.* **2001**, *123*, 576-587. (b) Ghosh, S.; Gorelsky, S. I.; Chen, P.; Cabrito, I.; Moura, J. J.; Moura, I.; Solomon, E. I. *J Am Chem Soc* **2003**, *125*, 15708-15709.

10. (a) Klein, E. L.; Khan, M. A.; Houser, R. P. *Inorg. Chem.* **2004**, *43*, 7272-7274. (b) Carrier, S. M.; Ruggiero, C. E.; Tolman, W. B.; Jameson, G. B. *J. Am. Chem. Soc.* **1992**, *114*, 4407-4408. (c) Halfen, J. A.; Tolman, W. B. *J. Am. Chem. Soc.* **1994**, *116*, 5475-5476.

11. Lee, W. Z.; Tolman, W. B. *Inorg. Chem.* **2002**, *41*, 5656-5658.

12. Nonoyama, M. *Inorg. Chim. Acta* **1975**, *13*, 5-10.

13. (a) Toscano, P. J.; Marzilli, L. G. *Inorg. Chem.* **1983**, *22*, 3342-3350. (b) Toscano, P. J.; Belsky, K. A.; Engelhardt, L. M.; Fordon, K. J.; White, A. H. *Inorg. Chem.* **1990**, *29*, 1357-1359.

14. Toscano, P. J.; Fordon, K. J.; Macherone, D.; Liu, S. C.; Zubieta, J. *Polyhedron* **1990**, *9*, 2375-2383.

15. Mondal, A.; Li, Y.; Khan, M. A.; Ross, J. H.; Houser, R. P. *Inorg. Chem.* **2004**, *43*, 7075-7082.

16. Elsayed, L.; Ragsdale, R. O. *Inorg. Chem.* **1967**, *6*, 1640-1643.

17. Addison, A. W.; Rao, T. N.; Reedijk, J.; Vanrijn, J.; Verschoor, G. C. *Dalt. Trans.* **1984**, 1349-1356.

18. (a) Torreggiani, A.; Tamba, M.; Fini, G. *Biopolymers* **2000**, *57*, 149-159. (b) Hynes, M. J.; Clarke, E. M. *J. Chem. Soc. Perk. Trans. 2* **1998**, 1263-1267.

19. (a) Garg, B. S.; Nandan Kumar, D.; Sarbhai, M.; Reddy, M. J. *Spectrochim. Acta Sec. A Mol. Biomol. Spectrosc.* **2003**, *59*, 2775-2783. (b) Haidar, R.; Ipek, M.; DasGupta, B.; Yousaf, M.; Zompa, L. J. *Inorg. Chem.* **1997**, *36*, 3125-3132.

20. Fry, F. H.; Fischmann, A. J.; Belousoff, M. J.; Spiccia, L.; Brugger, J. *Inorg. Chem.* **2005**, *44*, 941-950.

21.   Holland, P. L.; Tolman, W. B. *J. Am. Chem. Soc.* **2000**, *122*, 6331-6332.

22.   Randall, D. W.; George, S. D.; Holland, P. L.; Hedman, B.; Hodgson, K. O.; Tolman, W. B.; Solomon, E. I. *J. Am. Chem. Soc.* **2000**, *122*, 11632-11648.

23.   Holland, P. L.; Tolman, W. B. *J. Am. Chem. Soc.* **1999**, *121*, 7270-7271.

24.   (a) Fujisawa, K.; Morooka, Y.; Kitajima, N. *Chem.Comm.* **1994**, 623-624. (b) Osako, T.; Ueno, Y.; Tachi, Y.; Itoh, S. *Inorg. Chem.* **2004**, *43*, 6516-6518. (c) Ueno, Y.; Tachi, Y.; Itoh, S. *J. Am. Chem. Soc.* **2002**, *124*, 12428-12429. (d) Ohta, T.; Tachiyama, T.; Yoshizawa, K.; Yamabe, T.; Uchida, T.; Kitagawa, T. *Inorg. Chem.* **2000**, *39*, 4358-4369.

25.   Downes, J. M.; Whelan, J.; Bosnich, B. *Inorg. Chem.* **1981**, *20*, 1081-1086.

26.   (a) Houser, R. P.; Halfen, J. A.; Young, V. G.; Blackburn, N. J.; Tolman, W. B. *J. Am. Chem. Soc.* **1995**, *117*, 10745-10746. (b) John, E.; Bharadwaj, P. K.; Potenza, J. A.; Schugar, H. J. *Inorg. Chem.* **1986**, *25*, 3065-3069. (c) Kitajima, N.; Fujisawa, K.; Tanaka, M.; Morooka, Y. *J. Am. Chem. Soc.* **1992**, *114*, 9232-9233. (d) Paul, P. P.; Karlin, K. D. *J. Am. Chem. Soc.* **1991**, *113*, 6331-6332.

27.   Higashimura, H.; Kubota, M.; Shiga, A.; Fujisawa, K.; Moro-oka, Y.; Uyama, H.; Kobayashi, S. *Macromolecules* **2000**, *33*, 1986-1995.

28.   Lipscomb, J. D. *Biochemistry* **1980**, *19*, 3590-3599.

29.   (a) *X-ray data collection and cell refinement: SMART*, version 5.625; Bruker AXS, Inc.: Madison, WI, 2002. (b) *X-ray data reduction program: SAINT-plus*, version 6.28A; Bruker AXS, Inc.: Madison, WI, 2002.

30.   *X-ray structure solution and refinement program: SHELXTL*, version 6.12; Bruker AXS, Inc.: Madison, WI, 1997.

31.	*X-ray structure presentation software: Materials Studio,* version 2.1; Accelrys, Inc.: San Diego, CA, 2001.

CHAPTER 4.

COPPER(II) REDUCTION BY THIOETHER SULFUR: A SYNTHETIC MODEL OF THE COPPER(II) REDUCTION BY METHIONINE IN ALZHEIMER'S DISEASE AMYLOID-*β* PEPTIDES

4.1.   *Introduction*

The interesting chemistry with the new ligands described in chapter 3, particularly with ligand 2-HL^{N2S}, prompted us to consider variations of their designs.   We were specifically interested in the copper chemistry of 2-HL^{N2S} analogues that possess two amide and two thioether moieties. Ligand 2-HL^{N2S} is easily deprotonated to its mono-anionic amidate form when coordinated to copper(II) under basic conditions. In addition to the anionic ligand, the 2+ charge of the copper ion is balanced by an equatorially-coordinated chloride ligand to give a neutral complex. It was reasoned that two amide functionalities in an analogous ligands could both be deprotonated to afford neutral complexes where the ligand alone would balance the copper(II) charge. This project was, thus, conceived with the intent of developing new type 1 copper (Cu-I) center models as a direct extension of our previous work.

Interestingly, the reaction of one of the new ligands with copper(II) results in redox decomposition where the ligand thioether sulfurs are implicated as the copper(II) reductants, *vide infra*. This unprecedented synthetic result has direct relevance to the proposed mechanism of copper(I) and Reactive Oxygen Species (ROS) generation in the amyloid-*β* (A*β*) peptides associated with neurodegeneration in Alzheimer's Disease (AD).

AD is one of several neurodegenerative disorders where the pathogenesis is linked to amyloid plaques.[1] Postmortem analysis of AD brains reveals the presence of insoluble deposits of A*β* peptides, containing from 39 to 43 residues, proteolytically derived from transmembrane amyloid precursor glycoprotein (APP).[2]   The solution structure of A*β*(1-42), the principal form of A*β* deposits in AD brains, is shown in Figure

4-1.[3] Although the molecular basis for the neurotoxicity in AD has not yet been conclusively identified, one prevalent hypothesis suggests that oxidative stress associated with neurotoxicity results from the oxidation of the unique methionine residue (Met-35) in Aβ.[4-6]
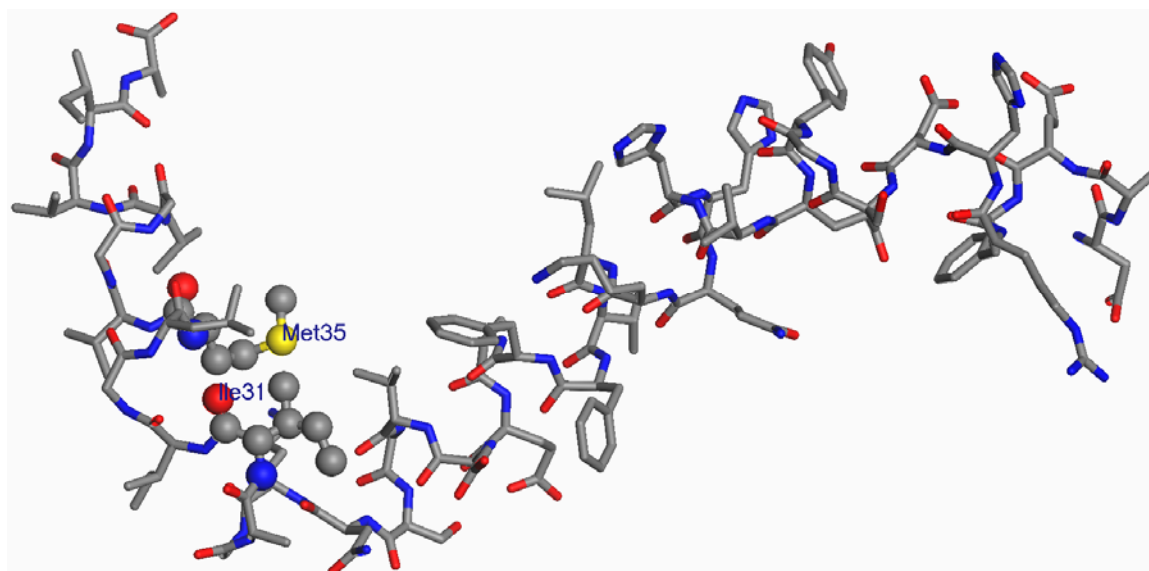
DAEFR⁵HDSGY¹⁰EVHHQ¹⁵KLVFF²⁰AEDVG²⁵SNKGA³⁰IIGLM³⁵VGGVV⁴⁰IA

Figure 4-1. Representation of the structure of Aβ(1-42). Met-35 and Ile-31 are highlighted as CPK spheres.

The histidine-rich N-terminus of Aβ is known to bind copper(II) with high affinity and the reduction of copper(II) has been linked to Aβ's neurotoxicity.[7, 8] Both Aβ neurotoxicity and its ability to reduce copper(II) are dependent on the methionine (Met-35) residue, leading to the notion that methionine sulfur reduces copper(II) with

concomitant generation of methionine cation radicals (reaction 1).[4, 6, 9] In the oxygen-rich environment of the brain, neuronal damage may be compounded by the formation of ROS through Fenton chemistry by copper(I) mediated generation of •OH from O_2 (reactions 2 - 5),[10] or perhaps through direct oxidation of cellular units (lipids, proteins, DNA) by Met($S^{+\bullet}$) itself.[11] Soluble oligomeric forms of Aβ have recently been shown to be responsible for neural dysfunction, possibly leading to onset of AD, raising the possibility that the chemistry involving Met-35 and copper(II) to generate copper(I), ROS, or Met($S^{+\bullet}$) may occur prior to formation of insoluble amyloid plaques.[12]

$$(A\beta)Met(S) + Cu^{II} \rightarrow (A\beta)Met(S^{+\bullet}) + Cu^{I} \tag{1}$$

$$O_2 + Cu^{I} \rightarrow Cu^{II} + O_2^{\bullet-} \tag{2}$$

$$O_2^{\bullet-} + O_2^{\bullet-} + 2\,H^+ \rightarrow H_2O_2 \tag{3}$$

$$O_2^{\bullet-} + Cu^{II} \rightarrow O_2 + Cu^{I} \tag{4}$$

$$H_2O_2 + Cu^{I} \rightarrow {}^{\bullet}OH + Cu^{II} + OH^{-} \tag{5}$$
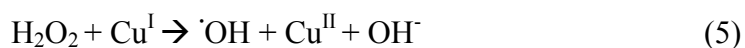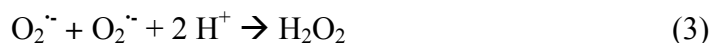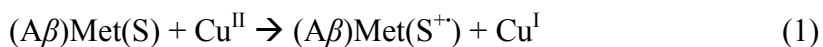
Normally, the reduction potentials for copper and methionine, or more generally thioethers, are not conducive for thermodynamically spontaneous redox reactions.[13, 14] The redox potential for the Met($S^{+\bullet}$)/Met(S) couple is 1.2 to 1.5 V vs. Ag/AgCl,[13] while typical $Cu^{II/I}$ redox potentials range from -0.6 to 0.6 V vs. Ag/AgCl, depending on solvent and ligand identity.[15] While the potential of copper in Aβ (0.5 V vs. Ag/AgCl)[8] is higher than in typical copper complexes, it is still far too low to oxidize methionine under

normal circumstances. Indeed, aside from the provocative proposal that Met(S) in Aβ reduces copper(II), there are no examples of spontaneous redox between copper(II) and methyl thioethers in the chemical or biochemical literature.

Thermochemical and theoretical studies have both revealed that the reduction potential of sulfides can be significantly modulated by two-center three-electron, so-called $\sigma\sigma^*$, interactions between the sulfur cation radical and an electronegative partner.[6, 13, 16] This type of interaction in Aβ between Met-35 and the Ile-31 backbone carbonyl was proposed to be responsible for its unusual ability to reduce copper.[11, 17]

This chapter describes the synthesis and copper chemistry of a new family of ligands based on 2-Methyl-2-(2-pyridinyl)-1,3-propanediamine.[18] One of these ligands carries out spontaneous reduction of bound copper(II) by its amide-activated thioether sulfur. The implication of this unprecedented synthetic reactivity on the proposed mechanism of neurotoxicity in AD is also discussed.

4.2.   Ligand Syntheses

2-Methyl-2-(2-pyridinyl)-1,3-propanediamine (**2**) was chosen as the diamine precursor from which to synthesize the new ligand described above. The synthesis of **2** was first reported by Friedrich, *et al.*, in 1997 and begins with the high temperature and high pressure reaction of 2-ethylpyridine with formaldehyde (Figure 4-2).[18] In reality, this reaction affords a mixture of equal amounts of mono- and di-alkylated products, along with unreacted starting materials. The desired dialcohol product, as shown in the figure, is obtained only after careful vacuum distillation of the reaction mixture, but still in low purity.
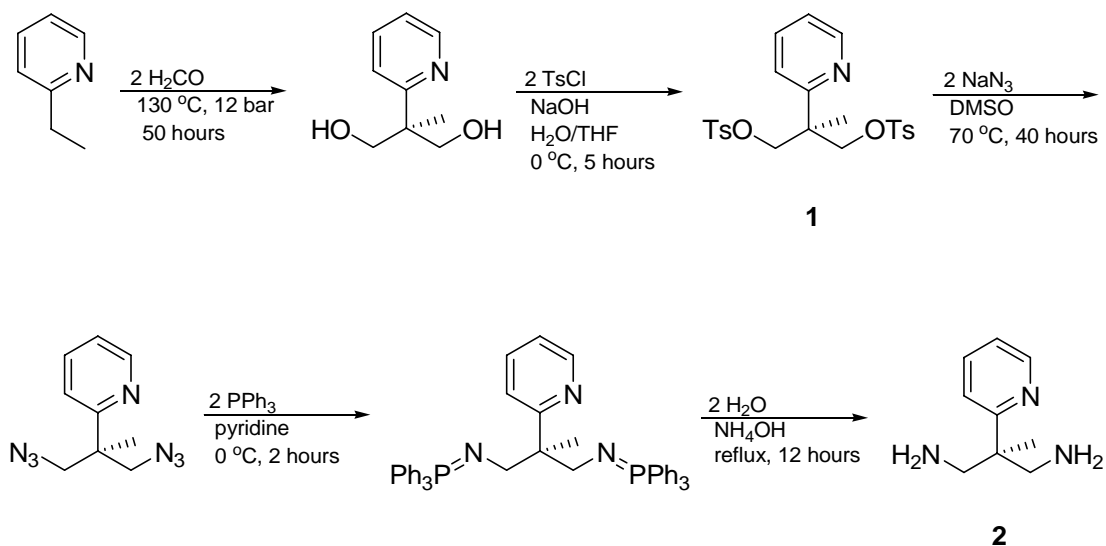
Figure 4-2. Synthesis of 2-Methyl-2-(2-pyridinyl)-1,3-propanediamine (**2**)

The purified dialcohol is then reacted with tosyl chloride to yield the ditosylate product, **1**.[18] In the published procedure for the synthesis **1**, pyridine is used as the solvent/base and the crude product is obtained as a tacky oil. Pure **1** is obtained from the tacky material after a complex workup procedure. Applying techniques used previously in our laboratory for the tosylation of ethylene glycol (see chapter 2),[19] both the yield and purity of **1** were dramatically improved by using sodium hydroxide as the base and H_2O/THF as the solvent mixture. Using this method, recrystallization of the desired product by direct addition of ethanol to the reaction mixture consistently gives analytically pure **1**, almost regardless of the purity of the dialcohol starting material.

1 is subsequently reacted with sodium azide in DMSO, resulting in azide displacement of tosylate and formation of the diazide product. Because of the potentially explosive character of organic azides,[20] the diazide product is not isolated at any step of the scale reaction. Instead, DMSO is replaced in portions with pyridine and the diazide is

immediately converted to the diamine, **2**, using the Staudinger reaction.[21] The structure of **2** is very similar to 2-picolylamine except for its central quaternary carbon and second amine arm. Metal complexes of several aryl amine derivatives of **2** have been reported, including Zr, Ti, and Hf,[18, 22] but there are no reported copper complexes of this ligand.

Inspired by the interesting copper(II) chemistry of *N*-(2-pyridylmethyl)acetamide (pmac) previously reported by our group,[23] the new ligand L$^{Py(ac)2}$ (**3**) was synthesized by reaction of **2** with acetic anhydride (Figure 4-3). The desired product is easily obtained as a fine pale-yellow powder following recrystallization from ethanol.
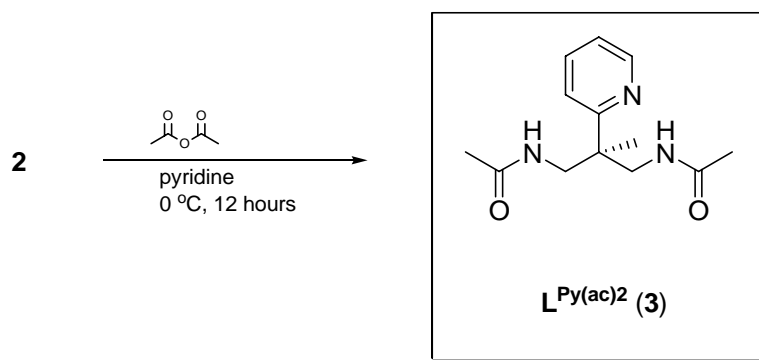
Figure 4-3. Synthesis of L$^{Py(ac)2}$ (**3**).

Toward our original synthetic goal, **2** was also reacted with (methylthio)acetic acid using DCC/HOBt peptide coupling reagents to yield L$^{Py(acSMe)2}$ (**4**) (Figure 4-4). This new ligand is the diamine dithioether analogue of 2-HL^{N2S},[24] and was envisioned to react with copper(II) to become anionic in its amidate form. The symmetric structure of **4**, with the methyl group of the quaternary carbon forcing the arms to the same side of the molecule, was expected to promote a capping coordination mode of the ligand by its

pyridyl and amidate nitrogens. Coordination of at least one thioether sulfur was also anticipated based on our previous experience.[24]
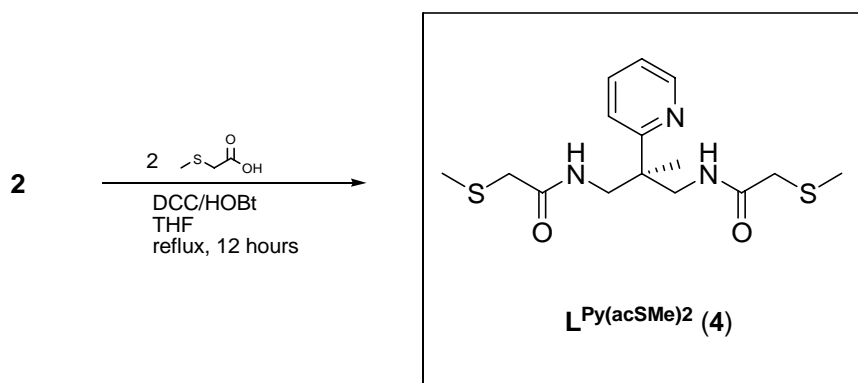
Figure 4-4. Synthesis of $L^{Py(acSMe)2}$ (**4**).

To systematically probe the effect(s) of each functional group in **4** on its coordination chemistry, and having already synthesized **3** which is essentially **4** without its methyl thioethers, modifications to the remainder of the ligand were carried out. Since amide nitrogens are poor ligands, we began with conversion of the amide groups of **4** to amines. Reaction of **4** with $LiAlH_4$ is sufficient for this reduction on a small scale and proceeds without adverse effects to the remainder of the ligand, yielding $L^{Py(SMe)2}$ (**5**) in high purity (Figure 4-5).
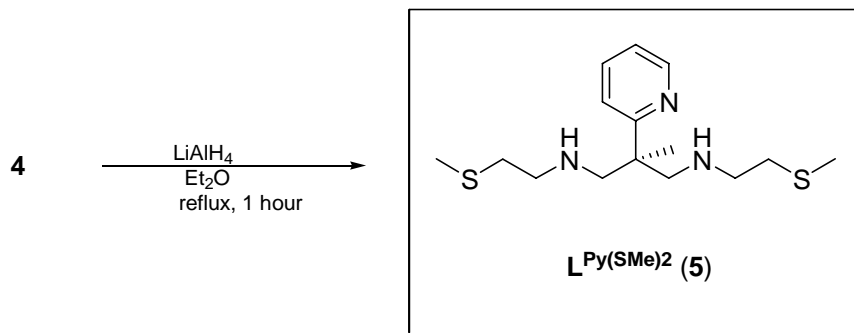
Figure 4-5. Synthesis of L$^{\text{Py(SMe)2}}$ (**5**)

With the methyl thioether and amide variants complete, the pyridyl ring itself was targeted next. Pyridyl-free **4** was obtained by simple reaction of 1,3-diaminopropane with (methylthio)acetic acid, yielding L$^{\text{(acSMe)2}}$ (**6**) (Figure 4-6). Other than the absence of pyridyl and methyl at the quaternary carbon, **6** is identical to **4** in all respects.
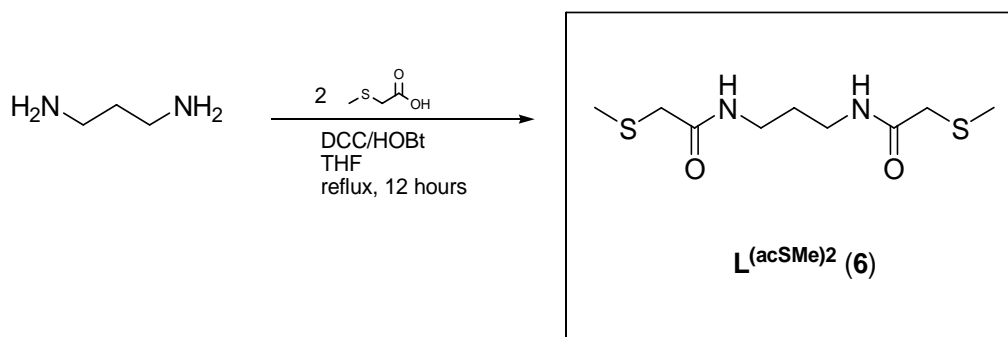
Figure 4-6. Synthesis of L$^{\text{(acSMe)2}}$ (**6**).

Finally, in an effort to improve the yield of **5** and simultaneously circumvent the requirement to reduce **4** with LiAlH$_4$ in preparative-scale syntheses of this compund, **2**

was mono-tosylated at each of its amine nitrogens to give 2-Methyl-*N,N'*-di(*p*-toluenesulfonyl)-2-pyridin-2-ylpropane-1,3-diamine (**7**). It was hoped that reaction of **7** with 2-(methylthio)ethyl tosylate followed by detosylation would more efficiently yield **5**. Numerous attempts to react **7** with 2-(methylthio)ethyl tosylate, however, continually resulted in a mixture of products (Figure 4-7). It was later discovered that 2-(methylthio)ethyl tosylate is unstable due to its susceptibility to intramolecular nucleophilic attack by its thioether sulfur, especially at elevated temperatures, eliminating tosylate.[25] This process initially results in the formation of three-member sulfonium rings that subsequently polymerize.
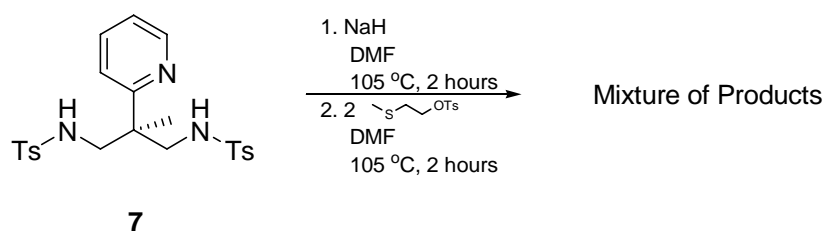
Figure 4-7. Attempted reaction of **7** with 2-(methylthio)ethyl tosylate

The instability problem was surmounted and the synthesis improved by reversal of the reagent functional groups. Instead of reacting **7** with unstable 2-(methylthio)ethyl tosylate, **1** was reacted with 2-(methylthio)-*N*-tosylethanamine.[26] This simple alteration resulted in the successful preparation of the tosyl-protected product, L^Py(TsSMe)2 (**8**) (Figure 4-8) and has the advantage of not requiring the preparation or use of **2**.[27]
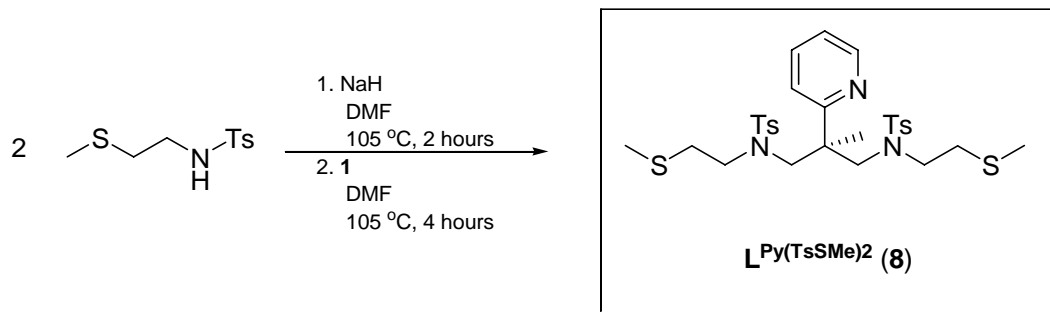
Figure 4-8. Synthesis of L$^{Py(TsSMe)2}$ (**8**).

X-ray quality crystals of **8** were obtained by slow solvent evaporation from a concentrated ethanol solution of the purified product. The X-ray crystal structure of **8** clearly shows its tosyl-protected amines, methyl thioether arms, pyridyl ring, and central quaternary carbon, all possessing normal geometric parameters (Figure 4-9).[27] More careful examination of this structure reveals the relative positions of each of these groups. The methyl of the quaternary carbon forces the pyridyl nitrogen (N1) to be rotated 180° so that it faces the opposite side of the molecule. In addition, N2 and N3 of the thioether arms are also oriented in the same direction, creating what could be envisioned as a binding pocket. Unfortunately, all efforts to cleave the tosyl groups from **8** to produce **5** also result in simultaneous cleavage of the methyl thioether groups and a mixture of products is obtained. Despite this problem, the synthetic route described here could easily be adapted for the synthesis of other secondary amine derivatives directly from **1** without the need to proceed through **2**.
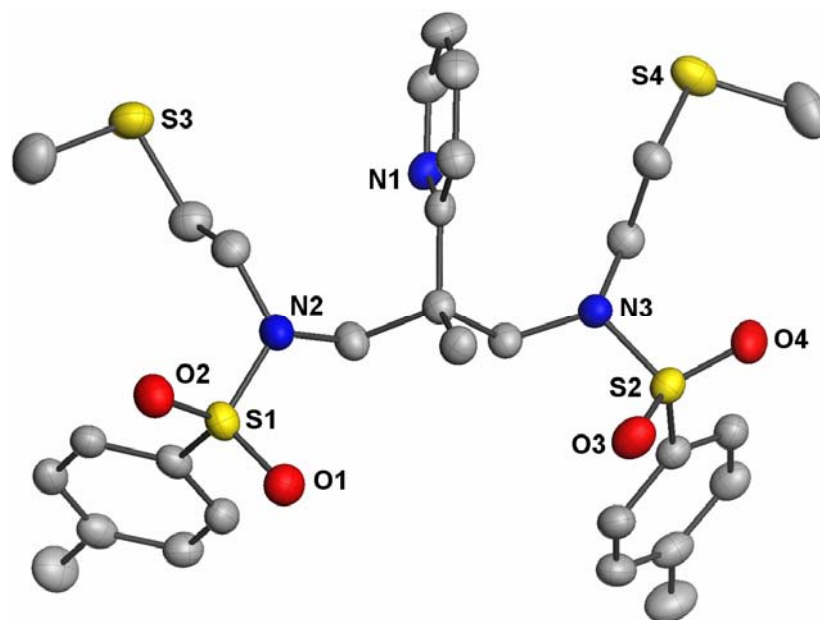
Figure 4-9. Representation of the X-ray crystal structure of $L^{Py(TsSMe)2}$ (**8**) possessing normal geometric parameters. H atoms have been removed for clarity.

4.3.   *Copper(II)-Ligand Reactivity*

The new ligand, **4**, consists of a pyridyl ring connected to two arms, each containing an amide and a methyl thioether.[18, 28] Solutions of copper(II) mixed with **4** initially yield a dark forest green solution, but the color steadily bleaches to produce a clear, light yellow solution at room temperature over the course of several hours. This unexpected decomposition was followed by ^{1}H NMR, EPR, and UV-vis spectroscopy.

The paramagnetically broadened ^{1}H NMR spectrum of the initial green solution sharpens over time, eventually producing a well-defined spectrum with chemical shifts that differ slightly from the spectrum of the free ligand (Figure 4-10). The observed differences in the chemical shifts of the ligand after decomposition compared to unreacted ligand, particularly in the aromatic region of the spectrum, suggest that the

ligand is coordinated to copper(I). Interestingly, the same spectrum cannot be replicated by direct reaction of **4** with copper(I) salts, implying some change to the ligand has also occurred in the decomposition.
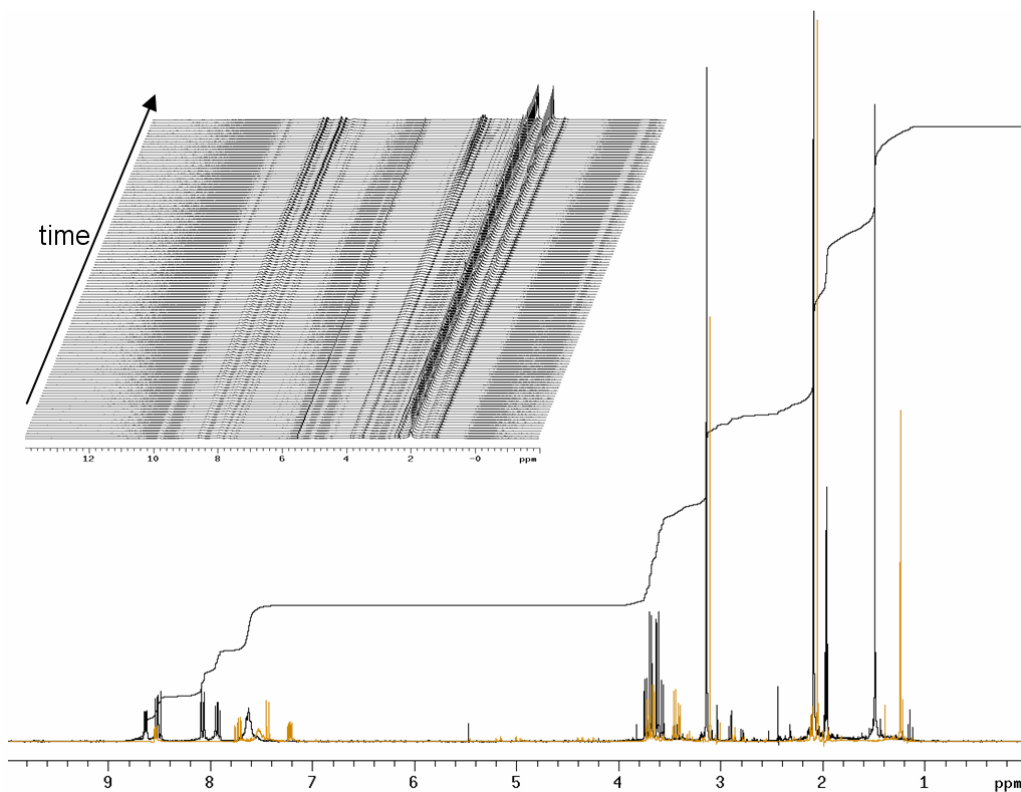
Figure 4-10. The 300 MHz ^{1}H NMR spectrum of the L$^{Py(acSMe)2}$ copper(I) decomposition mixture in acetonitrile-d_3 after 48 hours (black). The ^{1}H NMR spectrum of pure L$^{Py(acSMe)2}$ in the same solvent (orange) is overlaid for comparison. The inset shows the 300 MHz ^{1}H NMR array plot. Individual scans were collected at 300 second intervals over 10 hours.

The X-band EPR spectrum of the initial green solution displays a predominant axial signal that is typical of a tetragonal copper(II) species ($g_{\parallel}$ = 2.24, $A_{\parallel}$ = 153 x 10^{-4} cm^{-1}, $g_{\perp}$ = 2.05) (Figure 4-11). An apparent copper hyperfine signal of lower intensity is

134

also discernable in the spectrum, centered at $g_\parallel$ = 2.30, and has otherwise identical parameters as the more intense signal. The observed EPR signals completely disappear into the baseline over the course of the decomposition reaction, clearly showing the complete consumption of the paramagnetic copper(II) species in the decomposition.

$g_\parallel$=2.24
$A_\parallel$=153 x 10^{-4} cm^{-1}

$g_\perp$= 2.05

Field (Gauss)
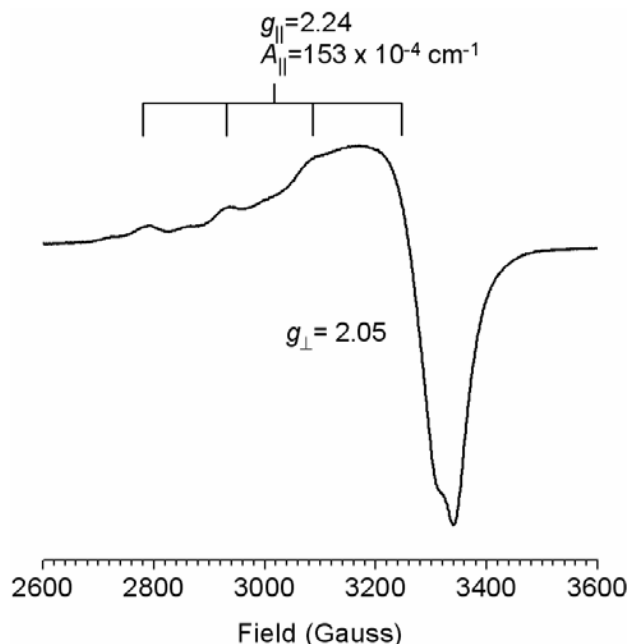
Figure 4-11. X-band EPR spectrum of the initial green solution of L$^{Py(acSMe)2}$ (**4**) with copper(II) triflate in CH$_3$CN at 77 K.

Finally, the UV-vis spectrum of the initial green solution is dominated by two absorption bands centered at 360 and 710 nm that both disappear over the course of the decomposition reaction (Figure 4-12). The UV-vis experiments also reveal that a single ligand molecule reduces two copper ions. When 2:1 ratios of copper(II) to **4** are reacted, the copper(II) chromophores at 360 and 710 nm completely disappear. Higher Cu:**4** ratios result in residual unreduced copper(II). The redox decomposition also proceeds

135

regardless of either the copper(II) salt or solvent identity, proving that the reducing moiety must be in the ligand. Ligand impurities were ruled out as potential reducing agents by the analytical purity of **4** coupled with the known 2:1 stoichiometry of the reaction.
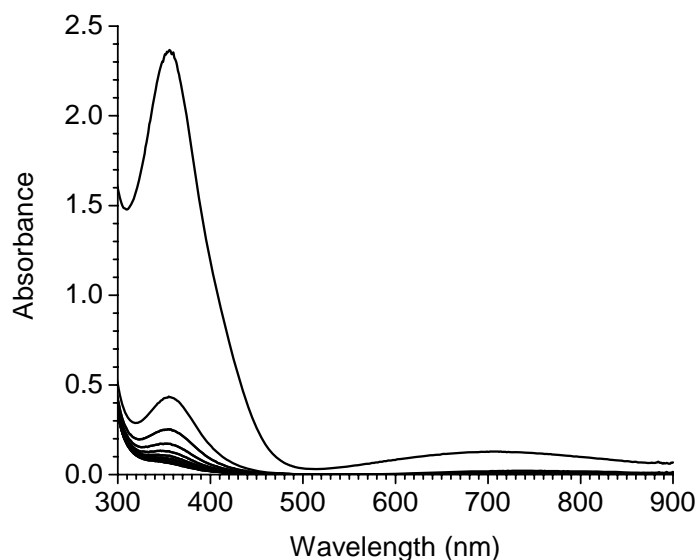
Figure 4-12. UV-vis spectrum of the 2:1 redox reaction between cupric triflate (3.3 mM) and $L^{Py(acSMe)2}$ (**4**) (1.7 mM) in acetonitrile. Individual scans were recorded at 15 minute intervals for 25 hours.

All of the spectroscopic results presented above are consistent with reduction of copper(II) to copper(I). This conclusion was further verified by quantitative recrystallization of $[Cu(CH_3CN)_4](OTf)$ directly from an acetonitrile solution of the reaction mixture after complete decomposition.

Attempts to characterize the electrochemical properties of **4** and the initial dark green complex formed immediately after addition of copper(II) salts to **4** were carried out

using cyclic voltammetry (CV). While the cyclic voltammogram of **4** in acetonitrile exhibits only a completely irreversible oxidation at +1200 mV (Ag/AgCl), assigned as the thioether sulfur oxidation, the cyclic voltammogram of the green complex is devoid of this feature, exhibiting a single irreversible reduction peak at -276 mV, assigned as the $Cu^{II} \rightarrow Cu^{I}$ reduction. If the potential is scanned to -500 mV or greater, however, the copper becomes fully reduced to Cu^{0} and is deposited on the electrode surface as evidenced by a very sharp irreversible oxidation in the reverse scan. Interestingly, the irreversible +1200 ligand oxidation peak reappears after the formation of Cu^{0} as a result of liberated ligand at the electrode surface. Although work is still underway to ascertain more details about the electronic structure of the green redox-active complex, this initial result is indicative of a direct thioether sulfur interaction with the copper(II) ion of the green complex.

The fact that copper(II) is reduced by **4** is unambiguous. Many examples of copper(II) thioether complexes are known and complexes with ligands similar to **4** have been reported by our group and others.[24, 29] There are, however, no examples of spontaneous redox in synthetic copper(II) thioether complexes without addition of external reducing agents, despite their generally higher reduction potentials.[30]

Previously in our laboratory, copper(II) complexes of 2-HL^{N2S} and pmac were synthesized and characterized.[23, 24] Stable, crystallographically characterized copper(II) complexes of 2-HL^{N2S} were shown to coordinate to copper(II) in a tridentate mode via the ligand pyridyl nitrogen atom, amidate nitrogen atom, and the thioether sulfur atom (see chapter 3).[24] Pmac, which differs from 2-HL^{N2S} only in the absence of the methyl thioether group, coordinates in a related manner via the two nitrogen atoms and a

bridging oxygen atom to form clusters.[23] Importantly, reduction of copper(II) was *never* observed with either 2-HL^{N2S} or pmac.

2-HL^{N2S}   **pmac**
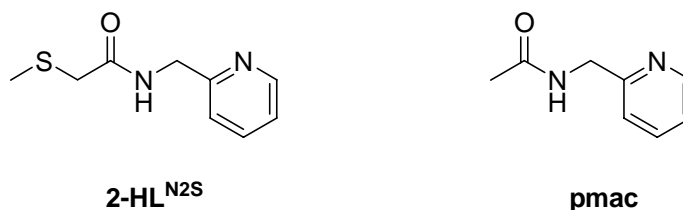
While pmac contains no thioether group, the key difference between **4** and 2-HL^{N2S} is that **4** possesses *two* amido-thioether arms attached to the pyridyl ring. To more systematically evaluate the mutual dependence of the observed redox decomposition on the amide, pyridyl, and thioether functional groups of **4**, we synthesized ligands **3**, **5**, and **6** (see section 4.2). **3** is identical to **4** except for the thioether groups, which are absent. **5** is also identical to **4** except that the amide groups have been reduced to amines. Solutions of copper(II) with **3** or **5** appear green immediately upon mixing, suggesting coordination, but no further color change was observed, indicating that the complexes are stable in the 2+ oxidation state. Thus, both of the thioethers and the amides are necessary for the reduction of copper.
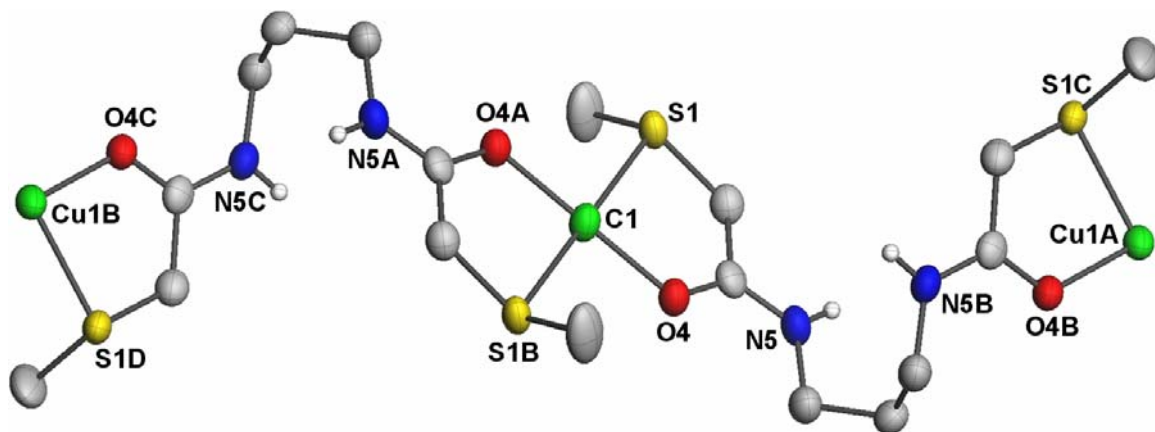
Bond Lengths (Å)		Angles (deg)	
Cu1–S1	2.323(2)	S1–Cu1–S1B	180.0(0)
Cu1–O4	1.924(2)	S1–Cu1–O4	87.2(1)
Cu⋯Cu	9.078(2)	S1–Cu1–O4A	92.8(1)
		O4–Cu1–O4A	180.0(2)

Figure 4-13. Representation of the X-ray crystal structure of $[Cu(L^{(acSMe)2})](OTf)_2$ (**9**) as 50% thermal ellipsoids. All non-amide H atoms have been omitted for clarity. Selected bond distances (Å) and angles (deg) relevant to copper coordination and the amide groups are tabulated.

To assess the importance of the pyridyl group in **4**, **6** was synthesized. **6** contains the amide and thioether functional groups, but the pyridyl ring is absent. Reactions of **6** with copper(II) salts result in the formation of stable complexes with no evidence of reduction, suggesting that the pyridyl ring in copper(II) complexes of **4** facilitates redox by organizing the ligand and copper ion and/or raising the $Cu^{II/I}$ redox potential. X-ray quality crystals of the product, $[Cu(L^{(acSMe)2})](OTf)_2$ (**9**), were obtained by diffusing

diethyl ether into a concentrated methanol solution of the reaction mixture. The X-ray crystal structure confirms both the identity and stability of the complex (Figure 4-13). In the crystal structure of **9**, ligand **5** forms infinite linear chains between copper(II) ions and coordinates in a square planar geometry via its amide oxygen (O4) and thioether sulfur (S1) atoms. The amide nitrogen atoms are not involved in coordination. Outer-sphere triflate ions, located between the chains, balance the charge of the cations.

Finally, since the ability of **4** to reduce copper(II) had now been established and all evidence strongly pointed to the mutual importance of the pyridyl, amide, and thioether functional groups of the ligand to promote the reduction, an attempt was made to investigate the copper(II) chemistry of **8**, containing sulfonamides instead of amides. It was proposed that the sulfonyl groups of **8** could possibly promote thioether activation in the same way that the amide carbonyl is suggested to do in the copper(II) complex of **4**. Indeed, the reaction of copper(II) with **8** results in an initial blue solution that slowly bleaches to pale yellow, indicative of copper(II) reduction. Work is currently underway to investigate this preliminary result quantitatively and to compare its chemistry to that of **4**. A summary of the observed copper chemistry with the ligands described in this section is provided in Table 4-1.

Table 4-1. Summary of ligand reactivity with copper(II).

Ligand		Observation
$L^{Py(ac)2}$	**(3)**	Forms stable green Cu^{II} product
$L^{Py(acSMe)2}$	**(4)**	Decomposes from dark green Cu^{II} to pale yellow Cu^{I} product
$L^{Py(SMe)2}$	**(5)**	Forms stable green Cu^{II} product
$L^{(acSMe)2}$	**(6)**	Forms stable green Cu^{II} product
$L^{Py(TsSMe)2}$	**(8)**	Decomposes from green Cu^{II} to pale yellow Cu^{I} product
2-HL^{N2S}		Forms stable dark blue Cu^{II} product[24]
Pmac		Forms stable blue Cu^{II} product[23]

Ligand Structures:

L$^{Py(ac)2}$ **(3)**   L$^{Py(SMe)2}$ **(5)**   L$^{Py(TsSMe)2}$ **(8)**

L$^{Py(acSMe)2}$ **(4)**   L$^{(acSMe)2}$ **(6)**
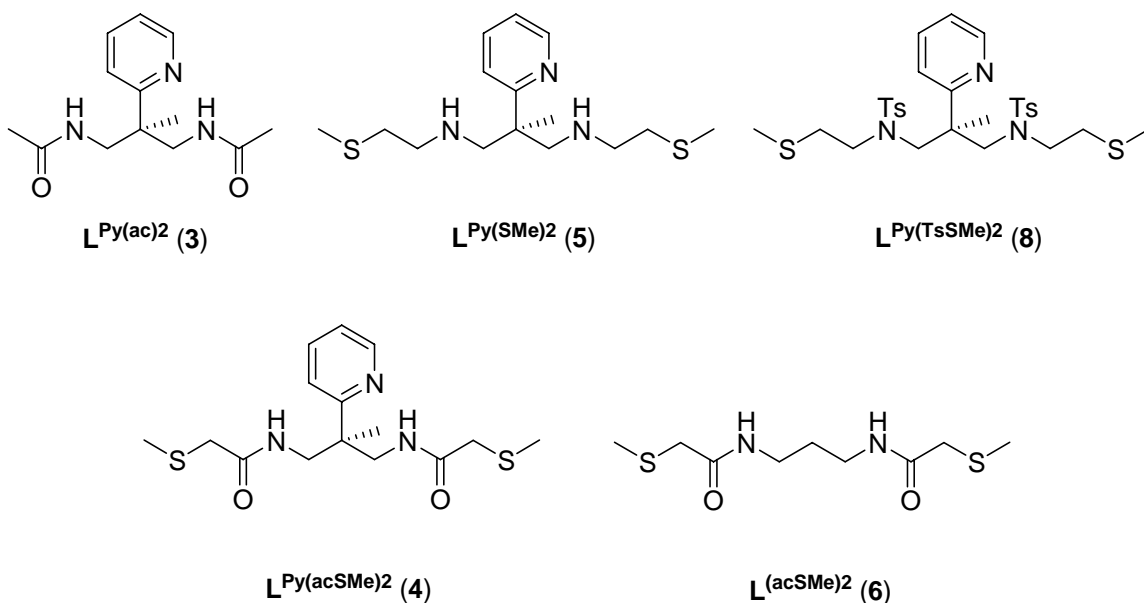
4.4.   Conclusions

Our results provide clear evidence that, under the appropriate conditions, thioether sulfur can be activated to reduce copper(II). In ligand **4**, the presence of the pyridyl ring, two thioether groups and two amide groups are *all* required for spontaneous redox to occur. Preliminary experiments with ligand **8** show that similar results can also be

obtained using sulfonamide groups instead of amides, supporting the notion that the thioether sulfurs of **4** are activated by amide carbonyl interactions. If the tosyl groups of **8** are removed and the resulting ligand, **5**, is reacted with copper(II), no redox is observed and a stable copper(II) product is obtained. The importance of two amide and two thioether groups, highlighted by the difference in reactivity between **4** and 2-HL^{N2S}, suggests that the amide group of one arm modulates the redox potential of the thioether group from the other arm, but cannot activate the thioether in the same arm, perhaps due to structural constraints or coordination effects. The very close proximity of Met-35 and the Ile-31 amide carbonyl in Aβ may activate it for redox with copper(II) in the same way. In addition to sulfur activation, it is also likely that the copper redox potential is significantly modulated by its coordination environment and that the redox chemistry occurs as a consequence of shifting both the copper and sulfur redox potentials in these special systems. This is supported by the fact that no redox is observed with **6**, which contains no pyridyl group.

Since the neurotoxicity in AD is known to be related to soluble Aβ oligomers,[12] we believe that the proposed copper(II)-thioether redox may occur by way of an intermolecular mechanism, where the redox-active species is composed of two interacting Aβ peptides in solution. Specifically, we envision a scenario where the activated Met-35 residue of one peptide directly coordinates the bound copper(II) of a second peptide, allowing for conditions that promote unusually facile inner-sphere electron transfer. This arrangement is consistent with the properties and reactivity of the model system presented in this chapter, where very specific conditions are required for redox to occur.

To our knowledge, no other examples of spontaneous redox between methyl thioether sulfur and copper(II) have been reported in the literature to date. The preliminary observations presented in this work, as such, may provide the first synthetic evidence supporting the feasibility of the unusual decomposition mode that is proposed to take place in Aβ peptides. Further studies of our system to elucidate the details of its redox mechanism and the identity of the organic ligand decomposition product(s) are currently underway.

4.5. *Experimental*

General. All reagents were purchased from commercial sources and used without additional purification unless otherwise noted. Solvents were dried and purified under nitrogen using standard methods. Et$_2$O, THF, and pentane were distilled over NaK$_2$ alloy, CH$_3$CN and CH$_2$Cl$_2$ over CaH$_2$, MeOH over Mg(OMe)$_2$, and toluene over Na. Degassing of the dried solvents was achieved by triple freeze-pump-thaw degas cycles. Oxygen- and/or water-sensitive reactions were carried out using Schlenk vacuum line techniques and/or by using an M. Braun UNILab inert atmosphere glovebox with nitrogen as its working gas. Procedures for the syntheses of 2-methyl-2-(2-pyridinyl)-1,3-propan-diol, 2-methyl-2-(2-pyridinyl)-1,3-bis(*p*-toluenesulfonate)-propane, and 2-methyl-2-(2-pyridinyl)-1,3-propanediamine are published elsewhere.[18] The improved syntheses of 2-methyl-2-(2-pyridinyl)-1,3-bis(*p*-toluenesulfonate)-propane and 2-methyl-2-(2-pyridinyl)-1,3-propanediamine are also included here.

Spectroscopy. Infrared (IR) spectra were prepared by pressing the sample into a KBr "glass" and were collected using a Nicolet NEXUS 470 FTIR spectrophotometer coupled to a computer running OMNIC E.S.P (version 5.1) software for spectrum

display, background baseline correction, scaling, and automatic peak-picking. Unless otherwise stated, samples for electronic absorption (UV-vis) spectroscopy were prepared at 5 mM concentrations in a 5 mL 1.00 cm path length quartz cuvette. UV-vis data were obtained using a Shimadzu UV2401PC UV-vis spectrophotometer capable of a 200 - 1100 nm scan range and having a dedicated variable temperature Neslab RTE-140 circulating heater/chiller and computer interface running Shimadzu UV Probe (v. 1.00) for instrument control and spectrum display. All UV-vis spectra were obtained at 298.0 K unless otherwise noted. ^{1}H and ^{13}C NMR spectra were measured at room temperature on a Varian 300 MHz (Mercury) spectrometer or a Varian 400 MHz spectrometer coupled to the Varian VNMR software package. Solvent was used as an internal chemical shift standard unless otherwise stated. All signals are reported in ppm relative to the reported value(s) for the solvent. X-band (~9.45 GHz) EPR spectra were obtained using a Bruker EMX spectrometer fitted with a either a liquid nitrogen finger dewer or a liquid nitrogen cryostat (BVT-3000). Temperature and *g* value calibrations were performed as described.[31]

Physical Methods. Capillary Gas Chromatography Mass Spectrometry (GC-MS) analyses were performed in a Trace GC 2000 and Thermoquest GCQ/Polaris mass spectrometer (ThermoQuest Finnigan, San Jose, CA). The software controlling the system was Xcalibur (version 1.1) from ThermoQuest Finnigan. Electron impact (EI) was the ionization source and the typical electron energy was set to 70 eV with the ion source temperature maintained at 200 $^{\circ}$C. The instrument was calibrated with the perfluorotributyl amine FC-43 over a *m/z* range of 50-650 Da. Organic components were separated in an Alltech-ECCNO-OAP (30 m x 0.25 mm x 0.25 μm). The injector

temperature was set at 210 °C and a splitless mode of injection was used in all analyses. The GC temperature gradient was set to 50 °C, holding for 5 minutes, then increased at 20 °C/minute to 250 °C holding for 20 minutes. The GC system was run at a constant flow rate of 1.0 mL/minute of helium gas (Minimum Purity 99.999%). ElectroSpray Ionization Mass Spectrometry (ESI-MS) data were recorded using a Q-TOF quadrupole time-of flight mass spectrometer (Micromass, Manchester, UK) equipped with a Z-spray electrospray ionization (ESI) source. The software controlling the instrument was MassLynx (version 4.0). A Harvard syringe pump (Harvard Apparatus, South Natick, MA, USA) was used to deliver the sample solution to the electrospray source at a flow rate of 5 μl/min. The electrospray capillary voltage was set at 3000 V and the cone voltage was typically set to 30 V. The temperature for desolvation and source was set to 90 °C. The desolvation gas (nitrogen, 99.99%) flow rate was set to 250 liters per hour. Nebuliser gas flow was set to 20 liters per hour. The mass spectrometer was calibrated over a mass range of 50-1500 Da using a 0.05 μg/μL CsI and 2 μg/μL NaI solution in methanol.

2-Methyl-2-(2-pyridinyl)-1,3-bis(*p*-toluenesulfonate)-propane (**1**). Sodium hydroxide (34.2 g, 854 mmol) was dissolved in 200 mL of water in a 2 L beaker. To this solution was added 2-methyl-2-(2-pyridinyl)-1,3-propanediol (50.0 g, 299 mmol) in 200 mL of THF. This mixture was cooled to 0 °C and a solution of *p*-toluenesulfonyl chloride (114.1 g, 568.1 mmol) in 200 mL of THF was added dropwise over 2 hours. During this time, the solution was rapidly stirred and the temperature was maintained at 0 °C. A yellow-white precipitate began to form. After the addition was complete, the reaction

mixture was stirred at room temperature for an additional 2 hours. The reaction mixture was then poured into 500 mL of ice water and stirred for 1 hour, resulting in the formation of more yellow-white precipitate. The precipitate was filtered from the solution, repeatedly washed with ethanol, and trace solvents were removed under reduced pressure to yield the desired product in high purity as a fine white powder (66.1g, 49%). ^{1}H NMR (200 MHz, CDCl$_3$) δ 8.30-8.34 (m, 1H), 7.55-7.67 (m, 5H), 7.10-7.32 (m, 6H), 4.27 (s, 4H), 2.44 (s, 6H), 1.34 (s, 3H) ppm. Anal. Calcd for C$_{23}$H$_{25}$NO$_6$S$_2$: C, 58.09; H, 5.30; N, 2.95; S, 13.48. Found: C, 58.05; H, 5.26; N, 2.95; S, 13.38.

2-Methyl-2-(2-pyridinyl)-1,3-propanediamine (**2**). **1** (50.00 g, 105 mmol) was dissolved in 500 mL DMSO in a 1 L Schlenk flask under a nitrogen atmosphere. To this rapidly-stirring solution at 70 ^{o}C was added anhydrous NaN$_3$ (20.48 g, 315 mmol) in a single portion. The resulting mixture was stirred for 40 hours at 70 ^{o}C, allowed to cool to room temperature, and poured into 700 mL of 30 v/v% ethanol in water in a 2 L separation funnel. This resulted in the formation of colorless oil that settled to the bottom of the funnel after agitation. The oil was extracted into 400 mL of Et$_2$O. The Et$_2$O extraction was repeated 2 more times. The combined Et$_2$O solution was reduced in volume to 400 mL, washed with 100 mL of water, dried over Na$_2$SO$_4$, and then filtered into a clean 2 L flask. To the remaining 400 mL Et$_2$O solution was added 150 mL pyridine and the total volume then reduced to 100 mL under reduced pressure (**NOTE**: Due to the explosive nature of organic azides, the azide intermediate was *not* isolated from solvent at any time). The same flask was fitted with an addition funnel containing PPh$_3$ (66.07 g, 252.8 mmol) in 125 mL of pyridine, the contents of which were added

drop-wise to the stirring pyridine solution at 0 °C. After complete addition, the reaction mixture was allowed to warm to room temperature, stirred for 2 hours, and the solvent then removed *in vacuo* to reveal a thick yellow oil. 600 mL of 25 % NH$_4$OH were added to this oil and the flask was fitted with a condenser. This mixture was heated to reflux (~150 °C) in an oil bath for 12 hours. After cooling to room temperature, the colorless NH$_4$OH solution was filtered into a clean 2 L flask. To the remaining PPh$_3$O in the first flask was added 600 mL of fresh 25 % NH$_4$OH and the mixture was refluxed for 1 hour in order to further extract the desired product. After cooling, the NH$_4$OH solution was filtered and combined with the first 600 mL solution. The 25% NH$_4$OH solvent was then removed by heating under high vacuum to reveal a yellow oil that was subsequently dissolved into an equal volume of dichloromethane and washed with 4 M aqueous NaOH. The aqueous wash was extracted with dichloromethane until the extracts were colorless. The combined dichloromethane solution was dried over Na$_2$SO$_4$ and the solvent removed *in vacuo* to yield the desired product as a low-viscosity yellow oil (16.80 g, 97%). ^{1}H NMR (200 MHz, CDCl$_3$) δ 8.24-8.28 (m, 1H), 7.32-7.38 (m, 1H), 7.01-7.06 (m, 1H), 6.80-6.87 (m, 1H), 2.61-2.87 (m, 4H), 2.05 (s, 4H), 1.03 (s, 3H) ppm. ^{13}C NMR (200 MHz, CDCl$_3$) δ 162.77, 148.11, 135.79, 120.80, 120.50, 49.24, 28.39, 20.57 ppm.

N,N'-(2-Methyl-2-pyridin-2-ylpropane-1,3-diyl)-bis(acetamide) (**L$^{Py(ac)2}$**, **3**). **2** (3.00 g, 18.2 mmol) was dissolved in 12 mL of pyridine in a 100 mL flask. To this rapidly-stirring solution was poured 15 mL of acetic anhydride in a single portion. After stirring for 12 hours at room temperature, 30 mL of water were added and the mixture was stirred for 5 more minutes. The solvent and excess acetic anhydride were removed by gentle

heating under reduced pressure, resulting in a thick yellow-orange oil that was then dissolved into an equal volume of dichloromethane and washed with 4 M aqueous NaOH. The aqueous wash was extracted with additional dichloromethane until the extracts were colorless. The combined dichloromethane solution was dried over Na_2SO_4 and filtered. Following removal of the filtrate solvent *in vacuo*, Et_2O (10 mL) was added to the obtained yellow oil and the desired product recrystallized as a white solid that was filtered from the Et_2O solution and washed with fresh Et_2O (2.92 g, 65%). ^{1}H NMR (200 MHz, $CDCl_3$) δ 8.43-8.46 (m, 1H), 7.58 - 7.67 (m, 1H), 7.34 - 7.38 (m, 1H), 7.08 - 7.24 (m, 3H), 3.79 - 3.91 (m, 2H), 3.05 - 3.15 (m, 2H), 1.96 (s, 6H), 1.16 (s, 3H) ppm. ^{13}C NMR (200 MHz, $CDCl_3$) δ 170.89, 164.37, 148.20, 136.77, 121.70, 121.46, 46.08, 43.94, 23.29, 22.77 ppm. FTIR (KBr): 3286, 3090, 3009, 2984, 2970, 2932, 2843, 2015, 1900, 1674, 1653 (υ_{CO}), 1589, 1553, 1468, 1441, 1426, 1388, 1364, 1356, 1340, 1284, 1258, 1222, 1164, 1128, 1089, 1052, 1038, 1029, 993, 908, 893, 853, 800, 756, 705, 649, 624, 587, 585, 527, 519, 515, 499, 472, 464, 453, 441, 426, 410 cm^{-1}. Anal. Calcd for $C_{13}H_{19}N_3O_2$: C, 62.63; H, 7.68; N, 16.85. Found: C, 62.58; H, 7.43; N, 16.74.

N,N'-(2-Methyl-2-pyridin-2-ylpropane-1,3-diyl)-bis[2-(methylthio)acetamide]

(**L$^{Py(acSMe)2}$, 4**). A solution of **2** (6.03 g, 36.5 mmol), (methylthio)acetic acid (7.75 g, 73.0 mmol), and HOBt (9.86 g, 73.0 mmol) in 250 mL of 50 v/v% THF/DMF was cooled to 0 ^{o}C. To this rapidly-stirring mixture was added a solution of DCC (15.06 g, 73.0 mmol) in a minimal volume of THF. The reaction mixture was stirred for one hour at 0 ^{o}C after the DCC addition was complete and then allowed to warm to room temperature and stirred for an additional 4 hours during which time dicyclohexylurea (DCU) byproduct had

precipitated from the solution. The reaction mixture was cooled to -40 °C and the solution filtered away from the DCU precipitate. Solvent was removed from the filtrate by gentle heating under reduced pressure, revealing a thick yellow-orange oil. An equal volume of toluene was added to this oil and the mixture was stirred for one hour at room temperature during which time more DCU precipitated. The DCU was filtered away and the toluene was removed from the filtrate *in vacuo*. The remaining yellow oil was dissolved into a minimal volume of dichloromethane and washed with 4 M aqueous NaOH. The aqueous wash was extracted with more dichloromethane until the extracts were colorless. The combined organic solution was dried over Na_2SO_4, filtered, and the solvent was removed under reduced pressure to give the desired product as a viscous yellow-orange oil (10.44 g, 84%). ^{1}H NMR (200 MHz, $CDCl_3$) δ 8.43 - 8.49 (m, 1H), 7.87 - 7.98 (m, 2H), 7.52 - 7.68 (m, 1H), 7.33 - 7.39 (m, 1H), 7.06 - 7.15 (m, 1H), 3.78 - 3.90 (m, 2H), 3.13 - 3.29 (m, 2H), 3.13 (s, 4H), 2.01 (s, 6H), 1.21 (s, 3H) ppm. ^{13}C NMR (200 MHz, $CDCl_3$) δ 169.31, 163.72, 148.22, 136.69, 121.69, 121.22, 46.17, 44.34, 38.02, 22.65, 16.10 ppm. FTIR (KBr): 3312, 3062, 2972, 2918, 2858, 1653 (C=O), 1589, 1522, 1473, 1431, 1385, 1362, 1302, 1225, 1155, 1120, 1072, 1050, 1021, 993, 963, 892, 867, 826, 789, 750, 696, 618, 543, 467, 449, 404 cm^{-1}. EIMS: *m/z* (Int.); 342 [M^+] (100%). Anal. Calcd for $C_{15}H_{23}N_3O_2S_2$: C, 52.76; H, 6.79; N, 12.30; S, 18.78. Found: C, 53.82; H, 6.85; N, 12.03; S, 17.95.

2-Methyl-*N,N'*-bis[2-(methylthio)ethyl]-2-pyridin-2-ylpropane-1,3-diamine
(**L$^{Py(SMe)2}$**, **5**). LiAlH$_4$ (1.40 g, 35.1 mmol) was added in small portions directly to a stirring solution of **4** (1.00 g, 2.93 mmol) in 100 mL dry diethyl ether under nitrogen.

The reaction mixture was refluxed for 12 hours. After cooling to room temperature, excess LiAlH$_4$ was quenched by slow addition of water under a continuous nitrogen purge. The ether level was maintained during quenching. The resulting mixture was transferred to a 1 L separation funnel and extracted with fresh diethyl ether (4 x 200 mL). The combined organic extract was dried over Na$_2$SO$_4$, filtered, and the solvent was removed under reduced pressure to give the desired product as a viscous yellow-orange oil (0.78 g, 85 %). ^{1}H NMR (300 MHz, CDCl$_3$) δ 8.47 - 8.51 (m, 1H), 7.54 – 7.62 (m, 1H), 7.00 – 7.10 (m, 2H), 2.33 -3.07 (m, 12H), 1.97 – 2.12 (m, 8H), 1.34 (s, 3H) ppm. ESI/MS: *m/z* = 314 (M + 1).

N,N'-Propane-1,3-diylbis[2-(methylthio)acetamide] (**L$^{(SMe)2}$**, **6**). 1,3-diaminopropane (0.815 g, 10.99 mmol), (methylthio)acetic acid (2.334 g, 21.99 mmol), and HOBt (3.368 g, 21.99 mmol) were dissolved in 250 mL of 50 v/v% THF/DMF and cooled to 0 ^{o}C. To this rapidly-stirring solution was added a solution of DCC (4.537 g, 21.99 mmol) in a minimal volume of THF. The reaction mixture was stirred for one hour at 0 ^{o}C and then allowed to warm to room temperature and stirring was continued for an additional 4 hours. Dicyclohexylurea (DCU) byproduct precipitated from the solution during this time. The reaction mixture was cooled to -40 ^{o}C and the solution filtered away from the DCU precipitate. Solvent was removed from the filtrate by gentle heating under reduced pressure, revealing a pale yellow solid. This was dissolved into a minimal volume of dichloromethane and washed with 4 M aqueous NaOH. The aqueous wash was extracted with more dichloromethane until the extracts were colorless. The combined organic solution was dried over Na$_2$SO$_4$, filtered, and the solvent was removed under reduced

pressure. The desired product was obtained from this as a white solid following recrystallization from 5 % ethanol in toluene (1.62 g, 59 %). ^{1}H NMR (300 MHz, CDCl$_3$) δ 7.22 – 7.44 (m, 2H), 3.30 – 3.38 (m, 4H), 3.22 (s, 4H), 2.14 (s, 6H), 1.64 – 1.76 (m, 2H) ppm. ^{13}C NMR (300 MHz, CDCl$_3$) δ 169.75, 38.46, 36.54, 30.03, 16.76 ppm.

2-Methyl-*N,N'*-di(*p*-toluenesulfonyl)-2-pyridin-2-ylpropane-1,3-diamine (**7**). A mixture of **2** (2.000 g, 12.12 mmol), K$_2$CO$_3$ (3.1 g, 22 mmol), and water (10 mL) was cooled to 0 °C in a 150 mL Erlenmeyer flask. To this was added a solution of *p*-toluenesulfonyl chloride (4.593 g, 24.1 mmol) in THF (20 mL) over 2 hours. The reaction mixture was then allowed to warm to room temperature and stirring was continued for 12 hours after which time it was poured into 250 mL of ice water in a 500 mL separation funnel. This aqueous solution was extracted with chloroform (3 x 100 mL). The combined chloroform solution was dried over Na$_2$SO$_4$, filtered, and the solvent removed *in vacuo* to yield the crude product as a thick orange oil that was subsequently recrystallized from 150 mL of 10 v/v% ethanol in diethyl ether. The desired product was filtered then washed with ethanol and diethyl ether to yield the desired product as a white crystalline powder (2.59 g, 45.1 %). ^{1}H NMR (300 MHz, CDCl$_3$) δ 8.38 - 8.42 (m, 1H), 7.75 (d, *J* = 8, 4H), 7.62 - 7.69 (m, 1H), 7.28 - 7.35 (m, 5H), 7.12 - 7.18 (m, 1H), 5.95 - 6.03 (m, 2H), 3.07 - 3.27 (m, 4H), 2.42 (s, 6H), 1.34 (s, 3H) ppm. ^{13}C NMR (300 MHz, CDCl$_3$) δ 163.64, 148.64, 143.62, 137.47, 137.24, 130.05, 127.14, 122.46, 121.59, 48.78, 45.33, 22.55, 21.76. Anal. Calcd for C$_{23}$H$_{27}$N$_3$O$_4$S$_2$: C, 58.33; H, 5.75; N, 8.87. Found: C, 58.11; H, 5.65; N, 8.71.

2-Methyl-*N*,*N*'-bis[2-(methylthio)ethyl]-*N*,*N*'-di(*p*-toluenesulfonyl)-2-pyridin-2-ylpropane-1,3-diamine (L$^{Py(TsSMe)2}$, 8). *N*-[2-(Methylthio)ethyl]-*p*-toluenesulfonamide (6.618 g, 27.01 mmol) was dissolved in 120 mL of DMF and heated to 105 °C in a 3-neck flask. Sodium hydride (60 % dispersion in oil) (2.72 g, 113.4 mmol) was slowly added to this rapidly-stirring solution, resulting in the immediate evolution of hydrogen gas. Sirring and heating were continued for one hour following complete addition and the cessation of hydrogen gas evolution. The reaction mixture was then cooled to room temperature and the DMF solution was filtered from excess sodium hydride. **1** (6.416 g, 13.50 mmol) in 120 mL of DMF was added drop-wise to this solution over the course of two hours at 105 °C. Stirring at 105 °C was continued for two additional hours and the reaction mixture was then cooled to room temperature and poured into 250 mL of water in a 500 mL separation funnel. The aqueous solution was extracted with chloroform (4 x 125 mL). The organic extracts were combined and the chloroform removed *in vacuo* to yield a red-brown oil. The desired product was obtained from this crude product as a white powder following recrystallization from 100 mL of ethanol at room temperature (2.46 g, 29.3 %). X-ray quality crystals of the product were obtained by slow evaporation of a concentrated ethanol solution of the powder. ^{1}H NMR (300 MHz, CDCl$_3$) δ 8.45 - 8.49 (m, 1H), 7.59 - 7.66 (m, 5H), 7.36 - 7.41 (m, 1H), 7.22 - 7.26 (m, 4H), 7.10 - 7.15 (m, 1H), 3.70 (d, *J* = 14 Hz, 2H), 3.39 (d, *J* = 14 Hz, 2H), 2.43 - 2.70 (m, 8H), 2.36 (s, 6H), 1.74 (s, 6H), 1.55 (s, 3H) ppm. ^{13}C NMR (300 MHz, CDCl$_3$) δ 163.13, 149.34, 143.82, 137.25, 136.29, 130.04, 127.68, 122.51, 122.35, 57.82, 50.51, 46.90, 31.75, 21.77, 19.80, 15.52 ppm. Anal. Calcd for C$_{29}$H$_{39}$N$_3$O$_4$S$_4$: C, 56.01; H, 6.32; N, 6.76. Found: C, 55.99; H, 6.30; N, 6.59.

[Cu(L$^{(SMe)2}$)](OTf)$_2$ (9). A solution of L$^{(SMe)2}$ (**6**) (0.048 g, 0.19 mmol) in 5 mL of methanol was slowly added to a rapidly stirring solution of Cu(OTf)$_2$ in 5 mL of methanol (0.070 g, 0.19 mmol). The resulting clear dark green solution was stirred for 30 minutes at room temperature. X-ray quality crystals of the desired product were obtained by concentrating the reaction mixture and diffusing diethyl ether into it (0.095 g, 85 %). ESI-MS: *m/z* (Int.); 712, {[Cu(L$^{(SMe)2}$)$_2$](OTf)}$^+$, (77 %); 463 , {[Cu(L$^{(SMe)2}$)](OTf)}$^+$, (43 %). Anal. Calcd for C$_{11}$H$_{18}$CuF$_2$N$_2$O$_8$S$_4$: C, 21.60; H, 2.94; N, 4.58. Found: C, 21.84; H, 3.01; N, 4.62.

X-ray Crystallography.   **L$^{Py(TsSMe)2}$** (**8**):   A colorless crystal of dimensions 0.47 x 0.33 x 0.31 mm was selected for structural analysis. Intensity data for this compound were collected using an instrument with a Bruker APEX ccd area detector with graphite-monochromated Mo Kα radiation (λ = 0.71073 Å).[32]   Important crystallographic information is summarized in table 4-2. The sample was cooled to 97(2) K. Cell parameters were determined from a non-linear least squares fit of 6458 peaks in the range 2.25 < θ < 28.27°. A total of 17215 data were measured in the range 2.25 < θ < 26.00° using ω oscillation frames. The data were corrected for absorption by the semi-empirical method giving minimum and maximum transmission factors of 0.8572 and 0.902.[33] The data were merged to form a set of 6174 independent data with R(int) = 0.0227 and a coverage of 100.0 %.

The monoclinic space group *P*(1) was determined by systematic absences and statistical tests and verified by subsequent refinement. The structure was solved by direct

methods and refined by full-matrix least-squares methods on F^2.[34] Hydrogen atom positions were initially determined by geometry and refined by a riding model. Non-hydrogen atoms were refined with anisotropic displacement parameters. Hydrogen atom displacement parameters were set to 1.2 (1.5 for methyl) times the displacement parameters of the bonded atoms. A total of 316 parameters were refined against 121 restraints and 6174 data to give w$R(F^2)$ = 0.1219 and S = 1.005 for weights of w = 1/[σ^2 (F^2) + (0.0660 P)^2 + 0.9400 P], where P = [$F_o^2 + 2F_c^2$] / 3. The final R(F) was 0.0437 for the 5852 observed, [$F > 4\sigma(F)$], data. The largest shift/s.u. was 0.006 in the final refinement cycle. The final difference map had maxima and minima of 0.872 and -0.488 e/Å^3, respectively. The final structure was graphically presented using the Accelrys Materials Studio software package.[35]

[Cu(L$^{\text{Py(TsSMe)2}}$)](OTf)$_2$ (9): A blue prism-shaped crystal of dimensions 0.30 x 0.28 x 0.10 mm was selected for structural analysis. Intensity data for this compound were collected using an instrument with a Bruker APEX ccd area detector with graphite-monochromated Mo Kα radiation (λ = 0.71073 Å).[32] Important crystallographic information is summarized in table 4-2. The sample was cooled to 110(2) K. Cell parameters were determined from a non-linear least squares fit of 6458 peaks in the range 2.25 < θ < 28.27°. A total of 8083 data were measured in the range 2.25 < θ < 26.00° using ω oscillation frames. The data were corrected for absorption by the semi-empirical method giving minimum and maximum transmission factors of 0.660 and 0.865.[33] The data were merged to form a set of 2118 independent data with R(int) = 0.0165 and a coverage of 100.0 %.

The monoclinic space group $P2/n$ was determined by systematic absences and statistical tests and verified by subsequent refinement. The structure was solved by direct methods and refined by full-matrix least-squares methods on F^2.[34] Hydrogen atom positions were initially determined by geometry and refined by a riding model. Non-hydrogen atoms were refined with anisotropic displacement parameters. Hydrogen atom displacement parameters were set to 1.2 (1.5 for methyl) times the displacement parameters of the bonded atoms. A total of 222 parameters were refined against 137 restraints and 2118 data to give w$R(F^2)$ = 0.1005 and S = 1.013 for weights of w = $1/[\sigma^2(F^2) + (0.0660\ P)^2 + 0.9400\ P]$, where P = $[F_o^2 + 2F_c^2] / 3$. The final R(F) was 0.0339 for the 1938 observed, $[F > 4\sigma(F)]$, data. The largest shift/s.u. was 0.006 in the final refinement cycle. The final difference map had maxima and minima of 0.889 and -0.513 e/Å^3, respectively. The final structure was graphically presented using the Accelrys Materials Studio software package.[35]

Table 4-2. Summary of crystallographic data for compounds **8** and **9**.

	8	9
empirical formula	$C_{29}H_{39}N_3O_4S_4$	$C_{11}H_{18}CuF_6N_2O_8S_4$
formula weight	621.97	612.07
crystal system	triclinic	monoclinic
space group	P(1)	P2/n
a (Å)	11.446 (2)	11.770(4)
b (Å)	12.166 (2)	7.182(2)
c (Å)	12.584 (2)	12.792(5)
α (deg)	92.881 (3)	90
β (deg)	112.681 (3)	95.232(5)
γ (deg)	99.595 (3)	90
V (Å^{-3})	1581.5 (5)	1076.8(6)
Z	2	2
density (calcd)	1.306 g/cm^3	1.888 g/cm^3
temperature (K)	97(2)	110(2)
crystal size (mm)	0.47 x 0.33 x 0.31	0.30 x 0.28 x 0.10
diffractometer	Bruker Apex	Bruker Apex
absorption coefficient	0.338 mm^{-1}	1.496 mm^{-1}
radiation, λ (Å)	Mo Kα, λ = 0.71073	Mo Kα, λ = 0.71073
2θ max (deg)	52.0	48.0
reflections collected	17215	8083
independent reflections	6174	2118
observed reflections	5852	1938
variable parameters	361	552
$R1$ [$I > 2\sigma(I)$]	0.0437	0.0339
w$R2$ [$I > 2\sigma(I)$]	0.1219	0.1005
goodness-of-fit	1.005	1.013
largest diff. peak and hole (e^{-1} Å^{-3})	0.872, -0.488	0.889, -0.513

4.6.   References

1.   Caughey, B.; Lansbury, P. T. *Annu. Rev. Neurosci.* **2003**, *26*, 267-298.

2.   Mattson, M. P. *Physiol. Rev.* **1997**, *77*, 1081-1132.

3.   Crescenzi, O.; Tomaselli, S.; Guerrini, R.; Salvadori, S.; D'Ursi, A. M.; Temussi, P. A.; Picone, D. *Eur. J. Biochem.* **2002**, *269*, 5642-5648.

4.   Varadarajan, S.; Kanski, J.; Aksenova, M.; Lauderback, C.; Butterfield, D. A. *J. Am. Chem. Soc.* **2001**, *123*, 5625-5631.

5.   Butterfield, D. A.; Boyd-Kimball, D. *Biochim. Biophys. Acta* **2005**, *1703*, 149-156.

6.   Rauk, A.; Armstrong, D. A.; Fairlie, D. P. *J. Am. Chem. Soc.* **2000**, *122*, 9761-9767.

7.   Curtain, C. C.; Ali, F.; Volitakis, I.; Cherny, R. A.; Norton, R. S.; Beyreuther, K.; Barrow, C. J.; Masters, C. L.; Bush, A. I.; Barnham, K. J. *J. Biol. Chem.* **2001**, *276*, 20466-20473.

8.   Huang, X.; Cuajungco, M. P.; Atwood, C. S.; Hartshorn, M. A.; Tyndall, J. D.; Hanson, G. R.; Stokes, K. C.; Leopold, M.; Multhaup, G.; Goldstein, L. E.; Scarpa, R. C.; Saunders, A. J.; Lim, J.; Moir, R. D.; Glabe, C.; Bowden, E. F.; Masters, C. L.; Fairlie, D. P.; Tanzi, R. E.; Bush, A. I. *J. Biol. Chem.* **1999**, *274*, 37111-37116.

9.   Schoneich, C.; Pogocki, D.; Hug, G. L.; Bobrowski, K. *J. Am. Chem. Soc.* **2003**, *125*, 13700-13713.

10.   Pogocki, D. *Acta Neurobiol. Exp.* **2003**, *63*, 131-145.

11.   Butterfield, D. A.; Bush, A. I. *Neurobiol. Aging* **2004**, *25*, 563-568.

12. Cleary, J. P.; Walsh, D. M.; Hofmeister, J. J.; Shankar, G. M.; Kuskowski, M. A.; Selkoe, D. J.; Ashe, K. H. *Nat. Neurosci.* **2005**, *8*, 79-84.

13. Armstrong, D. A., In *S-Centered Radicals*, Alfassi, Z. B., Ed. Wiley: New York, 1999; pp 27-61.

14. Glass, R. S., In *Topics In Current Chemistry*, Page, P. C. B., Ed. Springer-Verlag: Berlin Heidelberg, 1999; Vol. 205, pp 1-87.

15. Karlin, K. D.; Gultney, Y., In *Prog. Inorg. Chem.*, Lippard, S. J., Ed. 1987; Vol. 35, pp 219-328.

16. Bobrowski, K.; Pogocki, D.; Schoneich, C. *J. Phys. Chem. A* **1998**, *102*, 10512-10521.

17. (a) Kanski, J.; Aksenova, M.; Schoneich, C.; Butterfield, D. A. *Free Radic. Biol. Med.* **2002**, *32*, 1205-1211. (b) Pogocki, D.; Schoneich, C. *Chem. Res. Toxicol.* **2002**, *15*, 408-418.

18. Friedrich, S.; Schubart, M.; Gade, L. H.; Scowen, I. J.; Edwards, A. J.; McPartlin, M. *Chem. Ber./Recueil* **1997**, *130*, 1751-1759.

19. Halfen, J. A., Unpublished work. In 1999.

20. (a) Tobias, B. I. *Chemical & Engineering News* **1991**, *69*, 2-2. (#) Cardillo, P. *J. Loss Prev. Proc. Indust.* **2001**, *14*, 69-76. (b) Klapotke, T. M.; Rienacker, C. M. *Propell. Expl. Pyrotech.* **2001**, *26*, 43-47.

21. Vaultier, M.; Knouzi, N.; Carrie, R. *Tet. Lett.* **1983**, *24*, 763-764.

22. (a) Schrock, R. R.; Adamchuk, J.; Ruhland, K.; Lopez, L. P. H. *Organometallics* **2003**, *22*, 5079-5091. (b) Mehrkhodavandi, P.; Schrock, R. R.; Bonitatebus, P. J. *Organometallics* **2002**, *21*, 5785-5798. (c) Araujo, J. P.; Wicht, D. K.;

Bonitatebus, P. J.; Schrock, R. R. *Organometallics* **2001**, *20*, 5682-5689. (d) Galka, C. H.; Trosch, D. J. M.; Schubart, M.; Gade, L. H.; Radojevic, S.; Scowen, I. J.; McPartlin, M. *Eur. J. Inorg. Chem.* **2000**, 2577-2583. (e) Mehrkhodavandi, P.; Bonitatebus, P. J.; Schrock, R. R. *J. Am. Chem. Soc.* **2000**, *122*, 7841-7842.

23. Mondal, A.; Li, Y.; Khan, M. A.; Ross, J. H.; Houser, R. P. *Inorg. Chem.* **2004**, *43*, 7075-7082.

24. Klein, E. L.; Khan, M. A.; Houser, R. P. *Inorg. Chem.* **2004**, *43*, 7272-7274.

25. (a) Mcmanus, S. P.; Sedaghatherati, M. R.; Harris, J. M. *Tet. Lett.* **1987**, *28*, 5299-5300. (b) Mcmanus, S. P.; Neamatimazraeh, N.; Hovanes, B. A.; Paley, M. S.; Harris, J. M. *J. Am. Chem. Soc.* **1985**, *107*, 3393-3395.

26. Mizukami, A.; Kono, M. Bactericidal N-(2-alkylthioethyl)sulfonamides. 1970.

27. Michels, J. T.; O'Malley, B. G.; Klein, E. L.; Yang, L.; Grohmann, A.; Houser, R. P. *Acta Cryst. Sec. E* **2005**, *61*, 2824-2826.

28. (a) Grohmann, A.; Knoch, F. *Inorg. Chem.* **1996**, *35*, 7932-7934. (b) Grohmann, A. *Adv. Inorg. Chem.* **2004**, *56*, 179-210.

29. (a) Nonoyama, M.; Tomita, S.; Yamasaki, K. *Inorg. Chim. Acta* **1975**, *12*, 33-37. (b) Nonoyama, M. *Inorg. Chim. Acta* **1975**, *13*, 5-10. (c) Karlin, K. D.; Dahlstrom, P. L.; Stanford, M. L.; Zubieta, J. *Chem. Comm.* **1979**, 465-467. (d) Champloy, F.; Benali-Cherif, N.; Bruno, P.; Blain, I.; Pierrot, M.; Reglier, M.; Michalowicz, A. *Inorg. Chem.* **1998**, *37*, 3910-3918.

30. Ambundo, E. A.; Deydier, M. V.; Grall, A. J.; Aguera-Vega, N.; Dressel, L. T.; Cooper, T. H.; Heeg, M. J.; Ochrymowycz, L. A.; Rorabacher, D. B. *Inorg. Chem.* **1999**, *38*, 4233-4242.

31.   Lipscomb, J. D. *Biochemistry* **1980**, *19*, 3590-3599.

32.   (a) *X-ray data collection and cell refinement: SMART*, version 5.625; Bruker AXS, Inc.: Madison, WI, 2002. (b) *X-ray data reduction program: SAINT-plus*, version 6.28A; Bruker AXS, Inc.: Madison, WI, 2002.

33.   Sheldrick, G. M. *SADABS. Program for Empirical Absorption Correction of Area Detector Data.*, University of Göttingen: Göttingen, Germany, 2002.

34.   *X-ray structure solution and refinement program: SHELXTL*, version 6.12; Bruker AXS, Inc.: Madison, WI, 1997.

35.   *X-ray structure presentation software: Materials Studio*, version 2.1; Accelrys, Inc.: San Diego, CA, 2001.